

# Synthesizing Quantum-Circuit Optimizers

AMANDA XU, University of Wisconsin-Madison, USA

ABTIN MOLAVI, University of Wisconsin-Madison, USA

LAUREN PICK, University of Wisconsin-Madison, USA

SWAMIT TANNU, University of Wisconsin-Madison, USA

AWS ALBARGHOUTHI, University of Wisconsin-Madison, USA

Near-term quantum computers are expected to work in an environment where each operation is noisy, with no error correction. Therefore, quantum-circuit optimizers are applied to minimize the number of noisy operations. Today, physicists are constantly experimenting with novel devices and architectures. For every new physical substrate and for every modification of a quantum computer, we need to modify or rewrite major pieces of the optimizer to run successful experiments. In this paper, we present *QUESO*, an efficient approach for automatically synthesizing a quantum-circuit optimizer for a given quantum device. For instance, in 1.2 minutes, *QUESO* can synthesize an optimizer with high-probability correctness guarantees for IBM computers that significantly outperforms leading compilers, such as IBM's *Qiskit* and *TKET*, on the majority (85%) of the circuits in a diverse benchmark suite.

A number of theoretical and algorithmic insights underlie *QUESO*: (1) An algebraic approach for representing rewrite rules and their semantics. This facilitates reasoning about complex *symbolic* rewrite rules that are beyond the scope of existing techniques. (2) A fast approach for probabilistically verifying equivalence of quantum circuits by reducing the problem to a special form of *polynomial identity testing*. (3) A novel probabilistic data structure, called a *polynomial identity filter* (PIF), for efficiently synthesizing rewrite rules. (4) A beam-search-based algorithm that efficiently applies the synthesized symbolic rewrite rules to optimize quantum circuits.

CCS Concepts: • **Software and its engineering** → **Compilers**; • **Hardware** → **Quantum computation**.

Additional Key Words and Phrases: quantum computing, probabilistic verification

## ACM Reference Format:

Amanda Xu, Abtin Molavi, Lauren Pick, Swamit Tannu, and Aws Albarghouthi. 2023. Synthesizing Quantum-Circuit Optimizers. *Proc. ACM Program. Lang.* 7, PLDI, Article 140 (June 2023), 70 pages. <https://doi.org/10.1145/3591254>

## 1 INTRODUCTION

The dream of quantum computing has been around for decades, but it is only recently that we have begun to witness promising physical realizations of quantum computers. Quantum computers enable efficient simulation of quantum mechanical phenomena, potentially opening the door to advances in quantum physics, chemistry, material design, and beyond. Near-term quantum computers with several dozens of qubits are expected to operate in a noisy environment without error correction, in a model of computation called *Noisy Intermediate Scale Quantum* (NISQ) computing [Preskill 2018].

Authors' addresses: Amanda Xu, University of Wisconsin-Madison, Madison, WI, USA, [axu44@wisc.edu](mailto:axu44@wisc.edu); Abtin Molavi, University of Wisconsin-Madison, Madison, WI, USA, [amolavi@wisc.edu](mailto:amolavi@wisc.edu); Lauren Pick, University of Wisconsin-Madison, Madison, WI, USA, [lpick2@wisc.edu](mailto:lpick2@wisc.edu); Swamit Tannu, University of Wisconsin-Madison, Madison, WI, USA, [stannu@wisc.edu](mailto:stannu@wisc.edu); Aws Albarghouthi, University of Wisconsin-Madison, Madison, WI, USA, [aws@cs.wisc.edu](mailto:aws@cs.wisc.edu).

Permission to make digital or hard copies of part or all of this work for personal or classroom use is granted without fee provided that copies are not made or distributed for profit or commercial advantage and that copies bear this notice and the full citation on the first page. Copyrights for third-party components of this work must be honored. For all other uses, contact the owner/author(s).

© 2023 Copyright held by the owner/author(s).

2475-1421/2023/6-ART140

<https://doi.org/10.1145/3591254>

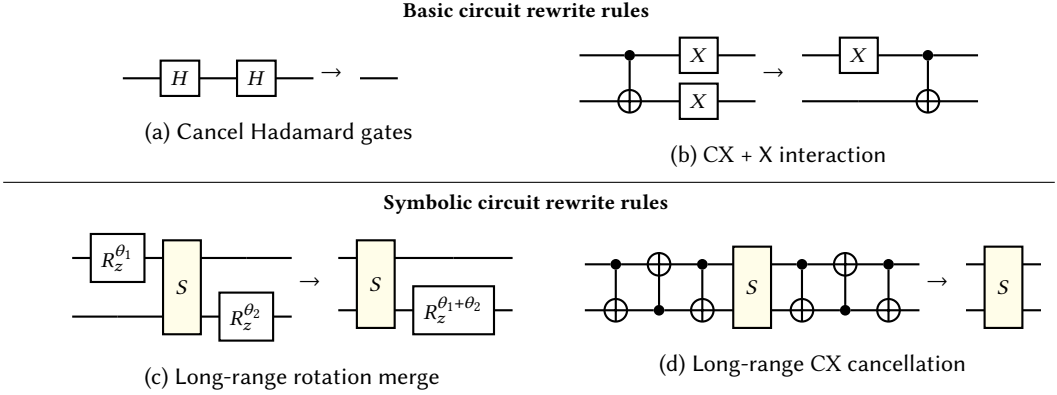


Fig. 1. Some optimizations QUESO can synthesize/verify ( $S$  is a symbolic gate satisfying some constraints)

In NISQ computers, each operation is noisy. Therefore, powerful quantum-circuit optimizers are absolutely crucial: we want to produce smaller circuits that are more tolerant to noise. Without careful optimization, one can easily end up with a circuit whose results are indistinguishable from random noise. However, the state of quantum hardware is in flux. There are so many physical realizations of quantum computers, and physicists are constantly experimenting with new devices and architectures—*neutral atoms, superconducting circuits, semiconductor devices* [Saffman 2019; Watson et al. 2018; Wilen et al. 2021]. **For every new physical substrate and for every modification of a quantum computer, we need to modify or rewrite major pieces of the optimizer to run experiments.** This is a bottleneck in our progress towards a quantum computing future: writing optimizers is a tedious, iterative, heuristic process, and one that is error-prone [Paltenghi and Pradel 2022].

Our goal in this paper is to answer the following question:

*Given a specification of a quantum architecture, can we automatically synthesize an efficient and correct quantum-circuit optimizer?*

Recent developments only partially address this question: The quantum-circuit optimizer, VOQC [Hietala et al. 2021], is manually written with machine-checked correctness proofs, and therefore is not automatically extensible to new quantum architectures. The superoptimizer, Quartz [Xu et al. 2022], automatically synthesizes semantics-preserving circuit rewrite rules; however, it can only synthesize simple rewrite rules and, as a superoptimizer, is heavily dependent on hand-crafted, device-specific optimization passes without which the synthesized rules have little impact.

We present QUESO, a new technique that rapidly synthesizes sophisticated, correct rewrite rules. QUESO then efficiently applies the synthesized rules to optimize quantum circuits. QUESO builds upon four critical ideas: (1) An algebraic approach for representing rewrite rules and their semantics. This allows us to reason about and synthesize complex optimizations beyond the scope of existing techniques. (2) A fast probabilistic verification approach for checking rewrite-rule correctness by reducing the problem to a special form of *polynomial identity testing* and demonstrating that the standard fast randomized algorithm applies. (3) A probabilistic data structure for efficiently synthesizing equivalent pairs of circuits without incurring a quadratic explosion. (4) A beam-search-based algorithm that efficiently applies synthesized rewrite rules to optimize circuits.

**Symbolic rules.** Typically, quantum-circuit optimizers apply a schedule of rewrite rules to shrink a given circuit. In its simplest form, a rewrite rule matches a specific subcircuit and rewrites it into a smaller, equivalent subcircuit. For instance, Fig. 1a shows two equivalent circuits: if we see two

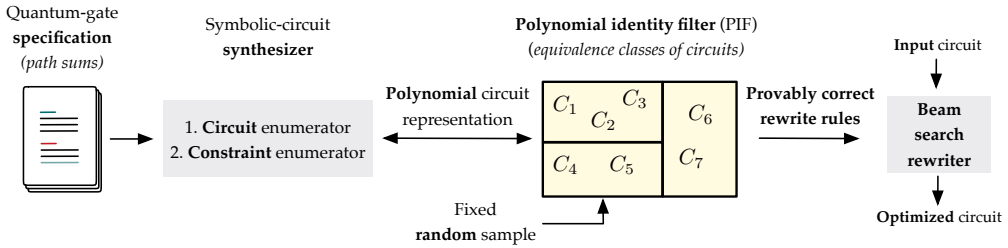


Fig. 2. Overview of the QUESO approach

Hadamard gates ( $H$ ) applied to the same qubit, we can eliminate them because they cancel each other out. Fig. 1b shows a rewrite rule over subcircuits with two qubits.

Automatically synthesizing such rules is relatively simple: enumerate pairs of circuits and verify their equivalence. This approach that has been applied in other domains, e.g., machine learning [Jia et al. 2019], traditional compilers [Sasnauskas et al. 2017], and recently quantum-circuit superoptimization [Xu et al. 2022]. However, there are complex and critical rules that cannot be discovered this way: subcircuits can have parameters, e.g., angles of rotations, or *completely unknown subcircuits*. Thus, we need a *symbolic approach* for reasoning about such rules. For instance, Fig. 1c shows a rewrite rule in which two rotations about the  $z$ -axis on different qubits can be merged into a single rotation, even if they are separated by arbitrarily many operations, denoted  $S$ , so long as  $S$  satisfies certain conditions. We think of  $S$  as an unknown, *symbolic* gate. Similarly, Fig. 1d shows a rule in which two distant sequences of CX gates can be cancelled.

To reason about symbolic circuits and rules, we utilize *path-sum*-based semantics. First introduced by Feynman, path sums compactly capture the semantics of a quantum system as an expression. Intuitively, one can think of a path sum as a transition relation specifying how a quantum system’s state evolves. Indeed, path sums have been used for quantum-circuit verification [Amy 2019; Chareton et al. 2021]. In this paper, we exploit the algebraic nature of path sums to reason about circuits with unknown parameters and unknown subcircuits. By reasoning using path sums, we show that we are able to synthesize *long-range* rules, like Figs. 1c and 1d, that cancel out far-apart quantum gates.

**Probabilistic verification and synthesis.** QUESO synthesizes rewrite rules following the standard synthesize-and-verify story: we enumerate circuits with symbolic components and verify equivalence of pairs of circuits. If two circuits  $C_1$  and  $C_2$  are proven equivalent, then we can soundly rewrite  $C_1$  to  $C_2$  or vice versa. Naïvely following this recipe, of course, does not scale due to the large space of pairs of circuits. Our first, and perhaps most critical, observation is that the equivalence-checking problem for two circuits can be reduced to a *constrained* form of *polynomial identity testing* (PIT)—the problem of checking equivalence of two polynomials—where the constraints are on the domain of the variables. We then demonstrate that this problem can be directly solved by the foundational Schwartz–Zippel randomized algorithm for PIT [Motwani and Raghavan 1995, Ch. 7], which is very fast, because it relies on a single random instantiation of the variables of a polynomial.

With this insight, we present a probabilistic data structure—the *polynomial identity filter* (PIF)—for constructing equivalence classes of circuits. The PIF builds upon the high-probability guarantees of Schwartz–Zippel to eliminate the quadratic explosion of checking equivalence of pairs of circuits. The PIF therefore enables fast construction of rewrite rules from equivalence classes.

**Applying rewrite rules.** Quantum-circuit optimizers, like voqc [Hietala et al. 2021] and TKET [Sivarajah et al. 2020], use a fixed schedule for applying optimizations that is chosen by

the compiler developer. In our setting, however, we synthesize tens of thousands of rules, and we simply cannot ask a developer to experiment with different schedules. We demonstrate that a simple, beam-search-based algorithm can quickly optimize quantum circuits by applying sequences of rewrite rules. The most algorithmically challenging piece is matching symbolic rewrite rules, which can match arbitrarily large subcircuits.

**Evaluation.** We implemented QUESO and used it to synthesize optimizers for four different quantum architectures with different operations (or gate sets)—including IBM, Rigetti, and *ion trap* computers. QUESO can synthesize all rewrite rules in about 2 minutes. Our results demonstrate that QUESO is able to outperform or match handwritten optimizers, like VOQC [Hietala et al. 2021], TKET [Sivarajah et al. 2020], and IBM Qiskit [Aleksandrowicz et al. 2019]. For instance, in 1.2 minutes, QUESO can synthesize an optimizer for IBM computers that significantly outperforms leading compilers, such as IBM’s Qiskit and TKET, on the majority (85%) of the circuits in a diverse benchmark suite, and can outperform or match VOQC on 72% of the benchmarks, outperforming it in 51% of the benchmarks. In comparison to the superoptimizer, Quartz [Xu et al. 2022], we demonstrate (1) that QUESO is radically faster at rule synthesis and (2) the critical importance of symbolic rewrite rules. For instance, on IBM, in a head-to-head comparison of synthesized rules (i.e., excluding any preprocessing), QUESO synthesizes rules an order of magnitude faster than Quartz and outperforms Quartz on 97% of the benchmarks.

**Contributions.** In summary, we make the following contributions:

- A path-sum-based circuit semantics that can compactly capture circuits with unknown, symbolic subcircuits. This enables us to synthesize sophisticated, long-range rewrite rules that are critical for quantum-circuit optimization. (§ 3)
- A fast quantum-circuit equivalence verifier that reduces the problem to a constrained form of polynomial identity testing, which can be solved using a fast randomized algorithm. (§ 4)
- A fast rule synthesizer that uses a novel probabilistic data structure, called *polynomial identity filter* (PIF), to avoid the quadratic explosion of rule enumeration. (§ 5)
- A beam-search-like algorithm that applies symbolic rewrite rules to optimize a circuit. (§ 6)
- A thorough evaluation of QUESO on four quantum architectures. Our results demonstrate that QUESO can outperform or match state-of-the-art optimizers. (§ 7)

## 2 BACKGROUND AND OVERVIEW

### 2.1 Quantum Circuits Background

**Quantum state.** A quantum bit (qubit) can be in state 0 or 1, the *computational basis states*, which are represented by the 2-dimensional vectors  $|0\rangle = \begin{bmatrix} 1 \\ 0 \end{bmatrix}$  and  $|1\rangle = \begin{bmatrix} 0 \\ 1 \end{bmatrix}$ , respectively. A qubit can also be in a linear combination (*superposition*) of the basis states,  $\alpha|0\rangle + \beta|1\rangle = \begin{bmatrix} \alpha \\ \beta \end{bmatrix}$ , where  $\alpha, \beta$  are complex numbers, called the *amplitudes*, such that  $|\alpha|^2 + |\beta|^2 = 1$ . The state of two qubits is a vector of four complex numbers, where each number is the amplitude of one of the basis states,  $|00\rangle, |01\rangle, |10\rangle$ , and  $|11\rangle$ . The state of  $n$  qubits is a vector of  $2^n$  complex numbers.

**Quantum gates.** Quantum operations (or *gates*) transform the state of the qubits of a system. Unlike in Boolean circuits, there are infinitely many possible quantum gate combinations that can be used to produce a *universal* quantum computer—one that can approximate arbitrary *unitary* transformations (the class of state transformations the rules of quantum mechanics admit) to arbitrary precision. Because of a variety of engineering challenges, different quantum computers provide different gate sets. We give examples of some standard gates below.

A classical gate like NOT (denoted  $X$ ) can be applied to a single qubit. If the qubit state is  $|0\rangle$ , it becomes  $|1\rangle$ , and vice versa, just like on a classical circuit. However, if the state of the qubit is a

superposition  $\alpha |0\rangle + \beta |1\rangle$ , applying  $X$  results in the state  $\beta |0\rangle + \alpha |1\rangle$ , i.e., swaps the amplitudes. The *Hadamard* gate, denoted  $H$ , takes a qubit from a basis state and puts it in superposition; for example, given the basis state  $|0\rangle$ , applying  $H$  results in  $\frac{1}{\sqrt{2}} |0\rangle + \frac{1}{\sqrt{2}} |1\rangle$ .

**Path sums.** Since quantum operations are *linear* transformations, they are represented uniquely by how they transform the basis states. We use the traditional *path-sum* notation [Amy 2019], which can be seen as a compact representation of a state-transition relation. For example, the path-sum representation of the  $X$ ,  $H$ , and  $R_z$  gates are defined as follows:

$$X : |x\rangle \rightarrow |\neg x\rangle \quad H : |x\rangle \rightarrow \frac{1}{\sqrt{2}} \sum_{y \in \{0,1\}} e^{i\pi xy} |y\rangle \quad R_z^\theta : |x\rangle \rightarrow e^{i(2x-1)\theta} |x\rangle$$

These are read as follows: Applying gate  $X$  to basis state  $|x\rangle$  results in the state  $|\neg x\rangle$ ; applying  $H$  to  $|x\rangle$  results in the state  $\frac{1}{\sqrt{2}} |0\rangle + \frac{1}{\sqrt{2}} e^{i\pi x} |1\rangle$ . The  $R_z$  gate is parameterized by an angle  $\theta$ , and only changes the amplitude of a given basis state. The *controlled*  $X$  (CX) gate can *entangle* two qubits, a critical operation in quantum computing:  $|x_1 x_2\rangle \rightarrow |x_1(x_1 \oplus x_2)\rangle$ . Given a basis state  $|x_1 x_2\rangle$ , CX produces the basis state  $|x_1(x_1 \oplus x_2)\rangle$ , where  $\oplus$  is XOR.

**Quantum circuits.** Quantum circuits are combinations of quantum gates. Consider the circuit in Fig. 3 (left) over two qubits,  $x_1$  and  $x_2$ , represented by the two horizontal wires. The circuit is read from left to right. The first gate is a CX gate applied to the two qubits. Then, an  $X$  gate and an  $R_z^{\pi/2}$  gate are applied to  $x_1$  and  $x_2$  in parallel.

We will use a linear representation of the circuit as a sequence of gates—Fig. 3 (right). Since  $X$  and  $R_z$  are applied in parallel to two different qubits, we can safely swap them in the linear representation. The semantics of the circuit can be represented in path-sum notation by *composing* the path-sum representation of the constituent gates.

**Executing circuits on hardware.** On quantum hardware, operations are imperfect and prone to errors. Typically, quantum computers provide single- and two-qubit gates, which are optimized to minimize errors. Despite these optimizations, the average single-qubit

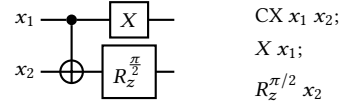


Fig. 3. Circuit and its linear representation

gate error rate is about 0.1%, while the two-qubit gate error is about 10-100x higher on most industrial quantum computers [IBM 2022; Quantum-AI 2021]. Therefore, to minimize circuit error rate, we need to eliminate as many two-qubit gates as possible, which not only corrupt the qubits involved in the operation, but also impose *crosstalk* errors on neighboring qubit devices, significantly degrading circuit reliability. See Appendix A for more details on hardware and errors.

## 2.2 Overview of QUESO

**High-level view.** Fig. 2 provides a high-level illustration of QUESO. First, the user provides a specification of the gate set of some quantum architecture, e.g., IBM's gate set, in the form of path sums. Then, a synthesis algorithm starts enumerating (symbolic) circuits along with constraints on the symbolic components. All circuits are inserted into a probabilistic data structure—the polynomial identity filter—which groups circuits into correct equivalence classes with high-probability guarantees. Finally, we construct rewrite rules from equivalent pairs of circuits and apply them following a beam-search-based algorithm to optimize a given circuit. We illustrate these pieces with examples.

**Example A.** Let us consider the rewrite rule in Fig. 1c. The two circuits on either side of the rule have three unknowns: the rotation angles,  $\theta_1$  and  $\theta_2$ , and the highlighted gate  $S$ . Our synthesis algorithm enumerates such circuits in order to discover equivalent pairs of circuits. However, in our

example, the gate  $S$  is completely unconstrained—we know nothing about it. We call  $S$  a *symbolic gate*. Therefore, QUESO needs to answer the following *abduction* question:

*Under what conditions on  $S$  are the two circuits equivalent?*

For this specific example, QUESO abduces the following constraint on  $S$ :

$$S : |x_1x_2 \dots\rangle \rightarrow \phi(x_1x_2 \dots) |x_2x_1 \dots\rangle$$

In other words, all we need to know about  $S$  for these two circuits to be equivalent is that  $S$  swaps the values of  $x_1$  and  $x_2$ . Note that  $S$  is allowed to change the amplitudes (denoted by an unconstrained function  $\phi$ , called the *amplitude transformer*) and may even apply gates to other qubits (denoted by the  $\dots$ ).

**Example B.** Fig. 1d shows another rewrite rule that QUESO can synthesize. This rewrite rule cancels two distant sequences of CX gates, separated by a symbolic gate  $S$ . QUESO abduces the following constraint on  $S$ .

$$S : |x_1x_2 \dots\rangle \rightarrow \phi(x_1x_2 \dots) |x_1x_2 \dots\rangle$$

Informally,  $S$  may change the amplitudes but should not change the first two bits of the state,  $x_1x_2$ .

**Proving equivalence.** To prove equivalence of two circuits, we observe that we can reduce the problem to a constrained form of *polynomial identity testing* (PIT), the problem of checking equivalence of two polynomials. Specifically, the amplitudes of every basis state will be represented as a polynomial over the complex field. In Example A, the polynomials describing the amplitudes will be over the variables  $\theta_1, \theta_2$ , and the function  $\phi$  (from the constraint on  $S$ ).

We show that our constrained PIT problem can be solved with the standard randomized algorithm—following the Schwartz–Zippel lemma [Motwani and Raghavan 1995]. Simply, randomly sample values for the variables and check if the two polynomials evaluate to the same value. If they do not, then we have a counterexample; if they do, then we have a high-probability guarantee that the polynomials are equivalent.

To give some intuition, for Example A (Fig. 1c), the amplitudes of the basis state  $|11\rangle$  for the left and right circuits are as follows (a full derivation is shown in Example 3.9):

$$e^{i\theta_1} \cdot \phi(11) \cdot e^{i\theta_2} = \phi(11) \cdot e^{i(\theta_1+\theta_2)}$$

where  $\phi$  is the unknown amplitude transformer of  $S$ . While these two expressions are clearly equivalent, it is not always immediate, and one generally requires algebraic manipulation to prove equivalence. Further, these two expressions are not polynomials. Luckily, as we show in § 4, we demonstrate that we can treat the above expressions as a special form of polynomials over the complex field and use Schwartz–Zippel to show their equivalence. Specifically,  $\phi(11)$  can be viewed as a complex variable and terms of the form  $e^{i\cdot}$  as complex variables *constrained* to the unit circle.

**Efficient synthesis.** To synthesize rewrite rules, we can simply enumerate pairs of circuits, abduce constraints, and verify their equivalence. But this blows up quadratically—say there are 1 million circuits, then we will need to consider  $10^{12}$  pairs.

To avoid the quadratic explosion we present a simple and efficient probabilistic data structure, the *polynomial identity filter* (PIF). The PIF takes a set of polynomials and returns a set of equivalence classes. The key idea underlying the PIF is that we can use a single random valuation of variables to evaluate each circuit’s polynomial representation, and store circuits with equal valuations in the same equivalence class. Using the guarantees of Schwartz–Zippel, the PIF data structure ensures that all of its equivalence classes are correct with a high probability (Thm. 5.1). From the generated equivalence classes, we construct a set of rewrite rules like those shown in Fig. 1.

**Applying rules.** Given a set of rewrite rules, QUESO uses a beam search approach to traverse the space of rewrite sequences and optimize the circuit by minimizing the number of gates. The



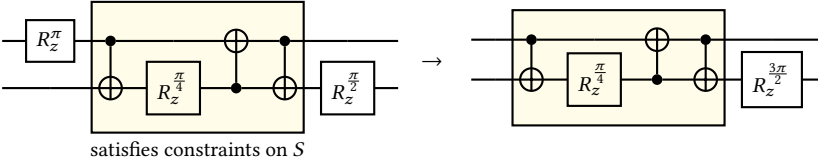


Fig. 4. Application of the long-range rotation merge optimization from Fig. 1c.

main challenge that QUESO addresses is a generic algorithm for applying symbolic rewrite rules. Specifically, it needs to discover a subcircuit that satisfies the constraints on the symbolic gate  $S$  in our examples. Fig. 4 demonstrates an application of the long-range rotation merge rule (Fig. 1c) to a circuit. The highlighted part of the circuit satisfies the constraints on the symbolic gate  $S$ , namely, the path-sum representation of the highlighted subcircuit is of the form  $|x_1 x_2 \dots\rangle \rightarrow \phi(x_1 x_2) |x_2 x_1 \dots\rangle$ .

### 3 PATH-SUM-BASED CIRCUIT SEMANTICS

We now formally define (symbolic) quantum circuits and their semantics using *path sums*. Our semantics is a direct adaptation of that of Amy [2019]. The novelty in this section is defining circuits with unknown, symbolic gates and what it means for such circuits to be equivalent (§ 3.3).

#### 3.1 States, Gates, and Path Sums

**Quantum states.** The state of a qubit is a linear combination of the computational basis states,  $|0\rangle$  and  $|1\rangle$ , written  $\alpha|0\rangle + \beta|1\rangle$ , where  $\alpha, \beta \in \mathbb{C}$ . The state of  $n$  qubits is a term of the form  $\sum_{\mathbf{x} \in \mathbb{Z}_2^n} \alpha_{\mathbf{x}} |\mathbf{x}\rangle$ , where  $\mathbb{Z}_2^n$  is the set of  $n$ -bit vectors and  $\alpha_{\mathbf{x}} \in \mathbb{C}$ . For bit vector  $\mathbf{x}$ , we use  $x_i$  to denote the  $i$ th bit of  $\mathbf{x}$ .

**Gates and path sums.** We consider two kinds of quantum gates, single- and multi-qubit gates. We will use  $G^\rho$  to denote a gate that takes a parameter  $\rho \in \mathbb{C}$  (e.g., angle of rotation), or simply  $G$  if the gate does not take parameters. For simplicity, we assume that gates have at most 1 parameter.

The semantics of a gate are defined in *path-sum* notation [Amy 2019] which shows how a gate transforms a basis state. From a verification perspective, a path sum is an expression defining the *transition relation*. Specifically, a single-qubit gate  $G^\rho$  is defined in the following fashion:

$$|x\rangle \rightarrow \sum_{y \in \mathbb{Z}_2} \phi(x, y, \rho) |f(x, y)\rangle \quad (1)$$

This path-sum specification says that for any basis state  $|x\rangle$ , applying  $G^\rho$  to  $|x\rangle$  transforms the state into  $\sum_{y \in \mathbb{Z}_2} \phi(x, y, \rho) |f(x, y)\rangle$ , where

- $\phi \in \mathbb{Z}_2 \times \mathbb{Z}_2 \times \mathbb{C} \rightarrow \mathbb{C}$  is the *amplitude transformer*, and
- $f \in \mathbb{Z}_2 \times \mathbb{Z}_2 \rightarrow \mathbb{Z}_2$  is the *state transformer*.

*Example 3.1.* For Hadamard  $H : |x\rangle \rightarrow \sum_{y \in \{0,1\}} \frac{1}{\sqrt{2}} e^{i\pi x y} |y\rangle$ ,  $\phi(x, y) = \frac{1}{\sqrt{2}} e^{i\pi x y}$  and  $f(x, y) = y$ .

**$n$ -qubit gates.**  $n$ -qubit gates are analogously defined; a gate  $G^\rho$  has a path sum of the form

$$|\mathbf{x}\rangle \rightarrow \sum_{\mathbf{y} \in \mathbb{Z}_2^n} \phi(\mathbf{x}, \mathbf{y}, \rho) |f(\mathbf{x}, \mathbf{y})\rangle$$

where  $\phi \in \mathbb{Z}_2^n \times \mathbb{Z}_2^n \times \mathbb{C} \rightarrow \mathbb{C}$  and  $f \in \mathbb{Z}_2^n \times \mathbb{Z}_2^n \rightarrow \mathbb{Z}_2^n$ . We write  $f(\mathbf{x}, \mathbf{y})_i$  for the  $i$ th bit of  $f(\mathbf{x}, \mathbf{y})$ .

**Monomial gates.** Some gates do not transform a basis state into *superposition* (non-trivial linear combination of basis states), and therefore their path-sums can be simplified as follows:

$$|\mathbf{x}\rangle \rightarrow \phi(\mathbf{x}, \rho) |f(\mathbf{x})\rangle$$

We call such gates *monomial* gates because their matrix representation is a monomial matrix (or a generalized permutation matrix). E.g., CX is a monomial gate with path sum  $|x_1 x_2\rangle \rightarrow |x_1 (x_1 \oplus x_2)\rangle$ .

$$\begin{aligned}
\llbracket G^\rho \rrbracket &\equiv \sum_{y \in \mathbb{Z}_2} \phi(x, y, \rho) |f(x, y)\rangle \\
\llbracket G^\rho i \rrbracket &\equiv \sum_{y \in \mathbb{Z}_2} \phi(x_i, y, \rho) |x_1 \dots x_{i-1} f(x, y) x_{i+1} \dots x_n\rangle \\
\llbracket C_1^\rho \rrbracket &\equiv \sum_{y_1 \in \mathbb{Z}_2^n} \phi_1(\mathbf{x}, y_1, \rho) |f_1(\mathbf{x}, y_1)\rangle & \llbracket C_2^\rho \rrbracket &\equiv \sum_{y_2 \in \mathbb{Z}_2^n} \phi_2(\mathbf{x}, y_2, \rho) |f_2(\mathbf{x}, y_2)\rangle \\
\llbracket C_1^\rho; C_2^\rho \rrbracket &\equiv \sum_{y_1 \in \mathbb{Z}_2^n} \phi_1(\mathbf{x}, y_1, \rho) (\llbracket C_2^\rho \rrbracket [x \leftarrow f_1(\mathbf{x}, y_1)])
\end{aligned}$$

EXTEND  
SEQ

Fig. 5. Path sum circuit semantics.  $\llbracket C_2^\rho \rrbracket [x \leftarrow f_1(\mathbf{x}, y)]$  is  $\llbracket C_2^\rho \rrbracket$  with every instance of  $\mathbf{x}$  replaced by  $f_1(\mathbf{x}, y)$ .

**Path sums are expressions.** Observe how the right-hand side of  $\rightarrow$  in a path sum is an expression of a quantum state parameterized by two variables,  $\mathbf{x}$  and  $\rho$ . Henceforth, for a gate  $G^\rho$ , we shall use  $\llbracket G^\rho \rrbracket$  to denote the expression on the right-hand side of its path sum.

*Example 3.2.*  $\llbracket H \rrbracket$  is  $\sum_{y \in \{0,1\}} \frac{1}{\sqrt{2}} e^{i\pi xy} |y\rangle$ .

We will use the notation  $\llbracket C_1^\rho \rrbracket \equiv \llbracket C_2^\rho \rrbracket$  to denote that  $\forall \mathbf{x}, \rho, \llbracket C_1^\rho \rrbracket = \llbracket C_2^\rho \rrbracket$ . In other words, the two path sums define the same quantum state for every valuation of the variables  $\mathbf{x}$  and  $\rho$ .

### 3.2 Circuit Semantics

**Circuits.** A quantum circuit over  $n$  qubits is a sequence of gates. Without loss of generality, we restrict ourselves to one- and two-qubit gates. We will write  $G^\rho i$  to denote the single-qubit gate  $G^\rho$  applied to the  $i$ th qubit, and  $G^\rho i j$  to denote the two-qubit gate  $G^\rho$  applied to the  $i$ th and  $j$ th qubits. A circuit  $C$  is defined by the following grammar:

$$C := G^\rho i \mid G^\rho i j \mid C_1; C_2 \quad (2)$$

where  $i, j \in [1, n]$ . We will use  $C^\rho$  to denote that the circuit has a number of parameters, a vector  $\rho$  containing the parameters of the circuit's constituent gates.

**Semantics of circuits.** The path-sum representation of a circuit  $\llbracket C^\rho \rrbracket$  follows the grammar recursively: Either it is the path sum of a single gate,  $\llbracket G^\rho i \rrbracket$  or  $\llbracket G^\rho i j \rrbracket$ , or the composition of the path sums of two circuits,  $\llbracket C_1; C_2 \rrbracket$ . See Fig. 5 for the definitions.

Consider the rule EXTEND in Fig. 5. Given a single-qubit  $G^\rho$  gate, EXTEND defines the path sum to denote that  $G^\rho$  is applied to the  $i$ th qubit of an  $n$ -qubit system. Intuitively, the state transformer of  $G^\rho i$  modifies the  $i$ th qubit, leaving the rest intact. EXTEND for two-qubit gates is analogous.

*Example 3.3.* Recall the Hadamard gate, where  $\llbracket H \rrbracket$  is  $\sum_{y \in \{0,1\}} \frac{1}{\sqrt{2}} e^{i\pi xy} |y\rangle$ . Following the EXTEND rule,  $\llbracket H i \rrbracket$  is  $\sum_{y \in \{0,1\}} \frac{1}{\sqrt{2}} e^{i\pi x_i y} |x_1 \dots x_{i-1} y x_{i+1} \dots x_n\rangle$ .

The rule SEQ defines the semantics of composition. Informally, composing two path sums stitches together the “final basis states” of the first with the “initial basis states” of the second.

*Example 3.4.* Consider  $\llbracket H \rrbracket$  and  $\llbracket R_z^\theta \rrbracket$ , which are  $\sum_{y \in \{0,1\}} \frac{1}{\sqrt{2}} e^{i\pi xy} |y\rangle$  and  $e^{i(2x-1)\theta} |x\rangle$ , respectively. For the single-qubit circuit  $H; R_z^\theta$ ,  $\llbracket H; R_z^\theta \rrbracket$  is the following:  $\sum_{y \in \{0,1\}} \frac{1}{\sqrt{2}} e^{i\pi xy} \underbrace{e^{i(2y-1)\theta} |y\rangle}_{\llbracket R_z^\theta \rrbracket [x \leftarrow y]}$ .

**Circuit equivalence.** Two circuits are equivalent if they have equivalent path sums.

*Definition 3.5 (Circuit equivalence).* Consider two circuits  $C_1^\rho$  and  $C_2^\rho$  over the same set of parameters,  $\rho$ . We say that the two circuits are equivalent iff  $\llbracket C_1^\rho \rrbracket \equiv \llbracket C_2^\rho \rrbracket$ .



*Example 3.6.* Consider the two equivalent single-qubit circuits,  $R_z^{\theta_1}; R_z^{\theta_2}$  and  $R_z^{\theta_1+\theta_2}$ , We have

$$\llbracket R_z^{\theta_1}; R_z^{\theta_2} \rrbracket \equiv e^{i(2x-1)\theta_1} e^{i(2x-1)\theta_2} |x\rangle \quad \llbracket R_z^{\theta_1+\theta_2} \rrbracket \equiv e^{i(2x-1)(\theta_1+\theta_2)} |x\rangle$$

It is easy to see that for any values of  $x$  and the parameters  $\theta_1$  and  $\theta_2$ , we have  $\llbracket R_z^{\theta_1}; R_z^{\theta_2} \rrbracket = \llbracket R_z^{\theta_1+\theta_2} \rrbracket$ .

### 3.3 Symbolic Circuits

**Symbolic gates.** We will often use unknown gates in a circuit. We will treat those *symbolic gates* as path sums where the amplitude and state transformers are undefined (or *uninterpreted*). We will use  $S$  to refer to a symbolic gate, where  $\llbracket S \rrbracket$  is of the form:

$$\phi^u(\mathbf{x}) |f^u(\mathbf{x})\rangle \quad (3)$$

where  $\phi^u$  and  $f^u$  are uninterpreted. Observe that  $S$  is a monomial gate; this practical assumption helps us restrict the space of interpretations of the state transformers.

**Symbolic circuits.** When a circuit uses a symbolic gate, we will call it a *symbolic circuit*. Given two symbolic circuits, ideally, we would like to discover constraints on the uninterpreted amplitude and state transformers under which the two circuits are equivalent. We simplify this problem and only consider constraints on state transformers,  $f^u$ , treating the amplitude transformers,  $\phi^u$ , as parameters of the circuit. The simplification is due to the fact that there are finitely many possible constraints on the Boolean function,  $f^u$ , while it is challenging to discover constraints on the complex-valued transformer,  $\phi^u$ .

**Interpretations of state transformers.** We will use  $I$  to denote an interpretation of the uninterpreted state transformers in a symbolic circuit  $C$ . We will use  $C(I)$  to denote  $C$  with all uninterpreted state transformers of symbolic gates replaced with their interpretation in  $I$ .

*Example 3.7.* Consider the symbolic gate  $S$  where  $\llbracket S \rrbracket \equiv \phi^u(\mathbf{x}) |f^u(\mathbf{x})\rangle$ . Let the interpretation  $I$  set  $f^u(\mathbf{x})$  to the identity function. Then,  $\llbracket S(I) \rrbracket \equiv \phi^u(\mathbf{x}) |x\rangle$ .

*Definition 3.8 (Unifying interpretations).* Consider two symbolic circuits  $C_1^P$  and  $C_2^P$  that use the same symbolic gates with amplitude transformers  $\phi_1^u, \dots, \phi_k^u$ . We say that  $I$  is a *unifying interpretation* of the two circuits if

$$\forall \phi_1^u, \dots, \phi_k^u, \mathbf{x}, \rho. \llbracket C_1^P(I) \rrbracket = \llbracket C_2^P(I) \rrbracket. \quad (4)$$

Intuitively, a unifying interpretation  $I$  creates two circuits that are equivalent, following Definition 3.5. The idea is that we can treat the amplitude transformers as if they are circuit parameters.

*Example 3.9.* Recall the two circuits in Fig. 1c; call them  $C_1$  and  $C_2$ . We have

$$\llbracket C_1 \rrbracket \equiv e^{i(2x_1-1)\theta_1} \cdot \phi^u(\mathbf{x}) \cdot e^{i(2f^u(\mathbf{x})_2-1)\theta_2} |x\rangle \quad \llbracket C_2 \rrbracket \equiv \phi^u(\mathbf{x}) \cdot e^{i(2f^u(\mathbf{x})_2-1)(\theta_1+\theta_2)} |x\rangle$$

Consider the unifying interpretation  $I$  where  $f^u(x_1x_2) = x_2x_1$ .

$$\llbracket C_1(I) \rrbracket \equiv e^{i(2x_1-1)\theta_1} \cdot \phi^u(\mathbf{x}) \cdot e^{i(2x_1-1)\theta_2} |x\rangle \quad \llbracket C_2(I) \rrbracket \equiv \phi^u(\mathbf{x}) \cdot e^{i(2x_1-1)(\theta_1+\theta_2)} |x\rangle$$

Observe that  $\llbracket C_1(I) \rrbracket \equiv \llbracket C_2(I) \rrbracket$ . However, e.g.,  $f^u(x_1x_2) = x_1x_2$  is *not* a unifying interpretation.

## 4 CIRCUIT EQUIVALENCE VERIFIER

We now present a fast approach for probabilistically verifying equivalence of two circuits, which will be key for synthesizing rewrite rules. We reduce the problem to a constrained form of *polynomial identity testing* (PIT), and demonstrate that it can be solved using a standard randomized algorithm for checking equivalence of polynomials. We begin with the foundations of polynomial identity testing.

#### 4.1 Polynomial Identity Testing & Schwartz–Zippel

We are given two polynomials  $p_1$  and  $p_2$  over the same set of  $n$  complex-valued variables. We want to check if  $p_1(\mathbf{v}) = p_2(\mathbf{v})$  for all values of  $\mathbf{v} \in \mathbb{C}^n$ , concisely denoted as  $p_1 = p_2$ . We will use  $d$  to denote the maximum degree of the two polynomials.

We can verify equivalence of  $p_1$  and  $p_2$  with high probability as follows.

- (1) Let  $R \subset \mathbb{C}$  be a finite subset of the complex numbers.
- (2) Sample  $n$  independent values,  $\alpha_1, \dots, \alpha_n$ , from the uniform distribution over  $R$ .
- (3) Return True if  $p_1(\boldsymbol{\alpha}) = p_2(\boldsymbol{\alpha})$ ; otherwise, return False.

The correctness of the above algorithm directly follows from the Schwartz–Zippel lemma [Motwani and Raghavan 1995, Ch. 7], which we adapt to our purposes here:

**THEOREM 4.1.** *If  $p_1 = p_2$ , the algorithm returns True. If  $p_1 \neq p_2$ , the algorithm returns True (false positive) with probability at most  $d/|R|$  (conversely, the algorithm returns False with probability at least  $1 - d/|R|$ ).*

**PROOF.** First case ( $p_1 = p_2$ ): the algorithm returns True since for any  $\boldsymbol{\alpha}$  we have  $p_1(\boldsymbol{\alpha}) = p_2(\boldsymbol{\alpha})$ . Second case ( $p_1 \neq p_2$ ): The Schwartz–Zippel lemma says that if we sample  $\alpha_1, \dots, \alpha_n$  independently and uniformly from the finite set  $R$ , the probability that  $p_1(\boldsymbol{\alpha}) = p_2(\boldsymbol{\alpha})$  is at most  $d/|R|$ .  $\square$

Observe that the algorithm has a small probability of a false positive: If the algorithm returns False, then we know that  $p_1 \neq p_2$ , since  $\boldsymbol{\alpha}$  serves as a counterexample to equivalence. However, given  $p_1 \neq p_2$ , the algorithm may return the wrong answer (True) with a small probability. The probability of failure  $d/|R|$  can be made arbitrarily small by sampling from a larger finite domain  $R$ .

*Example 4.2.* Suppose  $p_1$  and  $p_2$  are inequivalent, degree 10 polynomials. If we take  $R$  to be the set of 64-bit integers, we will have a failure probability on the order of  $10^{-19}$ .

**Constrained identity testing.** A nice property of PIT is that we can readily apply it to checking equivalence of two polynomials under the constraint that *some* variables have a restricted domain in  $\mathbb{C}$ . This is critical in our setting, since we will have variables constrained to the unit circle, denoted  $\mathbb{S} = \{c \in \mathbb{C} \mid |c| = 1\}$ . Specifically, say we want to prove the following:

$$p_1(\mathbf{u}, \mathbf{v}) = p_2(\mathbf{u}, \mathbf{v}) \text{ for all } \mathbf{u} \in \mathbb{C}^n \text{ and } \mathbf{v} \in Z^m, \text{ where } Z \subset \mathbb{C} \quad (5)$$

Then, we can simply apply PIT by using a finite sample space  $R \subseteq Z$ .

**COROLLARY 4.3 (CONSTRAINED PIT).** *Consider Eq. (5). Apply PIT to check  $p_1 = p_2$  with  $R \subseteq Z$ . If for all  $\mathbf{u} \in \mathbb{C}^n$  and  $\mathbf{v} \in Z^m$  we have  $p_1(\mathbf{u}, \mathbf{v}) = p_2(\mathbf{u}, \mathbf{v})$ , the algorithm returns True. Otherwise, if there exists  $\mathbf{u} \in \mathbb{C}^n$  and  $\mathbf{v} \in Z^m$  such that  $p_1(\mathbf{u}, \mathbf{v}) \neq p_2(\mathbf{u}, \mathbf{v})$ , the algorithm returns True with probability at most  $d/|R|$ .*

**PROOF.** First case ( $p_1 = p_2$ ): The algorithm will correctly return True because it samples each  $\alpha_i$  from  $R \subseteq Z \subset \mathbb{C}$ , and we know from Eq. (5) that  $p_1(\mathbf{u}, \mathbf{v}) = p_2(\mathbf{u}, \mathbf{v})$  for all  $\mathbf{u} \in \mathbb{C}^n$  and  $\mathbf{v} \in Z^m$ . Second case ( $p_1 \neq p_2$ ): following Schwartz–Zippel (Thm. 4.1), the algorithm returns True with probability  $\leq d/|R|$ .  $\square$

Observe how in the case the algorithm correctly returns True, you actually get a more general result than needed—a probabilistic guarantee that  $p_1 = p_2$  with no constraints on the  $\mathbf{v}$  variables.

## 4.2 Circuit-Equivalence Verification as Constrained Identity Testing

To prove equivalence of two circuits, we will check the equivalence of their amplitudes for every input basis state. While there are exponentially many amplitudes in the number of qubits, for synthesizing rewrite rules, we only care about circuits with a relatively small number of qubits, and so we do not suffer an exponential explosion. We will demonstrate that amplitude expressions are *constrained* polynomials, and therefore reduce the equivalence problem to PIT.

The following approach works for symbolic and non-symbolic pairs of circuits, under the assumption that all state transformers are interpreted. For simplicity, we assume that uninterpreted amplitude transformers are part of the circuit parameters.

**Amplitude equivalence.** Consider two circuits  $C_1^\rho$  and  $C_2^\rho$ . Fix a constant  $\mathbf{a} \in \mathbb{Z}_2^n$ , which we will use as the initial basis state. We can write  $\llbracket C_1^\rho \rrbracket[\mathbf{x} \leftarrow \mathbf{a}]$  and  $\llbracket C_2^\rho \rrbracket[\mathbf{x} \leftarrow \mathbf{a}]$  as follows:

$$\sum_{\mathbf{y} \in \mathbb{Z}_2^n} \psi_1^{\mathbf{a}}(\mathbf{y}, \rho) |y\rangle \qquad \sum_{\mathbf{y} \in \mathbb{Z}_2^n} \psi_2^{\mathbf{a}}(\mathbf{y}, \rho) |y\rangle$$

Intuitively,  $\psi_1^{\mathbf{a}}(\mathbf{y}, \rho)$  is an expression of the amplitude of basis state  $y$  if we apply  $C_1^\rho$  to state  $|\mathbf{a}\rangle$ .

*Example 4.4.* From Example 3.4,  $\llbracket H; R_z^\theta \rrbracket$  is  $\sum_{y \in \{0,1\}} \underbrace{\frac{1}{\sqrt{2}} e^{i\pi x y} e^{i(2y-1)\theta}}_{\psi^x(y,\theta)} |y\rangle$ .

The following lemma reframes circuit equivalence as checking the equality of amplitudes:

LEMMA 4.5.  $C_1^\rho$  and  $C_2^\rho$  are equivalent iff for all  $\mathbf{x}, \mathbf{y}$ , and  $\rho$ ,  $\psi_1^{\mathbf{x}}(\mathbf{y}, \rho) = \psi_2^{\mathbf{x}}(\mathbf{y}, \rho)$ .

We can eliminate the universal quantifier over  $\mathbf{x}$  and  $\mathbf{y}$  in Lem. 4.5 by turning it into a finite summation, following the basic arithmetic fact:

$$\text{If } \alpha = \beta \text{ and } \alpha' = \beta', \text{ then } z\alpha + z'\alpha' = z\beta + z'\beta' \text{ for all } z, z'.$$

THEOREM 4.6. For every  $\mathbf{a}, \mathbf{b} \in \mathbb{Z}_2^n$ , create a fresh complex-valued variable  $v_{\mathbf{a},\mathbf{b}}$ . Then,  $C_1^\rho$  and  $C_2^\rho$  are equivalent iff for all values of the parameters  $\rho$  and the fresh variables,

$$\sum_{\mathbf{a}, \mathbf{b} \in \mathbb{Z}_2^n} v_{\mathbf{a},\mathbf{b}} \cdot \psi_1^{\mathbf{a}}(\mathbf{b}, \rho) = \sum_{\mathbf{a}, \mathbf{b} \in \mathbb{Z}_2^n} v_{\mathbf{a},\mathbf{b}} \cdot \psi_2^{\mathbf{a}}(\mathbf{b}, \rho) \quad (6)$$

Observe that Eq. (6) is only over the freshly introduced ( $v$ ) variables and the parameters  $\rho$ .

*Example 4.7.* Continuing Example 4.4, if  $H; R_z^\theta$  is circuit  $C_1$  in Thm. 4.6, then the left-hand side of Eq. (6) will be  $\sum_{\mathbf{a}, \mathbf{b}} v_{\mathbf{a},\mathbf{b}} \underbrace{\frac{1}{\sqrt{2}} e^{i\pi \mathbf{a} \mathbf{b}} e^{i(2\mathbf{b}-1)\theta}}_{\psi^{\mathbf{a}}(\mathbf{b},\theta)} |b\rangle$ . After expanding:

$$\left( v_{0,0} \cdot \frac{1}{\sqrt{2}} \cdot e^{-i\theta} \right) + \left( v_{0,1} \cdot \frac{1}{\sqrt{2}} \cdot e^{i\theta} \right) + \left( v_{1,0} \cdot \frac{1}{\sqrt{2}} \cdot e^{-i\theta} \right) + \left( v_{1,1} \cdot \frac{e^{i\pi}}{\sqrt{2}} \cdot e^{i\theta} \right)$$

**Amplitudes are polynomials.** We make the observation that for all quantum gates of interest, the two sides of Eq. (6) can be reduced to constrained polynomials. Therefore, we can reduce checking Eq. (6) to constrained PIT. Specifically, each side of Eq. (6) can be written in the form

$$\sum_j c_j \prod_k t_k$$

where  $c_j$  is a constant and  $t_k$  is a term that can have three different forms:

- (1) variables  $v_{a,b}$ , introduced in Thm. 4.6,
- (2)  $(\phi^u(\mathbf{a}, \mathbf{b}))^n$ , where  $n \in \mathbb{N}$ ,
- (3) or  $(e^{i\theta})^n$ , where  $\theta$  is a parameter of the circuit and  $n \in \mathbb{Z}$ .

Observe therefore that Eq. (6) very much resembles a polynomial over complex variables, but only one of the three kinds of terms  $t_k$  is a complex variable ( $v_{a,b}$ ). We now show how to transform the rest of the terms into complex variables.

- First, applications of amplitude transformers,  $\phi^u(\mathbf{a}, \mathbf{b})$ , of symbolic gates. Since the domain of  $\phi^u$  is finite, we replace each application of the form  $\phi^u(\mathbf{a}, \mathbf{b})$  with a complex variable  $\phi_{a,b}^u$ .
- Second, terms of the form  $e^{i\theta}$ , which come from the gates in the circuit. Note that  $e^{i\theta}$  is a point on the complex unit circle,  $\mathbb{S}$ , parameterized by the angle  $\theta$ . Therefore, for every unique term  $e^{i\theta}$ , we replace  $e^{i\theta}$  with a complex-valued variable  $v_\theta$  and constrain it to  $\mathbb{S}$ .<sup>1</sup>

The above transformation reduces the problem in Thm. 4.6 to constrained PIT, which can be solved using Schwartz–Zippel (Cor. 4.3).

**THEOREM 4.8 (REDUCTION TO CONSTRAINED PIT).** *In the context of Thm. 4.6, assume that Eq. (6) has  $k$  unique terms of the form  $e^{i\theta_1}, \dots, e^{i\theta_k}$ . Apply the above transformation to Eq. (6) and let  $p_1 = p_2$  be the resulting equality. Then,  $C_1^P$  is equivalent to  $C_2^P$  iff  $p_1 = p_2$  under the constraint that  $v_{\theta_1}, \dots, v_{\theta_k} \in \mathbb{S}$ .*

*Example 4.9.* Suppose we want to check the following equality:  $e^{i\theta_1} \cdot \phi^u(00) \cdot e^{i\theta_2} = 0$ . We transform  $\phi^u(00)$  into a fresh variable  $\phi_{00}^u$  and  $e^{i\theta_1}$  and  $e^{i\theta_2}$  into  $v_{\theta_1}$  and  $v_{\theta_2}$ , respectively. This results in the following constrained PIT problem:  $v_{\theta_1} \cdot \phi_{00}^u \cdot v_{\theta_2} = 0$ , for all  $v_{\theta_1}, v_{\theta_2} \in \mathbb{S}$  and  $\phi_{00}^u \in \mathbb{C}$ .

## 5 REWRITE-RULE SYNTHESIZER

We now present our rewrite-rule synthesizer. The naïve approach is to enumerate pairs of circuits and check their equivalence—a quadratic explosion. To avoid this quadratic explosion, we will utilize a new probabilistic data structure in which circuits are inserted and stored in their respective equivalence classes. We call this data structure a *polynomial identity filter* (PIF), because it uses the high-probability guarantees of Schwartz–Zippel to populate circuits into equivalence classes.

### 5.1 The Polynomial Identity Filter (PIF)

We will now define the polynomial identity filter (PIF). Our goal is to design a data structure that groups polynomials into equivalence classes; when a new polynomial is *inserted*, it will assign it to the appropriate equivalence class. The PIF directly builds upon the insights of Schwartz–Zippel.

The key trick of the PIF is to randomly sample  $\alpha$  *only once* at initialization and use it to compare all inserted polynomials. Building upon the high-probability guarantees of Schwartz–Zippel, we ensure that all deduced equivalences are correct with a high probability.

**Initialization.** To define equivalence classes of polynomials, we will use a map  $M$  from complex numbers to *sets of polynomials*. We initialize our polynomial identity filter as follows:

- (1) Let  $M$  map every complex number to the empty set.
- (2) Let  $R \subset \mathbb{C}$  be a finite subset of the complex numbers.
- (3) Sample  $n$  independent values,  $\alpha_1, \dots, \alpha_n$ , from the uniform distribution over  $R$ . *These values are sampled once initially and used throughout the lifetime of the data structure.*

**Inserting a polynomial into PIF.** When a new polynomial  $p$  is inserted into the PIF, we update the map by adding  $p$  to the set  $M[p(\alpha)]$ . Intuitively, the set  $M[p(\alpha)]$  is the set of all polynomials that evaluate to the same complex number on the input  $\alpha$ .

<sup>1</sup>We can handle terms with negative exponents like  $e^{-i\theta}$  by multiplying both polynomials by  $e^{i\theta}$ . Terms with expressions such as  $e^{i(\theta_1+\theta_2)}$  can be expanded to  $e^{i\theta_1} e^{i\theta_2}$ .

**Correctness guarantees.** Suppose we insert  $\ell$  polynomials into the PIF. Intuitively, the PIF implicitly applies the PIT algorithm from § 4.1 to all pairs of polynomials, i.e.,  $\leq \ell^2$  polynomial identity checks. Since every identity test has a false positive probability (if the polynomials are not equal), the total failure probability of the PIF increases. Luckily, the high-probability guarantees of Schwartz–Zippel still provide us with a pretty good failure probability. Simply following the union bound, the failure probabilities add up, as formalized in the following theorem:

**THEOREM 5.1 (PIF WORST-CASE GUARANTEES).** *Suppose we insert  $\ell$  mutually inequivalent polynomials into a new PIF. Let  $d$  be the maximum degree of all  $\ell$  polynomials. The probability that one of the cells of  $M$  contains more than one polynomial is at most  $\ell^2 d/|R|$ .*

**PROOF.** Let  $p_1, \dots, p_\ell$  be mutually inequivalent polynomials over the same set of  $n$  variables. If we insert  $\ell$  polynomials into the PIF, it implicitly performs the following randomized computation:

- (1) Sample  $\alpha_1, \dots, \alpha_n$  independently and uniformly from  $R$ .
- (2) For every pair  $p_i$  and  $p_j$ , where  $i \neq j$ , check if  $p_i(\alpha) = p_j(\alpha)$ .

(Note that step 2 is performed efficiently by computing each  $p_i(\alpha)$  separately and inserting  $p_i$  into  $M[p_i(\alpha)]$ . All  $p_i, p_j$  such that  $p_i(\alpha) = p_j(\alpha)$  are therefore inserted into the same cell of  $M$ .)

Following Schwartz–Zippel (Thm. 4.1), for any pair of polynomials  $p_i$  and  $p_j$ , where  $i \neq j$ ,  $\Pr[p_i(\alpha) = p_j(\alpha)] \leq d/|R|$ . Therefore, following the union bound, the probability that one of the cells of  $M$  contains more than one polynomial is

$$\Pr[\exists i \neq j. p_i(\alpha) = p_j(\alpha)] \leq \sum_{i,j \in [1,\ell], i \neq j} \Pr[p_i(\alpha) = p_j(\alpha)] \leq \ell^2 d/|R|$$

□

*Example 5.2.* If we insert  $10^6$  mutually inequivalent polynomials of degree 10 into a new PIF, and we use 64-bit integers for  $R$ , then the probability of the PIF declaring a pair equivalent is  $\sim 10^{-7}$ .

**Implementation considerations.** To further minimize failure probability, if necessary, after populating the data structure, we can apply PIT (with freshly sampled values) to each pair of polynomials in each equivalence class. An equivalence class will typically contain a small number of polynomials, allowing us to enumerate all pairs and reverify their equivalence. To avoid floating-point errors, we can restrict our sample space  $R$  to rational numbers (see Appendix B for details).

## 5.2 Rewrite-Rule Synthesizer

We now have all the ingredients needed to describe our rewrite-rule synthesis technique.

**Symbolic-circuit grammar.** Fig. 6 shows the grammar of symbolic circuits that we consider. We fix finite sets of one- and two-qubit gates, symbolic gates, parameter variables ( $\theta$ ), and constants. We also allow for arithmetic expressions over parameters, e.g.,  $\theta_1 + \theta_2$ .

**The synthesis algorithm.** Alg. 1 synthesizes pairs of equivalent circuits. It starts with a PIF instance containing the empty circuit. Then, in a bottom-up-synthesis fashion, the algorithm enumerates circuits of increasing size, up to a bound  $k$ , and inserts them into the PIF. We assume that all circuits are transformed into polynomials, following Thm. 4.8, before inserting them into the PIF. We also assume that the polynomials all share the same  $v_{x,y}$  variables from Thm. 4.8.

For symbolic circuits, the algorithm considers every possible interpretation of the symbolic gates' state transformers ( $f^u$ ). Note that the space of interpretations is restricted to reversible functions because quantum operations are reversible.

**Algorithm 1** Circuit equivalence synthesizer**procedure** SYNTH-EQ

Construct a PIF instance and insert the empty circuit

Let  $\mathcal{F}$  be the space of all reversible functions in  $\mathbb{Z}_2^n \rightarrow \mathbb{Z}_2^n$

Let  $C$  be all circuits with size up to some fixed bound, following grammar in Fig. 6

**for**  $C \in C$  **do**

**if**  $C$  contains no symbolic gates **then** insert  $C$  into the PIF

**else**

        Let  $f_1, \dots, f_l$  be the uninterpreted state transformers in  $C$

**for** every interpretation  $I$  of  $f_1, \dots, f_l$  from  $\mathcal{F}$  **do**

            insert  $C(I)$  into the PIF

► in order of increasing size

After Alg. 1 completes, we take each equivalence class in the PIF and generate a set of rules. For every equivalent pair of circuits,  $(C_1, C_2)$ , where  $C_2$  is smaller than  $C_1$  (by number of gates), we generate the rewrite rule  $C_1 \rightarrow C_2$ . We call these *size-reducing* rules. For equivalent pairs of the same size, we generate  $C_1 \rightarrow C_2$  and  $C_2 \rightarrow C_1$ . We call these *size-preserving* rules. For symbolic circuits, we construct rewrite rules where the two circuits have the same interpretation.

$C := G_{1,1}^\rho i \mid G_{1,2}^\rho i \mid \dots$	1-qubit gates
$\mid G_{2,1}^\rho i j \mid G_{2,2}^\rho i j \mid \dots$	2-qubit gates
$\mid S_1 \mid S_2 \mid \dots$	symbolic gates
$\mid C_1; C_2$	sequential comp.
$\rho := \theta_1 \mid \theta_2 \mid \dots \mid -\rho \mid c\rho \mid \rho + \rho$	parameter expr.
$i, j \in [1, n]$	qubit indices
$c \in \{\pi, -\pi, \pi/2, \dots\}$	constants

Fig. 6. Circuit synthesis grammar

**Pruning techniques.** To prune unnecessary rules, we adopt two techniques from Quartz [Xu et al. 2022]: (1) Picking a representative circuit from each equivalence class to construct larger circuits with the grammar (any equivalent circuit can be rewritten to the representative and vice versa). (2) Prune rules where both sides have common subcircuits. We also incorporate some new heuristics such as pruning rules where the left-hand side contains functions in parameter expressions, e.g.,  $\theta_1 + \theta_2$ . The full list of additional pruning we perform is described in Appendix C.1.

## 6 CIRCUIT OPTIMIZER

Given a circuit, we apply the synthesized rewrite rules to minimize some cost function: Commonly, this is the number of gates in the circuit because each gate, particularly two-qubit gates, introduces noise in the computation. There are two critical challenges here:

- (1) How do we apply symbolic rules that can match arbitrary subcircuits? While there are standard algorithms for finding patterns in a quantum circuit, there are no general techniques for finding patterns that satisfy a given constraint.
- (2) In what order to apply the rules? Optimizers, like VOQC and TKET, employ a fixed schedule of optimizations chosen by the compiler designer. QUESO synthesizes tens of thousands of rules, and we simply cannot ask a developer to experiment with different schedules.<sup>2</sup>

To address these challenges, we present (1) an algorithm for matching and applying symbolic rewrite rules, and (2) a beam-search-based optimization algorithm.

### 6.1 Rule-Matching Algorithm

Given a quantum circuit  $C$  and a rewrite rule  $C_l \rightarrow C_r$ , we want to find subcircuits of  $C$  that match the pattern  $C_l$ , and rewrite them to  $C_r$ . For non-symbolic rewrite rules, this is a standard process.

<sup>2</sup>Equality saturation, as realized in the state-of-the-art library, egg [Willsey et al. 2021], cannot scale to large numbers of rules, especially *multi-pattern* ones, and cannot apply symbolic rules natively.



**Algorithm 2** Maximal beam search

---

```

procedure MAX-BEAM( $C$ )
  Create priority queue  $Q$  of bounded size, and add  $C$  to  $Q$ 
   $C_{best} \leftarrow C$ 
  while  $Q$  is not empty do
    dequeue circuit  $C'$ 
    if  $\text{COST}(C') < \text{COST}(C_{best})$  then
       $C_{best} \leftarrow C'$ 
    for every rewrite rule  $R$  do
       $C'_R \leftarrow \text{APPLY-MAX}(R, C')$ 
      if  $\text{COST}(C'_R) \leq \text{COST}(C_{best})$  and  $C'_R$  has not been seen before then
        add  $C'_R$  to  $Q$ 
  return  $C_{best}$ 

```

---

First, a quantum circuit is represented as a directed-acyclic graph (DAG), just like in our graphical representations of circuits in, e.g., Fig. 1. Finding the pattern  $C_l$  in  $C$  boils down to the following problem: Find a subgraph in  $C$  that is *isomorphic* to  $C_l$ .<sup>3</sup> Since this is a well-known problem, we use  $\text{MATCH}(C_l, C)$  to denote the procedure that returns *all* subgraphs in  $C$  that match the pattern  $C_l$ .

**Matching symbolic patterns.** For simplicity, and without loss of generality, we consider symbolic rewrite rules that contain a single symbolic gate  $S$ . We fix a rule of the form  $C_l; S; C'_l \rightarrow C_r; S; C'_r$ , where the state transformer of  $S$  is interpreted by  $I$ . We want to formalize matching the pattern  $C_l; S; C'_l$  in a circuit  $C$ . We assume that  $\llbracket S(I) \rrbracket$  is of the form  $\phi^u(\mathbf{x}) |f(\mathbf{x})\rangle$  and that the circuit  $C$  has  $n$  qubits. The idea is that we will have to try every possible circuit that matches the path sum of  $S$ , as formalized in  $\text{MATCH-SYM}$ :

$$\text{MATCH-SYM}(C_l; S; C'_l, C) = \bigcup_{C_S \in \mathcal{S}} \text{MATCH}(C_l; C_S; C'_l, C) \quad (7)$$

where  $\mathcal{S} = \{C_S \mid C_S \text{ is a non-symbolic } n\text{-qubit circuit and } \llbracket C_S \rrbracket \text{ is of the form } \phi(\mathbf{x} \dots) |f(\mathbf{x} \dots)\rangle\}$ . Observe that the circuits  $C_S$  can apply operations to more qubits than in  $S$ , (as indicated by the  $\dots$ ). As formalized in Thm. 6.2, this procedure preserves the correctness of the rewrite rule.

*Example 6.1.* Consider the 2-qubit symbolic pattern in Fig. 7 (top), where  $\llbracket S(I) \rrbracket \equiv \phi^u(x_1 x_2) |x_2 x_1\rangle$ . The 3-qubit circuit in Fig. 7 (bottom) matches the symbolic pattern. The highlighted subcircuit has a path sum of the form  $e^{i(2x_2-1)\pi/4} |x_2 x_1 \dots\rangle$ , which matches  $\llbracket S(I) \rrbracket$ , because it swaps the first two qubits,  $x_1$  and  $x_2$ .

**THEOREM 6.2 (SOUNDNESS OF MATCH-SYM).** *Given a symbolic rewrite rule of the form  $C_l; S; C'_l \rightarrow C_r; S; C'_r$  and  $C_S \in \mathcal{S}$ ,  $C_l; C_S; C'_l \equiv C_r; C_S; C'_r$ .*

**Implementing MATCH-SYM.** We implement  $\text{MATCH-SYM}$  by restricting  $\mathcal{S}$  to the space of subcircuits of  $C$ . For efficiency, we limit  $\mathcal{S}$  by (1) only considering subcircuits of  $C$  over monomial gates, since  $S$  is monomial, and (2) limiting the search to subcircuits *between* the set of subcircuits that match  $C_l$  and  $C'_l$ . Additionally (see § 7) we limit the size of circuits in  $\mathcal{S}$ . Our approach for checking if a subcircuit is monomial is inspired by Nam et al. [2018]’s rotation-merging implementation.

<sup>3</sup>additionally the subgraph has to be *convex*.

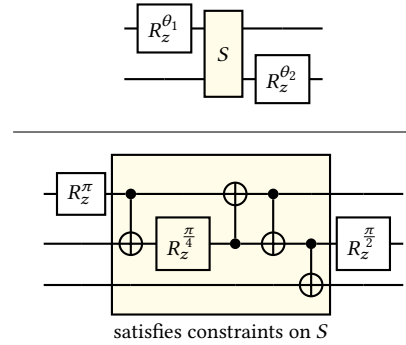


Fig. 7. Example of  $\text{MATCH-SYMB}$

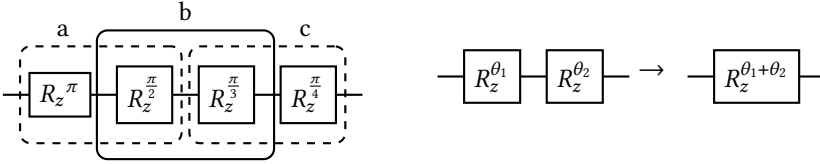


Fig. 8. Maximal match example

## 6.2 Maximal Beam Search

To find an optimal circuit, one needs to exhaustively consider every possible ordering of rewrite rule application. To limit the combinatorial explosion, the scheduling algorithm we propose, MAX-BEAM (Alg. 2), limits the size of the search space in two ways: (1) Instead of considering a single application of a rewrite rule in each step of the search, MAX-BEAM greedily considers *maximal* applications of a rewrite rule. (2) MAX-BEAM is a *beam search* through the space of rewrites.

*Definition 6.3 (Maximal matching set).* Consider a rewrite rule  $C_l \rightarrow C_r$  and a circuit  $C$ . A *maximal matching set* is a subset  $\mathcal{M} \subseteq \text{MATCH}(C_l, C)$  such that (1) no pair of subcircuits  $C'_i, C'_j \in \mathcal{M}$  overlap in  $C$ , and (2) there is no  $\mathcal{M}'$ , where  $\mathcal{M} \subset \mathcal{M}' \subseteq \text{MATCH}(C_l, C)$ , that satisfies condition (1). The same definition applies to symbolic rules.

*Example 6.4.* Consider the single-qubit circuit with a sequence of four rotations in Fig. 8 (left) and the rewrite rule that merges two rotations (right). The rule matches three subcircuits as shown by the three boxes. Matches (a) and (b) overlap, as well as (b) and (c). So APPLY-MAX chooses a set of matches that do not overlap—e.g., the dotted ones—and applies the rewrite to them.

The MAX-BEAM algorithm begins with a priority queue of fixed size containing the input circuit  $C$  that we wish to optimize. The priority queue uses a cost function,  $\text{COST}$ . The algorithm picks the next circuit from  $Q$  and rewrites it. For every rewrite rule  $R$ , it applies  $R$  *maximally* to the current circuit  $C'$ . Specifically, the function APPLY-MAX finds a maximal set of *non-overlapping* matches for the rewrite rule  $R$  in  $C'$  and rewrites all the matches, producing a new circuit  $C'_R$ . In practice, we implement APPLY-MAX greedily and do not try to find a *maximum* matching set, only a maximal one. MAX-BEAM can be terminated after a finite number of iterations or within some time limit.

## 7 IMPLEMENTATION AND EVALUATION

**Synthesized optimizers.** We implemented QUESO in  $\sim 3,700$  lines of Java. We evaluated QUESO on four different gate sets: (1) the standard gate set for IBM computers, (2) the gate set for Rigetti computers, (3) the gate set for *ion trap* computers (like IonQ [IonQ 2022b]), and (4) the gate set of Nam et al. [2018] (henceforth, Nam). The IBM and Rigetti gate sets support devices with superconducting qubits, which are the largest quantum devices physically realized so far. Ion trap architectures are attractive due to their all-to-all qubit connectivity, which reduces the need for expensive *swaps*. The Nam gate set is interesting to study because it closely resembles the *Clifford+T* universal gate set where Clifford gates can be efficiently simulated on a classical computer. However, unlike the other gate sets, the Nam gate set is not physically realized in any quantum hardware.

Table 1 summarizes the gate sets and the rules synthesized. For all gate sets, we limit rewrite rules to be over a maximum of 3 qubits and vary the maximum *size* of a rule: the number of gates on either side. We choose the largest size for which QUESO can synthesize rules within 3 minutes. For example, for IBM, in 72 seconds QUESO synthesizes 701 rules, out of which 48 rules are symbolic. Failure probability is an upper bound on the PIF returning an incorrect rule (Thm. 5.1). Observe how vanishingly small the failure probabilities are, e.g.,  $10^{-17}$  for IBM.

Table 1. Rewrite-rule synthesis results

Gate set	Gates	# Qubits	Size	# Possible Rules	# Rules	# Symbolic Rules	Failure Prob.	Time (s)
IBM	$U_1^\theta, U_2^{\theta_1, \theta_2}, U_3^{\theta_1, \theta_2, \theta_3}, CX$	3	4	$1.5 \times 10^{13}$	701	48	$10^{-17}$	72
Nam	$H, X, R_z^\theta, CX$	3	6	$5.4 \times 10^{18}$	14,544	2,365	$10^{-12}$	135
Rigetti	$R_x^\pi, R_x^{\pi/2}, R_x^{-\pi/2}, R_z^\theta, CZ$	3	5	$1.4 \times 10^{16}$	2,242	809	$10^{-14}$	70
Ion	$R_x^\theta, R_y^\theta, R_z^\theta, R_{xx}^\theta$	3	3	$1.6 \times 10^{11}$	1,519	24	$10^{-19}$	15

**Research questions.** We aim to answer the following research questions:

(Q1) How does QUESO compare to state-of-the-art optimizers?

(Q2) How does QUESO compare to superoptimization?

(Q3) Which synthesized rewrite rules are useful?

**Benchmarks.** Throughout, we will use a set of 33 benchmark circuits, comprised of those from prior work on optimization [Amy et al. 2014; Hietala et al. 2021; Nam et al. 2018; Xu et al. 2022] and a new class of circuits. The benchmarks from prior work include arithmetic circuits and Toffoli gate networks. We added *quantum approximate optimization algorithm* (QAOA) circuits that approximate the maximum cut in a 3-regular graph. QAOA is a promising and near-term application because it can approximate NP-hard combinatorial problems on NISQ machines without error correction.

**Instantiation of QUESO.** We use the total number of gates in a circuit as QUESO's cost function (cost in Alg. 2). We fix the priority queue size (in Alg. 2) to 8000 circuits. For matching symbolic circuits, we limit the number of qubits and size of the  $C_S$  circuits in Eq. (7) to 7 and 10, respectively.

**Metrics.** To compare tools, the main metric we use is the number of two-qubit gates, because they have *orders of magnitude* higher error rates compared to single-qubit gates. For instance, the error rates for single- and two-qubit gates on the IBM Toronto device are on the order of  $10^{-4}$  and  $10^{-2}$ , respectively [IBM 2022] (further, some single-qubit gates, like  $R_z$ , are error-free as they are simulated classically). To further illustrate the importance of two-qubit gate reduction, we use *fidelity* results (success probability), which we statically estimate based on publicly available error rates from the IBM Toronto [IBM 2022], Rigetti Aspen-11 [Rigetti 2022], and IonQ Aria [IonQ 2022a] devices. Fidelity is the probability that none of the gates in a circuit cause an error. For a circuit  $G_1; \dots; G_n$ , its fidelity is  $\prod_i (1 - \text{error rate of } G_i)$ .

### Q1: How does QUESO compare to state-of-the-art optimizers?

**Experimental setup.** We compared QUESO to four state-of-the-art optimizers: IBM Qiskit [Aleksandrowicz et al. 2019], Quilc [Smith et al. 2020], TKET [Sivarajah et al. 2020], and voqc [Hietala et al. 2021]. The first three are used in industrial toolkits; voqc is a formally verified and very effective optimizer.<sup>4</sup> For each benchmark, we set a time limit of 1 hour (we discuss running time of QUESO in Q3). To ensure a fair comparison of the optimization phases of the various tools, we provide all tools with the same decomposed input circuit in the target gate set.

We use *S-curves* to present the results. For each benchmark circuit, we compute the quantity

$$\frac{\# \text{ of gates with tool } X - \# \text{ of gates with QUESO}}{\# \text{ of gates in unoptimized circuit}}$$

and present the benchmarks in increasing order. Positive values imply that QUESO outperforms tool  $X$ . We compute the following quantity for fidelity:<sup>5</sup>  $\frac{\text{fidelity with QUESO} - \text{fidelity with tool } X}{\text{maximum of fidelity with QUESO and with tool } X}$ .

<sup>4</sup>We excluded the Nam et al. [2018] optimizer because it is proprietary and the existing data was not obtained from running on decomposed input circuits nor does it include the added benchmarks. We also excluded PyZX [Kissinger and van de Wetering 2019a] because it works well for reducing T gate count, which is useful for future fault-tolerant machines, but can often increase total gate count. A comparison of QUESO against PyZX with respect to T gate reduction is in Appendix E.1.

<sup>5</sup>We do not use the fidelity of the original circuit in the denominator here because it can be extremely small.

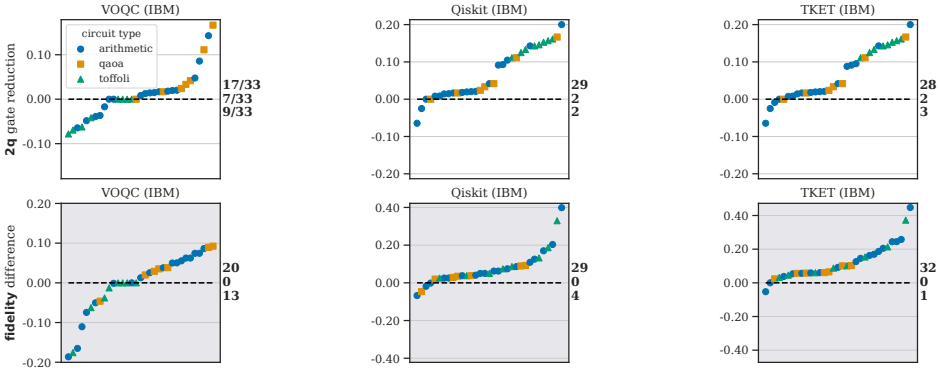


Fig. 9. Comparison against state-of-the-art optimizers on IBM. Each graph is annotated to the right with the number of circuits where QUESO outperforms, matches, and underperforms (top-to-bottom) the other tool.

**IBM.** Fig. 9 shows the S-curves for the IBM gate set. Consider, for instance, the top middle S-curve, which compares QUESO to IBM Qiskit. For the majority of the benchmarks, 29/33, QUESO outperforms Qiskit in two-qubit gate reduction—all the benchmarks above the dashed horizontal (0) line. We see similar results with TKET. QUESO can outperform VOQC in 17/33 benchmarks, and exactly match its performance on 7/33 benchmarks. The fidelity graphs, bottom row, depict a very similar story, indicating the close correspondence between two-qubit-gate count and fidelity.

**Nam.** Results on Nam are in the appendix because they resemble the results for the IBM gate set.

**Rigetti and Ion.** For the Rigetti and Ion gate sets, we compare against Quilc and Qiskit, respectively. Implemented by Rigetti, Quilc is specialized for optimizing the Rigetti gate set. To our knowledge, these are the only publicly available compilers that apply to those two gate sets. We also compare against TKET for the Rigetti gate set but we note that the optimized circuits TKET produces *do not* adhere to the allowed angles for  $R_x$  gates and therefore are not valid. See appendix for the results, which resemble the results for Quilc.

None of the tools are able to reduce two-qubit gate count for the majority of the benchmarks as shown in Fig. 10, where these benchmarks lay on the dashed line. However, we see reduction in single-qubit gates (see appendix), which is reflected in fidelity, as single-qubit gates errors dominate for all but 7/33 benchmarks. QUESO is able to outperform Quilc on a majority of the benchmarks for the Rigetti gate set (20/33). For the Ion gate set, we see an opposite story: QUESO outperforms Qiskit on 13/33 benchmarks and underperforms it on 20/33.

We investigated why Quilc and Qiskit are sometimes able to achieve reduction in two-qubit gates and isolated it to a powerful optimization that resynthesizes arbitrary two-qubit circuits [Cross et al. 2019]. We cannot fully capture such optimizations and leave it as an avenue for future work.

**Q1 summary.** QUESO is able to significantly outperform or match state-of-the-art optimizers on a majority of the benchmarks across all gate sets with respect to two-qubit gate reduction. The results are similar for fidelity except on the Ion gate set where QUESO only outperforms or matches Qiskit on 39% of the benchmarks.

## Q2: How does QUESO compare to superoptimization?

**Experimental setup.** Next, we compare against the Quartz *superoptimizer* [Xu et al. 2022]. Quartz is comprised of two phases that run in sequence: (1) The *preprocessing* phase: a manually written set of optimizations that decompose a circuit to the target gate set and applies rotation merging and other domain specific optimizations—e.g., Hadamard and CZ cancellation for Rigetti. (2) The

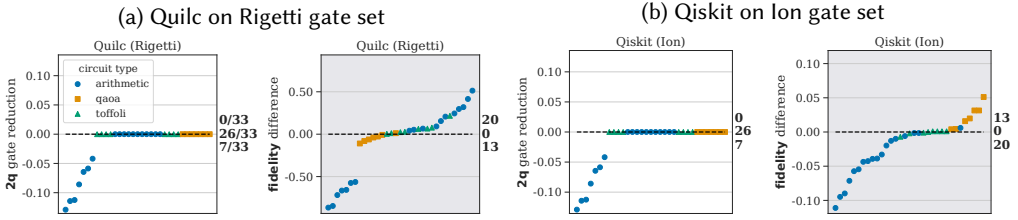


Fig. 10. Comparison against state-of-the-art optimizers on Rigetti and Ion trap.

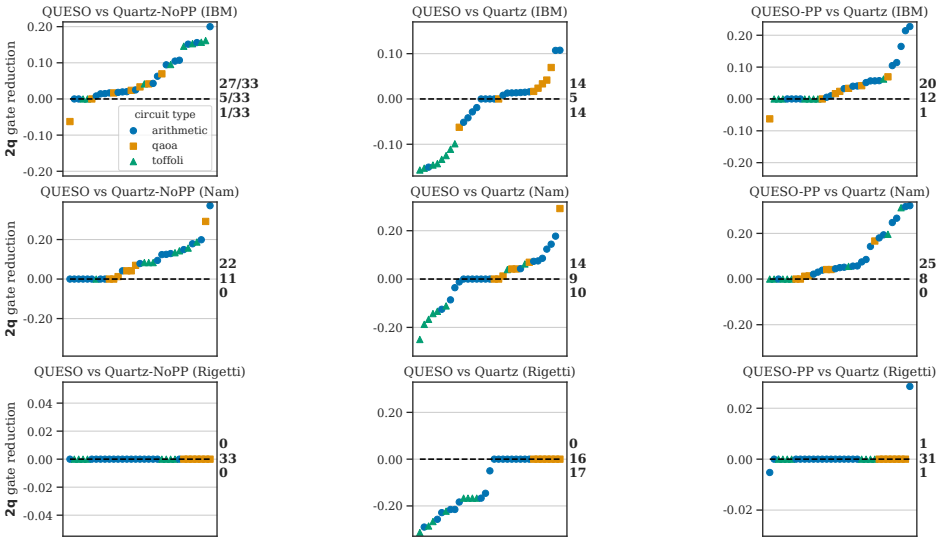


Fig. 11. **1 hour timeout** comparison against Quartz: (left column) Quartz without the preprocessing phase; (middle column) Quartz with both phases; (right column) QUESO with Quartz’s preprocessing phase vs Quartz with both phases.

*search* phase: applies automatically synthesized (non-symbolic) rewrite rules and applies them to a circuit by enumerating different orderings. The synthesized rules are verified with an SMT solver, but the manually written preprocessing phase is not verified.

We compare against Quartz along two dimensions: (1) the time to synthesize rules and (2) the quality of the synthesized rules. Both tools were allotted 1 hour of optimization time, 32GB of RAM, and 1 CPU core per benchmark. We do not compare against Quartz for the Ion gate set, which they do not currently support. To fairly compare against Quartz, we distinguish between two variants of the tool: (1) Quartz, the full tool with the two phases, and (2) Quartz-NoPP, which is Quartz without the preprocessing phase—just the synthesized rules.

**Results.** First, we observe that QUESO is able to synthesize rules an order of magnitude faster than Quartz: QUESO synthesizes rules in 70-135 seconds, whereas Quartz takes up to 2,303 seconds for rules of the same size. For example, QUESO synthesizes rules for the IBM gate set with up to 3 qubits and size 4 in 72 seconds while Quartz takes 2,193 seconds. Note that comparing rule-synthesis speed directly is challenging because QUESO synthesizes more expressive, symbolic rules. We attribute our fast rule synthesis to using a PIF for equivalence checking rather than an SMT solver.

Fig. 11 shows the results of the comparison to Quartz. The first column shows that QUESO is able to significantly outperform Quartz with preprocessing disabled (Quartz-NoPP) on most benchmarks

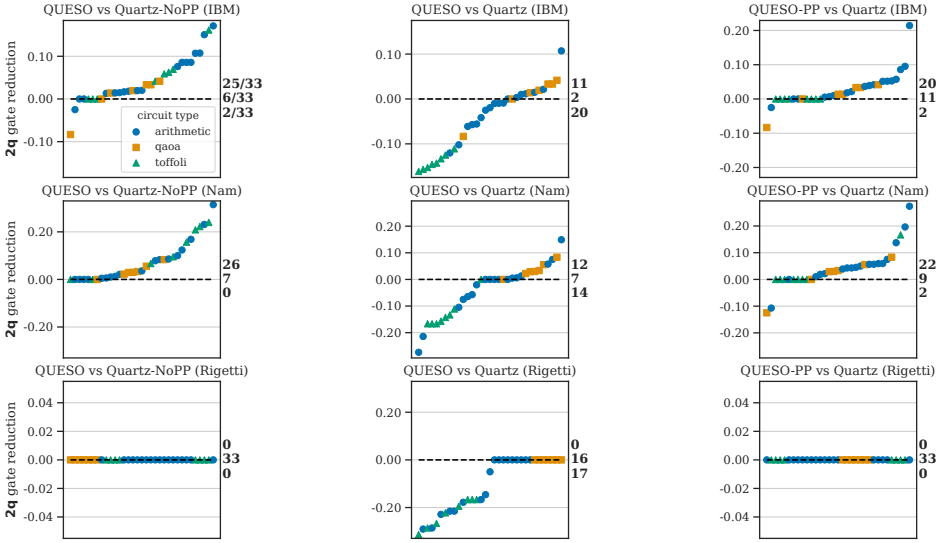


Fig. 12. 24 hour timeout comparison against Quartz

on IBM and Nam gate sets. For Rigetti, both `QUESO` and `Quartz-NoPP` cannot eliminate any two-qubit gates. These results demonstrate the power of our synthesized rules compared to `Quartz`'s.

Fig. 11 (middle column) shows the results against full `Quartz`, i.e., when enabling the hand-crafted preprocessing phase. Note that in this case we provide `Quartz` with circuits pre-decomposition—i.e., with Toffoli gates. For `QUESO`, we use the same decomposition for each Toffoli gate, whereas `Quartz`'s preprocessing greedily picks which decomposition to use. The results on IBM and Nam show `QUESO` and `Quartz` are close in performance; for Rigetti, thanks to the domain-specific optimizations in the preprocessing phase, `Quartz` is able to eliminate two-qubit gates in half of the benchmarks.

To further understand the effects of the preprocessing phase, `QUESO-PP` is the result of running `QUESO` on the output of `Quartz`'s preprocessing phase. As the third column of Fig. 11 shows, on IBM and Nam, `QUESO-PP` outperforms full `Quartz`, and matches it on Rigetti. These results further amplify the power of our symbolic rules in comparison with `Quartz`'s.

The results are similar when running both tools for the full 24 hour timeout used in `Quartz`'s original evaluation as shown in Fig. 12. The results for every one hour interval are included in the appendix. We observe that after 4 to 5 hours, `Quartz` (with preprocessing) catches up to `QUESO` (without preprocessing) on the IBM gate set on 6 of the benchmarks. With the longer timeout, `Quartz` overall performs slightly better than before on the IBM and Nam gate sets and remains the same on the Rigetti gate set. The notable exception is the comparison against `QUESO` and `Quartz-NoPP` on the Nam gate set where `QUESO` benefits from the longer timeout.

**Q2 Summary.** `QUESO` synthesizes rules for the same size and gate set up to 30x times faster than `Quartz`. When comparing synthesized rules, `QUESO` outperforms or matches `Quartz` on 97% of the benchmarks across all gate sets.

### Q3: Which synthesized rewrite rules are useful?

We explore this question at two levels of granularity: (A) Is there a subset of the rewrite rules that is sufficient for producing optimal circuits? (B) Which classes of rules are useful for optimization? We present results for the representative IBM gate set.



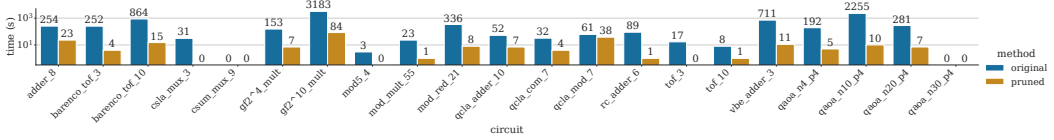


Fig. 13. Log-scale comparison of QUESO running time on IBM with pruned (35) vs original (701) rewrite rules.

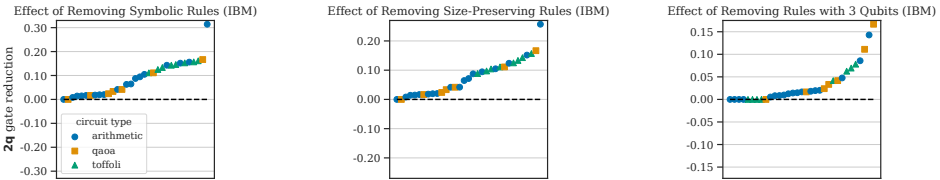


Fig. 14. Effect of different types of rules. Points > 0 indicate that removing the rules is detrimental.

**(A) Results.** We collect the set of all rewrite rules that result in the best circuit that QUESO can discover within 1 hour of execution time. Across all benchmarks, we observe that a fixed subset of only 35 rules out of 701 rules are used to reach the best solution. This implies that we can run QUESO with a subset of the rules and achieve similar results in a significantly smaller amount of time. We envision, for instance, that QUESO can be *finetuned* on a given class of problems to collect all relevant rules and discard the unnecessary ones.

To understand the time savings, we run QUESO with the *pruned* set of 35 rules and ask: how long does it take for it to reach a circuit of equal cost (in terms of two-qubit gate count) to that found by QUESO running on the full set of rules for 1 hour. Fig. 13 shows the results for a representative subset of the 33 benchmarks. We observe a drastic reduction in runtime. For instance, on the qaoa\_n10\_p4 benchmark, it takes QUESO 2,255 seconds to converge to the best circuit that can be found within 1 hour, but it takes the pruned version only 10 seconds to arrive at a circuit with the same number of two-qubit gates. Overall, we observe runtime reductions of up to 225x, making QUESO run in a few seconds to a minute on the majority of the benchmarks.

**(B) Rule classes.** Next, we study the effect of symbolic rules, size-preserving rules, and rules over 3-qubit circuits. Fig. 14 shows the S-curves comparing QUESO versus QUESO without a subset of the rules. The graphs show that removing each type of rule significantly affects the performance—almost all the points are above the dashed line. Most importantly, this shows that being able to synthesize and apply symbolic rules is critical. We also observe that greedily applying only size-reducing rules, results in a worse solution in almost all the benchmarks. Finally, we see a slightly less dramatic effect when removing rules with 3 qubits, i.e., restricting QUESO to rules with up to 2 qubits, but a majority of the benchmarks still rely on these rules.

**Q3 Summary.** Restricting QUESO to the small subset of rules used decreases the time to reach the best solution by up to 225x. Symbolic rules significantly contribute to QUESO’s performance and the ability to synthesize and apply them is critical.

## 8 RELATED WORK

**Rewrite-rule synthesis.** Most quantum-circuit compilers use hand-crafted optimizations for a given gate set [Aleksandrowicz et al. 2019; Hietala et al. 2021; Nam et al. 2018; Shi et al. 2019; Sivarajah et al. 2020; Smith et al. 2020]. Our approach is most similar to Quartz [Xu et al. 2022] (and its predecessor [Pointing et al. 2021]) and related work on rewrite-rule synthesis for computation graphs [Jia et al. 2019] and LLVM. QUESO differs from Quartz along two dimensions: expressivity and speed. QUESO can learn symbolic rules, unlike Quartz. These symbolic rules enable optimizations

similar to [Nam et al. \[2018\]](#)'s rotation merging, which Quartz applies as an unverified hand-crafted preprocessing step. Our synthesis phase is much faster due to the application of Schwartz–Zippel as opposed to SMT-based verification. Quartz implements a preprocessing pass to optimize the circuit before beginning to apply rewrite rules using a cost-based backtracking search. In contrast, we rely only on learned rules; as our goal is not superoptimization, we apply rules greedily, allowing our approach to find smaller circuits faster. ZX calculus-based optimizers use graphical rewrite rules [[Cowtan et al. 2020](#); [Kissinger and van de Wetering 2019a,b](#)]. However, PyZX's full optimization pass involves a subroutine [[PyZX 2023](#)] that only supports circuits with Clifford + T gates and does not support arbitrary rotation, making it rigid and not compatible with existing hardware platforms that execute gates with arbitrary rotation. QUESO is designed to leverage hardware gates to unlock broad optimization opportunities and enable flexibility to adapt to changes in the basis gates.

**Verified optimizers.** Compilers are hard to get right [[Sun et al. 2016](#)], and much progress has been made in building verified classical compilers [[Kumar et al. 2014](#); [Leroy 2009](#)]. This includes verified optimizing compilers, using interactive theorem proving [[Barthe et al. 2014](#); [Becker et al. 2022](#); [Courant and Leroy 2021](#); [Mullen et al. 2016](#)] and automated techniques like SMT-solving [[Lerner et al. 2003](#); [Lopes et al. 2021, 2015](#)]. In the quantum realm, similar efforts have included reversible circuit compilers verified in F\* [[Amy et al. 2017](#); [Rand et al. 2018](#)], the optimizer voqc [[Hietala et al. 2021](#)], which has been formally verified in Coq, and Giallar [[Tao et al. 2022](#)] for verification of Qiskit optimizations. Our work, in contrast to the above, automatically synthesizes probabilistically verified rewrite rules, relying on novel verification insights for this problem domain and a probabilistic data structure. Leveraging PIT for equivalence-checking has been applied in other areas such as program analysis [[Gulwani and Necula 2003](#)] and machine learning [[Wang et al. 2021](#)].

**Circuit resynthesis.** There are quantum-circuit optimizations that QUESO cannot discover. The most interesting is that of [Cross et al. \[2019\]](#). This optimization finds maximal disjoint blocks of gates that operate on a given control and target of a CX in the block. For each two-qubit block, the optimization computes a unitary operation and resynthesizes a subcircuit for the block using either exact techniques [[Bullock and Markov 2003](#); [Shende et al. 2004](#)] or approximation. Other similar optimizations include QUEST [[Patel et al. 2022](#)], which performs approximate resynthesis of circuits to reduce their CX count, and several exact resynthesis techniques for reducing the CX counts in circuits [[Davis et al. 2020](#); [de Brugière et al. 2020](#); [Meuli et al. 2018](#)].

## 9 CONCLUSIONS AND FUTURE WORK

We have described a technique for automatically generating quantum-circuit optimizers by synthesizing symbolic rewrite rules. Our results demonstrate the remarkable ability of our synthesized optimizers to outperform or rival state-of-the-art optimizers. For future work, we would like to explore (1) learning-based techniques for scheduling rewrite rules to speed up optimization, and (2) enhancements of symbolic rules to capture more sophisticated optimizations like those in Quilc.

## ACKNOWLEDGEMENTS

We thank the anonymous reviewers and our shepherd, Joseph Tassarotti, for their insightful feedback. We also thank Justin Hsu and Thomas Reps for their input during the writing process. We are grateful to Martin Diges, Mingkuan Xu, and the CHTC team for their assistance in our experimentation as well as Max Willsey for providing guidance during our exploration of egg.

This work is supported by NSF grants #1652140 and #2212232 and awards from Meta and Amazon. This research is also partially supported by the OVCRGE at the University of Wisconsin–Madison with funding from the Wisconsin Alumni Research Foundation. Lauren Pick is supported by NSF grant #2127309 to the Computing Research Association for the CIFellows Project.

## SOFTWARE AVAILABILITY

Our artifact is publicly available on Zenodo [Xu et al. 2023]. It contains the QUESO source code, evaluation infrastructure, and documentation.

## REFERENCES

- Gadi Aleksandrowicz, Thomas Alexander, Panagiotis Barkoutsos, Luciano Bello, Yael Ben-Haim, David Bucher, Francisco Jose Cabrera-Hernández, Jorge Carballo-Franquis, Adrian Chen, Chun-Fu Chen, Jerry M. Chow, Antonio D. Córcoles-Gonzales, Abigail J. Cross, Andrew Cross, Juan Cruz-Benito, Chris Culver, Salvador De La Puente González, Enrique De La Torre, Delton Ding, Eugene Dumitrescu, Ivan Duran, Pieter Eendebak, Mark Everitt, Ismael Faro Sertage, Albert Frisch, Andreas Fuhrer, Jay Gambetta, Borja Godoy Gago, Juan Gomez-Mosquera, Donny Greenberg, Ikko Hamamura, Vojtech Havlicek, Joe Hellmers, Lukasz Herok, Hiroshi Horii, Shaohan Hu, Takashi Imamichi, Toshinari Itoko, Ali Javadi-Abhari, Naoki Kanazawa, Anton Karazeev, Kevin Krsulich, Peng Liu, Yang Luh, Yunho Maeng, Manoel Marques, Francisco Jose Martin-Fernández, Douglas T. McClure, David McKay, Srujan Meesala, Antonio Mezzacapo, Nikolaj Moll, Diego Moreda Rodríguez, Giacomo Nannicini, Paul Nation, Pauline Ollitrault, Lee James O’Riordan, Hanhee Paik, Jesús Pérez, Anna Phan, Marco Pistoia, Viktor Prutyantov, Max Reuter, Julia Rice, Abdón Rodríguez Davila, Raymond Harry Putra Rudy, Mingi Ryu, Ninad Sathaye, Chris Schnabel, Eddie Schoute, Kanav Setia, Yunong Shi, Adenilton Silva, Yukio Siraichi, Seyon Sivarajah, John A. Smolin, Mathias Soeken, Hitomi Takahashi, Ivano Tavernelli, Charles Taylor, Pete Taylour, Kenso Trabing, Matthew Treinish, Wes Turner, Desiree Vogt-Lee, Christophe Vuillot, Jonathan A. Wildstrom, Jessica Wilson, Erick Winston, Christopher Wood, Stephen Wood, Stefan Wörner, Ismail Yunus Akhalwaya, and Christa Zoufal. 2019. *Qiskit: An Open-source Framework for Quantum Computing*. <https://doi.org/10.5281/zenodo.2562111>
- Matthew Amy. 2019. Towards Large-scale Functional Verification of Universal Quantum Circuits. *Electronic Proceedings in Theoretical Computer Science* 287 (01 2019), 1–21. <https://doi.org/10.4204/EPTCS.287.1>
- Matthew Amy, Dmitri Maslov, and Michele Mosca. 2014. Polynomial-Time T-Depth Optimization of Clifford+T Circuits Via Matroid Partitioning. *IEEE Transactions on Computer-Aided Design of Integrated Circuits and Systems* 33, 10 (2014), 1476–1489. <https://doi.org/10.1109/TCAD.2014.2341953>
- Matthew Amy, Martin Roetteler, and Krysta M. Svore. 2017. Verified Compilation of Space-Efficient Reversible Circuits. In *CAV (2) (Lecture Notes in Computer Science, Vol. 10427)*. Springer, 3–21. [https://doi.org/10.1007/978-3-319-63390-9\\_1](https://doi.org/10.1007/978-3-319-63390-9_1)
- Gilles Barthe, Delphine Demange, and David Pichardie. 2014. Formal Verification of an SSA-Based Middle-End for CompCert. *ACM Trans. Program. Lang. Syst.* 36, 1, Article 4 (mar 2014), 35 pages. <https://doi.org/10.1145/2579080>
- Heiko Becker, Robert Rabe, Eva Darulova, Magnus O. Myreen, Zachary Tatlock, Ramana Kumar, Yong Kiam Tan, and Anthony Fox. 2022. Verified Compilation and Optimization of Floating-Point Programs in CakeML. In *36th European Conference on Object-Oriented Programming (ECOOP 2022) (Leibniz International Proceedings in Informatics (LIPIcs), Vol. 222)*, Karim Ali and Jan Vitek (Eds.). Schloss Dagstuhl – Leibniz-Zentrum für Informatik, Dagstuhl, Germany, 1:1–1:28. <https://doi.org/10.4230/LIPIcs.ECOOP.2022.1>
- Stephen S. Bullock and Igor L. Markov. 2003. Arbitrary two-qubit computation in 23 elementary gates. *Phys. Rev. A* 68 (Jul 2003), 012318. Issue 1. <https://doi.org/10.1103/PhysRevA.68.012318>
- Christophe Charetton, Sébastien Bardin, François Bobot, Valentin Perrelle, and Benoît Valiron. 2021. An Automated Deductive Verification Framework for Circuit-building Quantum Programs. In *Programming Languages and Systems*, Nobuko Yoshida (Ed.). Springer International Publishing, Cham, 148–177. [https://doi.org/10.1007/978-3-030-72019-3\\_6](https://doi.org/10.1007/978-3-030-72019-3_6)
- Nathanaël Courant and Xavier Leroy. 2021. Verified Code Generation for the Polyhedral Model. *Proc. ACM Program. Lang.* 5, POPL, Article 40 (jan 2021), 24 pages. <https://doi.org/10.1145/3434321>
- Alexander Cowtan, Silas Dilkes, Ross Duncan, Will Simmons, and Seyon Sivarajah. 2020. Phase Gadget Synthesis for Shallow Circuits. *Electronic Proceedings in Theoretical Computer Science* 318 (04 2020), 214–229. <https://doi.org/10.4204/EPTCS.318.13>
- Andrew W. Cross, Lev S. Bishop, Sarah Sheldon, Paul D. Nation, and Jay M. Gambetta. 2019. Validating quantum computers using randomized model circuits. *Phys. Rev. A* 100 (Sep 2019), 032328. Issue 3. <https://doi.org/10.1103/PhysRevA.100.032328>
- Poulami Das, Swamit Tannu, Siddharth Dangwal, and Moinuddin Qureshi. 2021. ADAPT: Mitigating Idling Errors in Qubits via Adaptive Dynamical Decoupling. In *MICRO-54: 54th Annual IEEE/ACM International Symposium on Microarchitecture (Virtual Event, Greece) (MICRO ’21)*. Association for Computing Machinery, New York, NY, USA, 950–962. <https://doi.org/10.1145/3466752.3480059>
- Marc G. Davis, Ethan Smith, Ana Tudor, Koushik Sen, Irfan Siddiqi, and Costin Iancu. 2020. Towards Optimal Topology Aware Quantum Circuit Synthesis. In *2020 IEEE International Conference on Quantum Computing and Engineering (QCE)*. 223–234. <https://doi.org/10.1109/QCE49297.2020.00036>
- Timotheé Goubault de Brugière, Marc Baboulin, Benoît Valiron, Simon Martiel, and Cyril Allouche. 2020. Quantum CNOT Circuits Synthesis for NISQ Architectures Using the Syndrome Decoding Problem. In *Reversible Computation*, Ivan Lanese and Mariusz Rawski (Eds.). Springer International Publishing, Cham, 189–205. <https://doi.org/10.1007/978-3-030-52482-2>

## 1\_11

- Sumit Gulwani and George C. Necula. 2003. Discovering Affine Equalities Using Random Interpretation. In *Proceedings of the 30th ACM SIGPLAN-SIGACT Symposium on Principles of Programming Languages* (New Orleans, Louisiana, USA) (POPL '03). Association for Computing Machinery, New York, NY, USA, 74–84. <https://doi.org/10.1145/604131.604138>
- Kesha Hietala, Robert Rand, Shih-Han Hung, Xiaodi Wu, and Michael Hicks. 2021. A Verified Optimizer for Quantum Circuits. *Proc. ACM Program. Lang.* 5, POPL, Article 37 (jan 2021), 29 pages. <https://doi.org/10.1145/3434318>
- IBM. 2022. IBM Toronto. [https://quantum-computing.ibm.com/services/resources?system=ibmq\\_toronto](https://quantum-computing.ibm.com/services/resources?system=ibmq_toronto).
- IonQ. 2022a. IonQ Aria. <https://ionq.com/posts/july-25-2022-ionq-aria-part-one-practical-performance>.
- IonQ. 2022b. IonQ Native Gates. <https://ionq.com/docs/getting-started-with-native-gates>.
- Zhihao Jia, Oded Padon, James Thomas, Todd Warszawski, Matei Zaharia, and Alex Aiken. 2019. TASO: Optimizing Deep Learning Computation with Automatic Generation of Graph Substitutions. In *Proceedings of the 27th ACM Symposium on Operating Systems Principles* (Huntsville, Ontario, Canada) (SOSP '19). Association for Computing Machinery, New York, NY, USA, 47–62. <https://doi.org/10.1145/3341301.3359630>
- Aleks Kissinger and John van de Wetering. 2019a. Pyzx: Large scale automated diagrammatic reasoning. *arXiv preprint arXiv:1904.04735* (2019).
- Aleks Kissinger and John van de Wetering. 2019b. Reducing T-count with the ZX-calculus. *arXiv preprint arXiv:1903.10477* (2019).
- Ramana Kumar, Magnus O. Myreen, Michael Norrish, and Scott Owens. 2014. CakeML: A Verified Implementation of ML. *SIGPLAN Not.* 49, 1 (jan 2014), 179–191. <https://doi.org/10.1145/2578855.2535841>
- Sorin Lerner, Todd Millstein, and Craig Chambers. 2003. Automatically Proving the Correctness of Compiler Optimizations. In *Proceedings of the ACM SIGPLAN 2003 Conference on Programming Language Design and Implementation* (San Diego, California, USA) (PLDI '03). Association for Computing Machinery, New York, NY, USA, 220–231. <https://doi.org/10.1145/781131.781156>
- Xavier Leroy. 2009. Formal Verification of a Realistic Compiler. *Commun. ACM* 52, 7 (jul 2009), 107–115. <https://doi.org/10.1145/1538788.1538814>
- Sophia Fuhui Lin, Sara Sussman, Casey Duckering, Pranav S. Mundada, Jonathan M. Baker, Rohan S. Kumar, Andrew A. Houck, and Frederic T. Chong. 2022. Let Each Quantum Bit Choose Its Basis Gates. In *2022 55th IEEE/ACM International Symposium on Microarchitecture (MICRO)*. 1042–1058. <https://doi.org/10.1109/MICRO56248.2022.00075>
- Norbert M Linke, Dmitri Maslov, Martin Roetteler, Shantanu Debnath, Caroline Figgatt, Kevin A Landsman, Kenneth Wright, and Christopher Monroe. 2017. Experimental comparison of two quantum computing architectures. *Proceedings of the National Academy of Sciences* 114, 13 (2017), 3305–3310. <https://doi.org/10.1073/pnas.1618020114>
- Nuno P. Lopes, Juneyoung Lee, Chung-Kil Hur, Zhengyang Liu, and John Regehr. 2021. Alive2: bounded translation validation for LLVM. In *PLDI*. ACM, 65–79. <https://doi.org/10.1145/3453483.3454030>
- Nuno P. Lopes, David Menendez, Santosh Nagarakatte, and John Regehr. 2015. Provably correct peephole optimizations with alive. In *PLDI*. ACM, 22–32. <https://doi.org/10.1145/2813885.2737965>
- David C McKay, Christopher J Wood, Sarah Sheldon, Jerry M Chow, and Jay M Gambetta. 2017. Efficient Z gates for quantum computing. *Physical Review A* 96, 2 (2017), 022330. <https://doi.org/10.1103/PhysRevA.96.022330>
- Giulia Meuli, Mathias Soeken, and Giovanni Micheli. 2018. SAT-based CNOT, T Quantum Circuit Synthesis: 10th International Conference, RC 2018, Leicester, UK, September 12-14, 2018, Proceedings. 175–188. [https://doi.org/10.1007/978-3-319-99498-7\\_12](https://doi.org/10.1007/978-3-319-99498-7_12)
- Rajeev Motwani and Prabhakar Raghavan. 1995. *Randomized algorithms*. Cambridge university press. <https://doi.org/10.1017/CBO9780511814075>
- Eric Mullen, Daryl Zuniga, Zachary Tatlock, and Dan Grossman. 2016. Verified peephole optimizations for CompCert. In *PLDI*. ACM, 448–461. <https://doi.org/10.1145/2908080.2908109>
- Prakash Murali, David C McKay, Margaret Martonosi, and Ali Javadi-Abhari. 2020. Software mitigation of crosstalk on noisy intermediate-scale quantum computers. In *Proceedings of the Twenty-Fifth International Conference on Architectural Support for Programming Languages and Operating Systems*. 1001–1016. <https://doi.org/10.1145/3373376.3378477>
- Yunseong Nam, Neil J Ross, Yuan Su, Andrew M Childs, and Dmitri Maslov. 2018. Automated optimization of large quantum circuits with continuous parameters. *npj Quantum Information* 4, 1 (2018), 1–12. <https://doi.org/10.1038/s41534-018-0072-4>
- Matteo Paltenghi and Michael Pradel. 2022. Bugs in Quantum computing platforms: an empirical study. *Proceedings of the ACM on Programming Languages* 6, OOPSLA1 (2022), 1–27. <https://doi.org/10.1145/3527330>
- Tirthank Patel, Ed Younis, Costin Iancu, Wibe de Jong, and Devesh Tiwari. 2022. QUEST: Systematically Approximating Quantum Circuits for Higher Output Fidelity. In *Proceedings of the 27th ACM International Conference on Architectural Support for Programming Languages and Operating Systems* (Lausanne, Switzerland) (ASPLOS 2022). Association for Computing Machinery, New York, NY, USA, 514–528. <https://doi.org/10.1145/3503222.3507739>

- Jessica Pointing, Oded Padon, Zhihao Jia, Henry Ma, Auguste Hirth, Jens Palsberg, and Alex Aiken. 2021. Quanto: Optimizing Quantum Circuits with Automatic Generation of Circuit Identities. *CoRR* abs/2111.11387 (2021).
- John Preskill. 2018. Quantum computing in the NISQ era and beyond. *Quantum* 2 (2018), 79. <https://doi.org/10.22331/q-2018-08-06-79>
- PyZX. 2023. PyZX Full API documentation. [https://pyzx.readthedocs.io/en/latest/api.html#pyzx.optimize.phase\\_block\\_optimize](https://pyzx.readthedocs.io/en/latest/api.html#pyzx.optimize.phase_block_optimize).
- Google Quantum-AI. 2021. Quantum Computer Datasheet. (Accessed on 11/22/2021).
- Robert Rand, Jennifer Paykin, Dong-Ho Lee, and Steve Zdancewic. 2018. ReQWIRE: Reasoning about Reversible Quantum Circuits. In *QPL (EPTCS, Vol. 287)*. 299–312. <https://doi.org/10.4204/EPTCS.287.17>
- Rigetti. 2022. Rigetti Aspen-11. <https://www.rigetti.com>.
- Mark Saffman. 2019. The next step in making arrays of single atoms.
- Raimondas Sasnauskas, Yang Chen, Peter Collingbourne, Jeroen Ketema, Gratian Lup, Jubi Taneja, and John Regehr. 2017. Souper: A synthesizing superoptimizer. *arXiv preprint arXiv:1711.04422* (2017).
- Vivek V. Shende, Igor L. Markov, and Stephen S. Bullock. 2004. Minimal universal two-qubit controlled-NOT-based circuits. *Phys. Rev. A* 69 (Jun 2004), 062321. Issue 6. <https://doi.org/10.1103/PhysRevA.69.062321>
- Yunong Shi, Runzhou Tao, Xupeng Li, Ali Javadi-Abhari, Andrew W Cross, Frederic T Chong, and Ronghui Gu. 2019. CertiQ: A Mostly-automated Verification of a Realistic Quantum Compiler. *arXiv preprint arXiv:1908.08963* (2019).
- Seyon Sivarajah, Silas Dilkes, Alexander Cowtan, Will Simmons, Alec Edgington, and Ross Duncan. 2020. t|ket>: a retargetable compiler for NISQ devices. *Quantum Science and Technology* 6, 1 (2020), 014003. <https://doi.org/10.1088/2058-9565/ab8e92>
- Robert S. Smith, Eric C. Peterson, Mark G. Skilbeck, and Erik J. Davis. 2020. An Open-Source, Industrial-Strength Optimizing Compiler for Quantum Programs. *CoRR* abs/2003.13961 (2020). <https://doi.org/10.1088/2058-9565/ab9acb>
- Chengnian Sun, Vu Le, Qirun Zhang, and Zhendong Su. 2016. Toward understanding compiler bugs in GCC and LLVM. In *Proceedings of the 25th International Symposium on Software Testing and Analysis, ISSTA 2016, Saarbrücken, Germany, July 18-20, 2016*, Andreas Zeller and Abhik Roychoudhury (Eds.). ACM, 294–305. <https://doi.org/10.1145/2931037.2931074>
- Runzhou Tao, Yunong Shi, Jianan Yao, Xupeng Li, Ali Javadi-Abhari, Andrew W. Cross, Frederic T. Chong, and Ronghui Gu. 2022. Giallar: Push-Button Verification for the Qiskit Quantum Compiler. In *Proceedings of the 43rd ACM SIGPLAN International Conference on Programming Language Design and Implementation (San Diego, CA, USA) (PLDI 2022)*. Association for Computing Machinery, New York, NY, USA, 641–656. <https://doi.org/10.1145/3519939.3523431>
- Haojie Wang, Jidong Zhai, Mingyu Gao, Zixuan Ma, Shizhi Tang, Liyan Zheng, Yuanzhi Li, Kaiyuan Rong, Yuanrong Chen, and Zhihao Jia. 2021. PET: Optimizing Tensor Programs with Partially Equivalent Transformations and Automated Corrections. In *15th USENIX Symposium on Operating Systems Design and Implementation (OSDI 21)*. USENIX Association, 37–54. <https://www.usenix.org/conference/osdi21/presentation/wang>
- TF Watson, SGJ Philips, Erika Kawakami, DR Ward, Pasquale Scarlino, Menno Veldhorst, DE Savage, MG Lagally, Mark Friesen, SN Coppersmith, et al. 2018. A programmable two-qubit quantum processor in silicon. *nature* 555, 7698 (2018), 633–637. <https://doi.org/10.1038/nature25766>
- Christopher D Wilen, S Abdullah, NA Kurinsky, C Stanford, L Cardani, G d’Imperio, C Tomei, L Faoro, LB Ioffe, CH Liu, et al. 2021. Correlated charge noise and relaxation errors in superconducting qubits. *Nature* 594, 7863 (2021), 369–373. <https://doi.org/10.1038/s41586-021-03557-5>
- Max Willsey, Chandrakana Nandi, Yisu Remy Wang, Oliver Flatt, Zachary Tatlock, and Pavel Panekha. 2021. Egg: Fast and extensible equality saturation. *Proceedings of the ACM on Programming Languages* 5, POPL (2021), 1–29. <https://doi.org/10.1145/3434304>
- Amanda Xu, Abtin Molavi, Lauren Pick, Swamit Tannu, and Aws Albarghouthi. 2023. *Synthesizing Quantum-Circuit Optimizers Artifact (QUESO)*. <https://doi.org/10.5281/zenodo.7809285>
- Mingkuan Xu, Zikun Li, Oded Padon, Sina Lin, Jessica Pointing, Auguste Hirth, Henry Ma, Jens Palsberg, Alex Aiken, Umut A. Acar, and Zhihao Jia. 2022. Quartz: Superoptimization of Quantum Circuits. In *Proceedings of the 43rd ACM SIGPLAN International Conference on Programming Language Design and Implementation (San Diego, CA, USA) (PLDI 2022)*. Association for Computing Machinery, New York, NY, USA, 625–640. <https://doi.org/10.1145/3519939.3523433>



## A QUANTUM HARDWARE

**What are different quantum hardware platforms?** Physically, a quantum bit (qubit) can be realized using superconducting, semiconductor, or atomic qubit devices. For example, IBM, Rigetti, and Google use superconducting architecture, whereas IonQ and Honeywell use atomic qubits. The design tradeoffs between different quantum hardware platforms are summarized in [Linke et al. 2017].

**How are gates performed on hardware?** Quantum hardware has two parts – (1) qubit devices and (2) a control computer. The control computer manipulates qubit states by sending control pulses to the qubit devices. For superconducting qubits, gates are performed by using the sequence of microwave control pulses, whereas shining laser pulses manipulate atomic qubits. The control computer can support different gates by changing the sequence or re-shaping these control pulses. Typically the pulse sequences and shapes are stored in the FPGAs, which drive the microwave signal generators or the lasers. We can add a gate to the basis by reprogramming the control FPGA.

**Why are two-qubit gates significantly error prone?** Two qubit gates entangle quantum bits using complex and relatively long control pulses to qubit devices. A qubit can decay to the lowest possible energy state during gate operations. Furthermore, the longer the gate duration, the exponentially higher the chances of qubit decay. As a result, the two-qubit gate error is about 10x higher, about 1%, on most industrial quantum computers [IBM 2022; IonQ 2022a; Quantum-AI 2021; Rigetti 2022]. Furthermore, two-qubit gates corrupt both the qubit devices involved in the operation and impose crosstalk errors on neighboring qubit devices, significantly degrading the output quality [Das et al. 2021; Murali et al. 2020].

**What are "perfect" virtual gates?** On most quantum hardware platforms,  $R_z$  gates are implemented in software virtually [McKay et al. 2017]. *These virtual gates have zero latency and perfect fidelity.* The insight behind the virtual gate is quite elegant.  $R_z$  gates affect the phase of the qubit state, which can be performed by simply adding a phase offset to the subsequent  $R_x$  or  $R_y$  gate pulses, such that the subsequent gate not only performs the intended operation but also adds the phase required by the  $R_z$  gate. If the subsequent gate is another  $R_z$  gate or sequence of  $R_z$  gates, then the phase offset corresponding to the sum of all rotation angles in the sequence is used. Due to this hardware optimization, reducing the  $R_z$  gate at the compiler level does not yield any fidelity benefits. Therefore, *to evaluate the effectiveness of QUESO, we count physical gates and omit "virtual"  $R_z$  gates that are perfect and do not degrade fidelity on real quantum hardware.*

**Why are basis gates changing?** On conventional computers and accelerators, instruction sets are rigid, as changing the instruction set involves physically redesigning the chip, whereas quantum hardware is highly reconfigurable. Engineers leverage this flexibility and continuously tune gates to enable higher gate fidelities. For example, all IBM platforms recently modified their basis gates to support less flexible but more noise-tolerant gates by upgrading their control computer firmware. With scaling quantum hardware, basis gates are expected to change as hardware is evolving rapidly with the innovation in qubit devices and qubit control. If we design compiler optimizations for fixed basis gates, we will need to hand-tune the optimization every time we change the basis gates. Recent work has also shown that it can be beneficial to allow basis gates to differ across qubits based on calibration data to minimize errors [Lin et al. 2022].



## B SAMPLING IN THE RATIONAL DOMAIN

To sample complex numbers on the unit circle, we note that every rational number  $r$  results in a unique rational coordinate on the unit circle:

$$\left( \frac{r^2 - 1}{1 + r^2}, \frac{2r}{1 + r^2} \right)$$

Specifically,  $r$  is the slope of the line between  $(1, 0)$  and the point above.

Therefore, if we uniformly sample  $r$  from any finite subset of  $\mathbb{Q}$  and apply the above formula, we have a complex number on the unit circle:

- Let  $X \subset \mathbb{Q}$ .
- Sample  $r$  uniformly from  $X$ .
- Return  $\frac{r^2-1}{1+r^2} + \frac{2r}{1+r^2}i$

**THEOREM B.1.** *The above procedure uniformly samples from the set*

$$\left\{ \frac{r^2 - 1}{1 + r^2} + \frac{2r}{1 + r^2}i \mid r \in X \right\}$$

**PROOF.** Follows from the fact that each  $r \in X$  produces a unique number on the unit circle,  $\frac{r^2-1}{1+r^2} + \frac{2r}{1+r^2}i$ . Since  $r$  is sampled uniformly from  $X$ , the output of the algorithm is uniformly distributed over the set  $\left\{ \frac{r^2-1}{1+r^2} + \frac{2r}{1+r^2}i \mid r \in X \right\}$ .  $\square$

## C MORE IMPLEMENTATION DETAILS

### C.1 Pruning techniques

In addition to the pruning adopted from Quartz described in § 5 we prune rules that satisfy the following:

- Either side is a disconnected graph. The way we enumerate circuits syntactically results in some rules that are unnecessary in the quantum setting such as the rule saying two gates on different qubits can commute.
- The pattern to search for contains a parameter with an arithmetic expression such as  $\theta_1 + \theta_2$ . Unless the parameter also appears in the replacement, the search would need to decompose an angle into a sum of two angles to find a match.
- The symbolic parameters in the replacement are not a subset of the symbolic parameters in the pattern. For example, this is possible when the symbolic parameters on both sides sum to zero.
- The qubits in the replacement are not a subset of the qubits in the pattern. This can happen in symbolic rules if the state transformer swaps the state of two qubits.
- A symbolic rule where the subcircuit before or after the symbolic gate in the pattern is empty. This is for efficiency and limits the search for a matching symbolic subcircuit to cases where it is more constrained. Additionally, rules of this form are almost always size-preserving rules, which Fig. 24 shows do not help in most cases.

### C.2 Experimental setup

**Instantiation of QUESO.** Table 2 shows the different parameters included in the grammar when synthesizing each gate set. For the IBM gate set, each parameter is only allowed to be used once in a circuit. We limit circuits with symbolic gates to have at most 2 qubits. We found that using symbolic rules of size at most 3 resulted in the best performance. The maximum sizes of non-symbolic rules

used are shown in Table 1. For the Ion gate set, we use a cost function that excludes  $R_z$  gates from the total gate count.

Table 2. Parameters allowed in synthesis

Gate set	Parameters
IBM	$\theta_1, \theta_2, \theta_3, \theta_1 + \theta_2, \theta_1 + \theta_2 + \theta_3$
Nam	$\theta_1, \theta_2, \theta_1 + \theta_2$
Rigetti	$\theta_1, \theta_2, \theta_1 + \theta_2, -\theta_1$
Ion	$\theta_1, \theta_2, \theta_1 + \theta_2, -\theta_1, \pi, \frac{\pi}{2}$

**Invoking other tools.** We invoked VOQC, TKET, Quilc, and Qiskit using their Python interfaces. We ran Quartz using the same parameters from [Xu et al. 2022]. Because Quartz behaves non-deterministically for the mod5\_4 benchmark on the Nam gate set, we report an average of 7 runs.

**Hardware.** All benchmarks were executed on a cluster of Intel® Xeon®, AMD EPYC™, and AMD Opteron™ CPUs clocked an average of 2.4GHz.

**Calculating fidelity.** We use the following publically reported gate fidelities for each device where  $f_1$  and  $f_2$  are the fidelities for single and two-qubit gates, respectively:

**IBM Toronto [IBM 2022]**  $f_1 = 0.999606, f_2 = 0.98719$

**Rigetti Aspen-11 [Rigetti 2022]**  $f_1 = 0.998, f_2 = 0.902$

**IonQ Aria [IonQ 2022a]**  $f_1 = 0.9995, f_2 = 0.996$

## D PROOFS

### D.1 Lem. 4.5

Follows directly from the definition of equivalence.

### D.2 Thm. 4.6

By contradiction: Suppose Eq. (6) does not hold but  $C_1$  and  $C_2$  are equivalent. By Lem. 4.5, we know that  $\psi_1^x(\mathbf{y}, \rho) = \psi_2^x(\mathbf{y}, \rho)$ , but there must be a value  $c$  such that  $c \cdot \psi_1^x(\mathbf{y}, \rho) \neq c \cdot \psi_2^x(\mathbf{y}, \rho)$ . Contradiction.

Conversely, suppose that Eq. (6) holds but  $C_1$  and  $C_2$  are not equivalent. By Lem. 4.5, this means that there is a valuation of the variables  $\mathbf{x}, \mathbf{y}, \dots$  such that  $\psi_1^x(\mathbf{y}, \rho) \neq \psi_2^x(\mathbf{y}, \rho)$ . Then, for  $v_{\mathbf{x}, \mathbf{y}} \neq 0$ , we have  $v_{\mathbf{x}, \mathbf{y}} \psi_1^x(\mathbf{y}, \rho) \neq v_{\mathbf{x}, \mathbf{y}} \psi_2^x(\mathbf{y}, \rho)$ . Hence, Eq. (6) does not hold.

### D.3 Thm. 4.8

We will prove this by way of the contrapositive. The idea is that the transformation induces a bijective correspondence between counterexamples to equivalence. Suppose first that  $C_1 \not\equiv C_2$ , where the amplitudes for  $C_1$  are given by

$$\psi_1^a(\mathbf{b}, \rho) = c_{\mathbf{a}, \mathbf{b}} \prod_{i=1}^p (\phi_i^u(\mathbf{a}, \mathbf{b}))^{m_i} \prod_{j=1}^k (e^{i\theta_j})^{n_j}$$

and the amplitudes for  $C_2$  are given by

$$\psi_2^a(\mathbf{b}, \rho) = c'_{\mathbf{a}, \mathbf{b}} \prod_{i=1}^p (\phi_i^u(\mathbf{a}, \mathbf{b}))^{m_i} \prod_{j=1}^k (e^{i\theta_j})^{n'_j}$$

This means that there is some  $\mathbf{a}, \mathbf{b} \in \mathbb{Z}_2^n$ , interpretation of the amplitude transformers  $\hat{\phi}_1^u, \dots, \hat{\phi}_p^u$  and value of the parameters  $\hat{\theta}_1 \dots \hat{\theta}_k$  such that

$$c_{\mathbf{a},\mathbf{b}} \prod_{i=1}^p (\hat{\phi}_i^u(\mathbf{a}, \mathbf{b}))^{m_i} \prod_{j=1}^k (e^{i\hat{\theta}_j})^{n_i} \neq c'_{\mathbf{a},\mathbf{b}} \prod_{i=1}^p (\hat{\phi}_i^u(\mathbf{a}, \mathbf{b}))^{m'_i} \prod_{j=1}^k (e^{i\hat{\theta}_j})^{n'_i}$$

Therefore, there is a point such that we have the following inequality between polynomials.

$$\sum_{\mathbf{x}, \mathbf{y} \in \mathbb{Z}_2^n} c_{\mathbf{x}, \mathbf{y}} v_{\mathbf{x}, \mathbf{y}} \prod_{i=1}^p (\hat{\phi}_{i, \mathbf{x}, \mathbf{y}}^u)^{m_i} \prod_{j=1}^k (v_{\theta_j})^{n_i} \neq \sum_{\mathbf{x}, \mathbf{y} \in \mathbb{Z}_2^n} c'_{\mathbf{x}, \mathbf{y}} v_{\mathbf{x}, \mathbf{y}} \prod_{i=1}^p (\hat{\phi}_{i, \mathbf{x}, \mathbf{y}}^u)^{m'_i} \prod_{j=1}^k (v_{\theta_j})^{n'_i}$$

Namely, set  $\hat{\phi}_{i, \mathbf{a}, \mathbf{b}}^u = \hat{\phi}_i^u(\mathbf{a}, \mathbf{b})$ ,  $v_{\theta_j} = e^{i\hat{\theta}_j}$ , and  $v_{\mathbf{a}, \mathbf{b}} = 1$  and all other variables to 0.

The other direction is similar. Given a point  $\hat{\phi}_{i, \mathbf{a}, \mathbf{b}}^u$ ,  $\hat{v}_{\theta_j}$ , and  $\hat{v}_{\mathbf{a}, \mathbf{b}}$  such that the polynomials are not equal, choose some  $\mathbf{a}, \mathbf{b}$  such that the corresponding terms evaluate to different values at this point. Then define an interpretation of the amplitude transformers by  $\hat{\phi}_i^u(\mathbf{a}, \mathbf{b}) = \hat{\phi}_{i, \mathbf{a}, \mathbf{b}}^u$ . Recall that each  $\hat{v}_{\theta_j}$  is in  $\mathbb{S}$ . Let  $\theta_j = \hat{\theta}_j$  where  $\hat{\theta}_j$  is the unique value in  $[0, 2\pi)$  satisfying  $\cos \hat{\theta}_j = \text{Re}(\hat{v}_{\theta_j})$  and  $\sin \hat{\theta}_j = \text{Im}(\hat{v}_{\theta_j})$ .

#### D.4 Thm. 6.2

Let  $\llbracket S(I) \rrbracket$  be of the form  $\hat{\phi}^u(\mathbf{x}) |f(\mathbf{x})\rangle$  where  $n = |\mathbf{x}|$ . That is, it has an interpreted state transformer but an uninterpreted amplitude transformer and operates over  $n$  qubits. Let  $\llbracket C_S \rrbracket$  be of the form  $\hat{\phi}(\mathbf{x} \dots) |f(\mathbf{x} \dots)\rangle$  where both the state and amplitude transformers are interpreted and  $C_S$  operates over  $k = |\mathbf{x} \dots| \geq n$  qubits. Consider the symbolic rewrite rule  $C_l; S; C'_l \rightarrow C_r; S; C'_r$ . From Alg. 1, this rule would only be synthesized if  $C_l; S; C'_l \equiv C_r; S; C'_r$ . Recall that any circuit that matches the state transformer of  $S$  will satisfy this equivalence because the amplitude transformer is uninterpreted and could therefore be anything. Observe that (1) a state transformer need only match  $S$  for the  $n$  qubits in  $S$  for the equivalence to hold because  $C_l$ ,  $C'_l$ ,  $C_r$ , and  $C'_r$  only operate on at most those  $n$  qubits and (2) the equivalence for the  $k - n$  qubits in  $C_S$  but not  $S$  have their equivalence trivially preserved because only  $C_S$  operates on those qubits. Combining (1) and (2), we get  $C_l; C_S; C'_l \equiv C_r; C_S; C'_r$ .

## E EXPERIMENTAL RESULTS CONTINUED

### E.1 How does QUESO compare to other optimizers in reducing T gate count?

**Results.** We compare against other optimizers with respect to T gate reduction using the Nam gate set. Although T gates can be efficiently simulated in the NISQ setting, they are the primary source of bottlenecks in fault tolerant quantum computing. Fig. 15 shows the results against other optimizers. Notably, we include PyZX now because its primary goal is to reduce T gate count. QUESO is not able to outperform other optimizers using a dedicated rotation merging pass despite being able to synthesize a symbolic rule capturing the essence of rotation merging.

**Summary.** With respect to T gate reduction, QUESO outperforms or matches optimizers that do not use a dedicated rotation merging pass and underperforms optimizers that do.

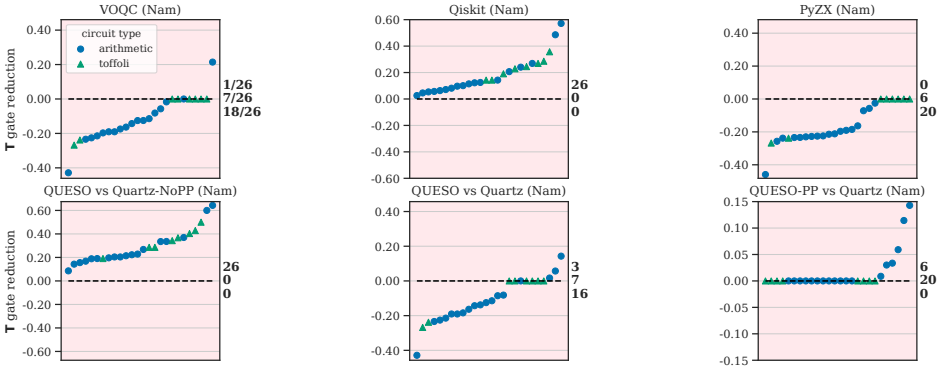


Fig. 15. Comparison against other optimizers with respect to T gate reduction on the Nam gate set.

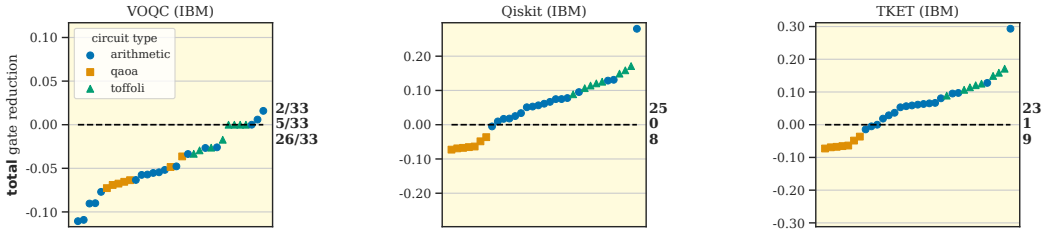
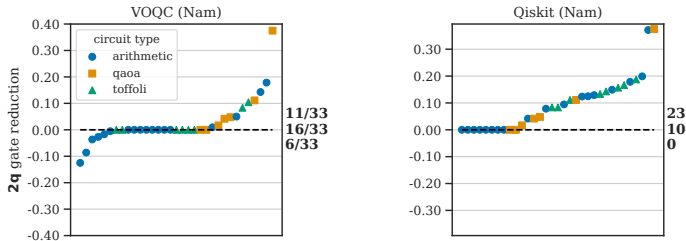


Fig. 16. Comparison against state-of-the-art optimizers for the IBM gate set with respect to total gate count reduction.

(a) Two-qubit gate reduction



(b) Total gate reduction

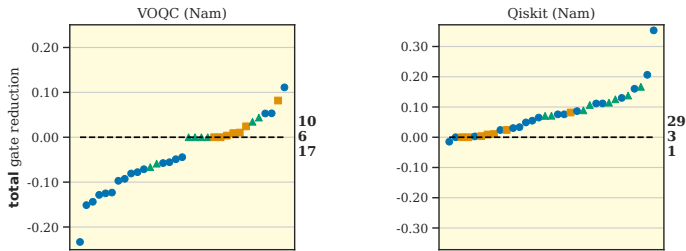


Fig. 17. Comparison against state-of-the-art optimizers for the Nam gate set.

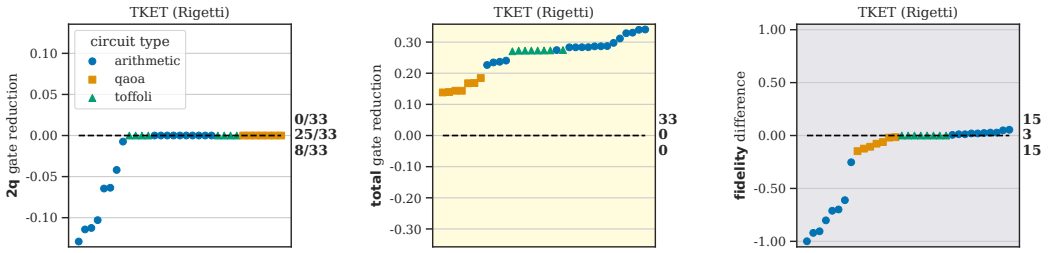


Fig. 18. TKET on Rigetti gate set

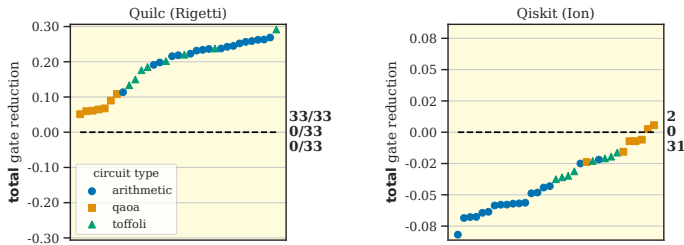


Fig. 19. Total gate reduction on Rigetti gate set compared to Quilc and Ion gate set compared to Qiskit. The cost function for the Ion gate set is excluding  $R_z$  gates.

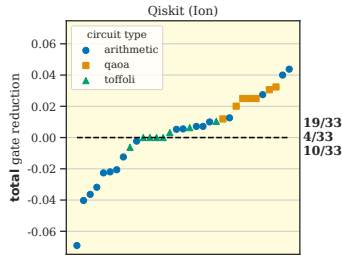


Fig. 20. Total gate reduction on Ion gate set with cost function including  $R_z$  gates.

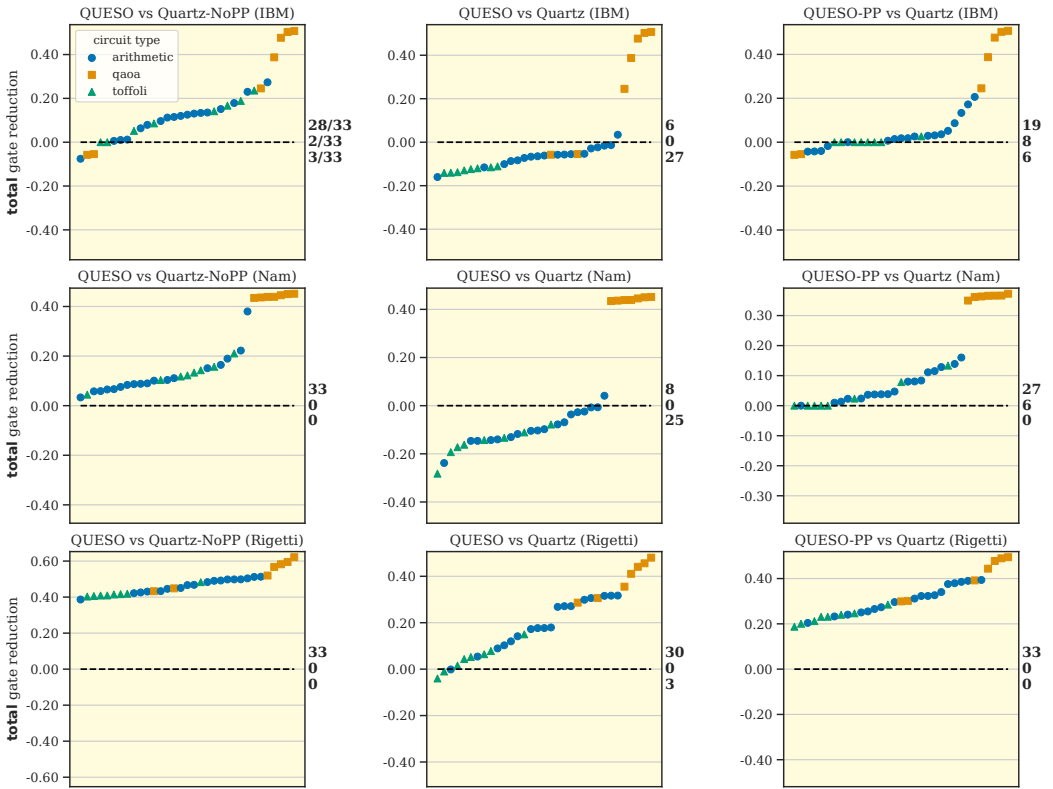


Fig. 21. 1 hour timeout comparison against Quartz on reduction in total gate count with preprocessing disabled and enabled. QUESO-PP is our tool run on the result of Quartz’s preprocessing.



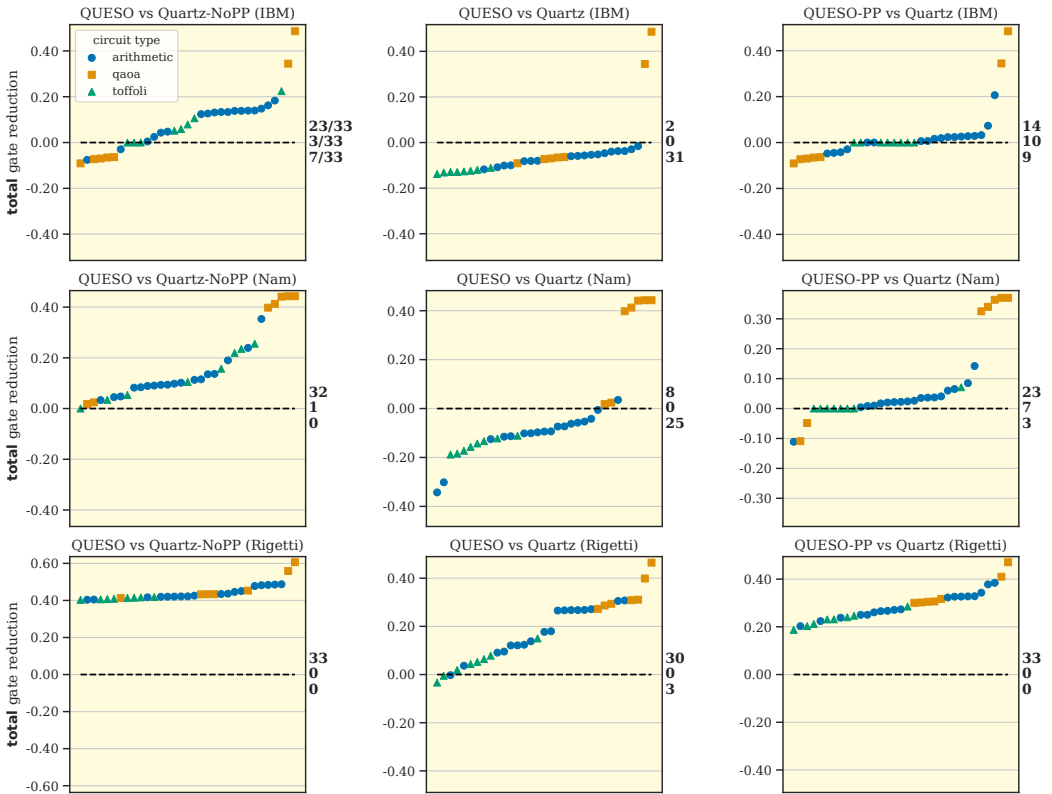


Fig. 22. 24 hour timeout comparison against Quartz on reduction in total gate count with preprocessing disabled and enabled. QUESO-PP is our tool run on the result of Quartz's preprocessing.

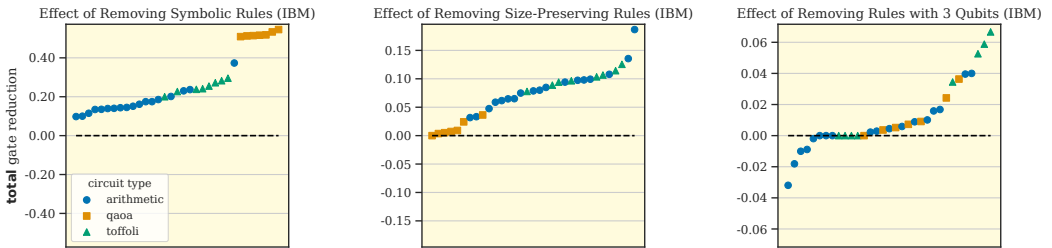


Fig. 23. Comparison between running QUESO using a baseline set of rules and various subsets for total gate reduction.

Effect of Adding Size-Preserving Symbolic Rules (IBM)

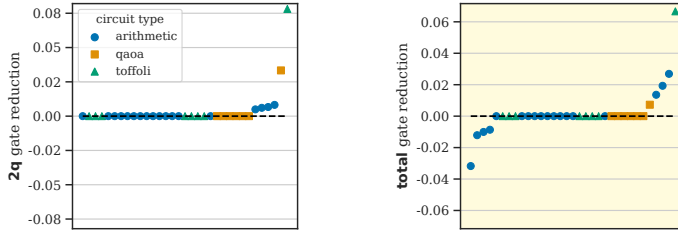


Fig. 24. Comparison between running QUESO using a baseline set of rules and adding size-preserving symbolic rules.

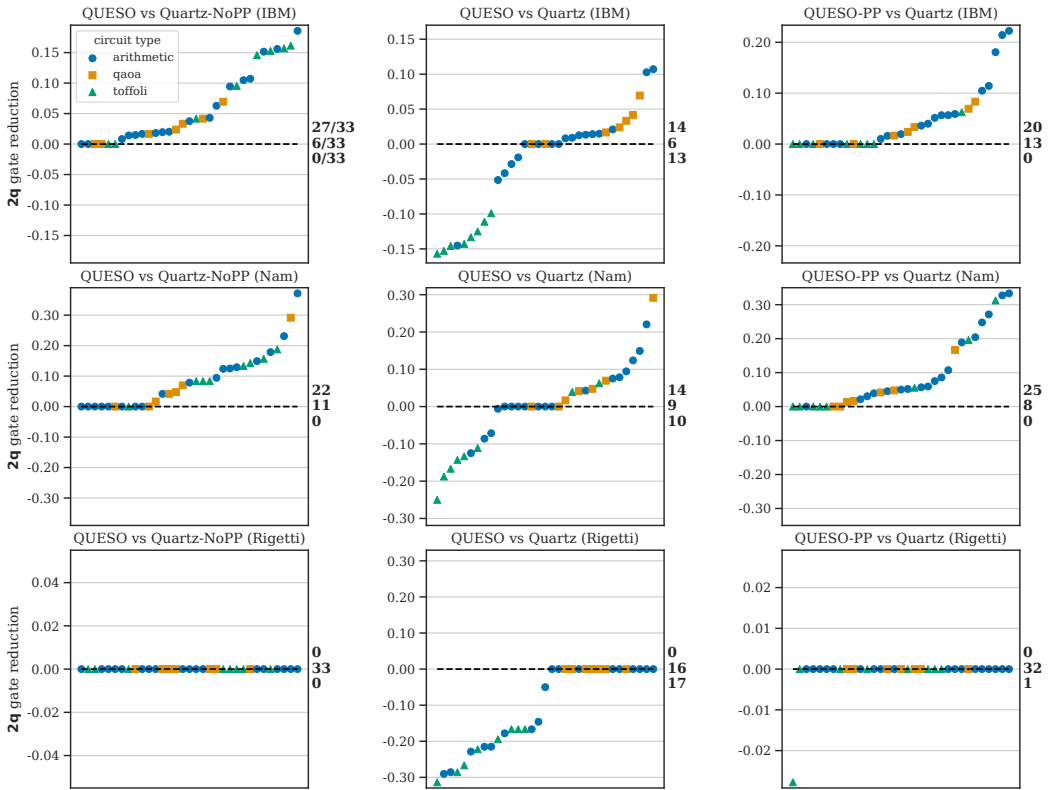


Fig. 25. 2 hour timeout comparison against Quartz.

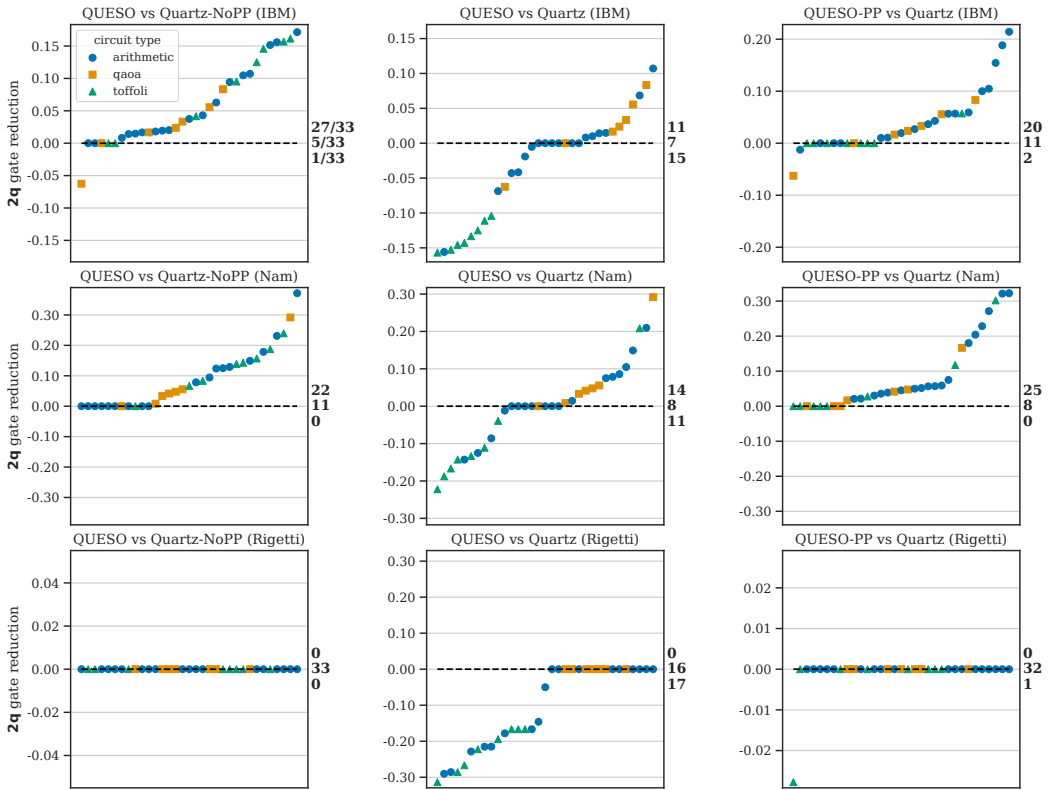


Fig. 26. 3 hour timeout comparison against Quartz.

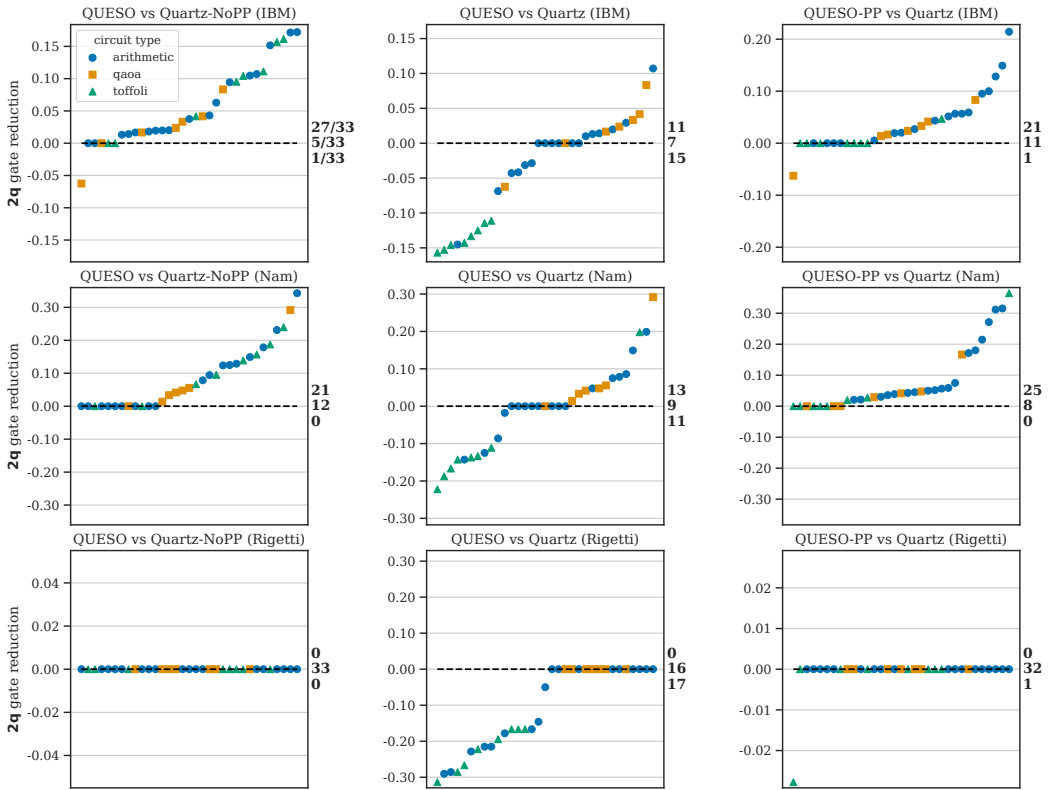


Fig. 27. 4 hour timeout comparison against Quartz.

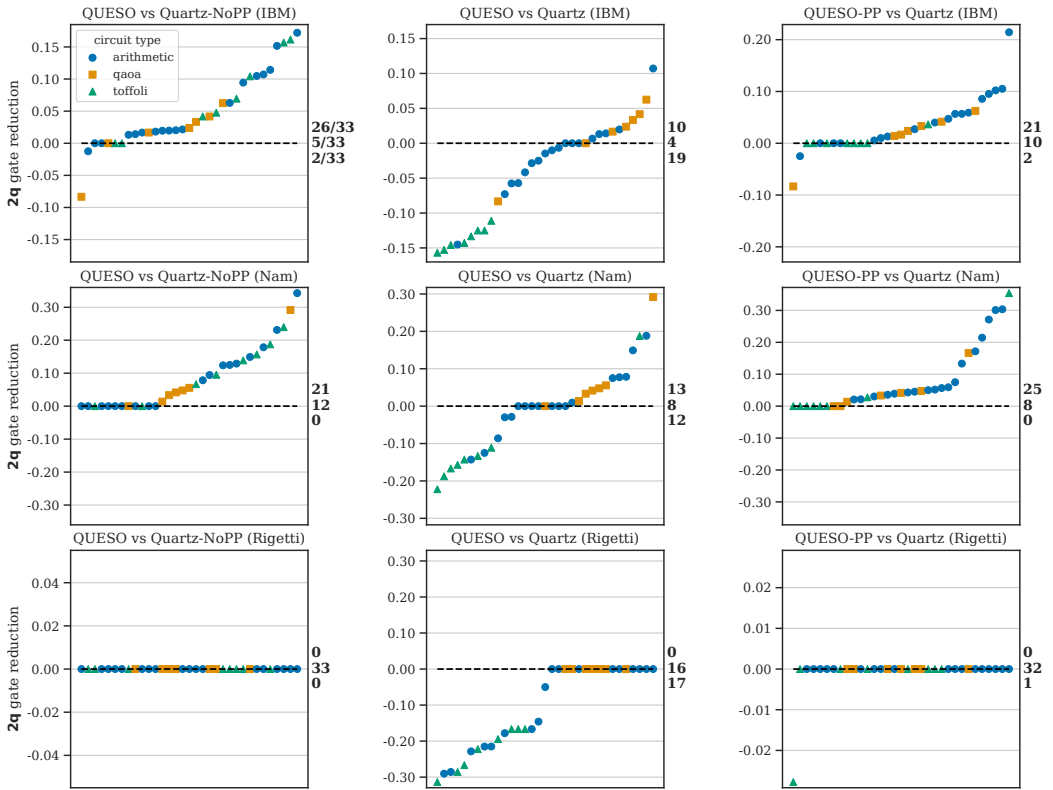


Fig. 28. 5 hour timeout comparison against Quartz.

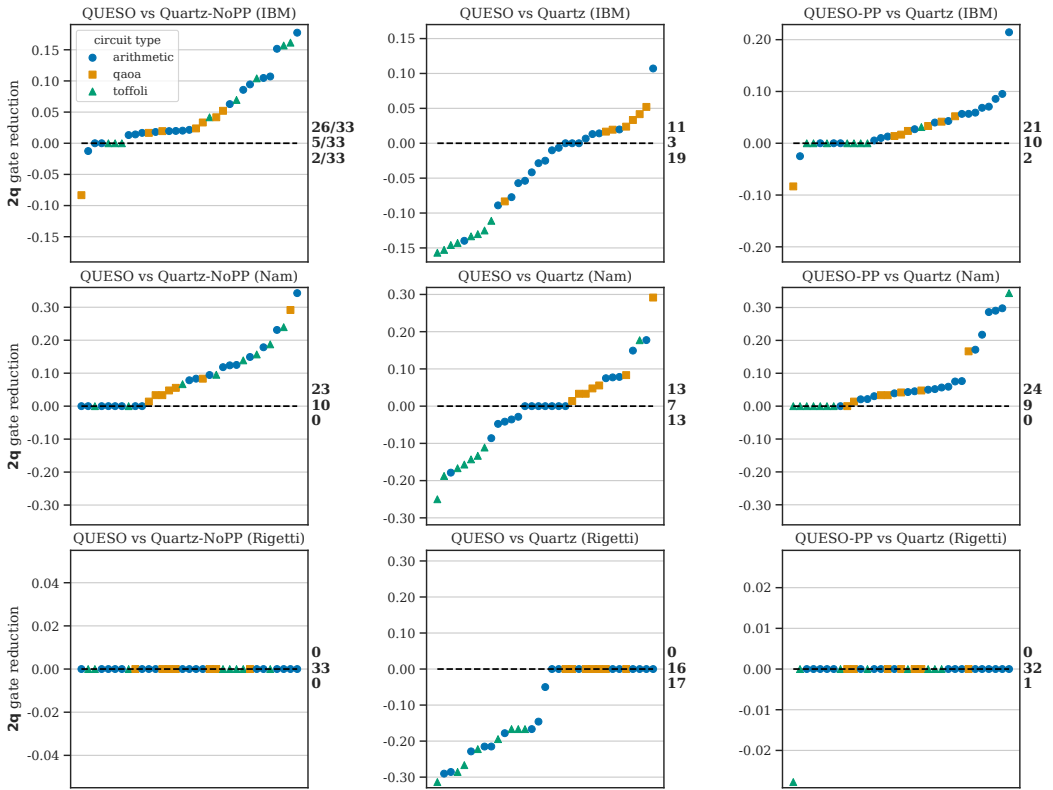


Fig. 29. 6 hour timeout comparison against Quartz.



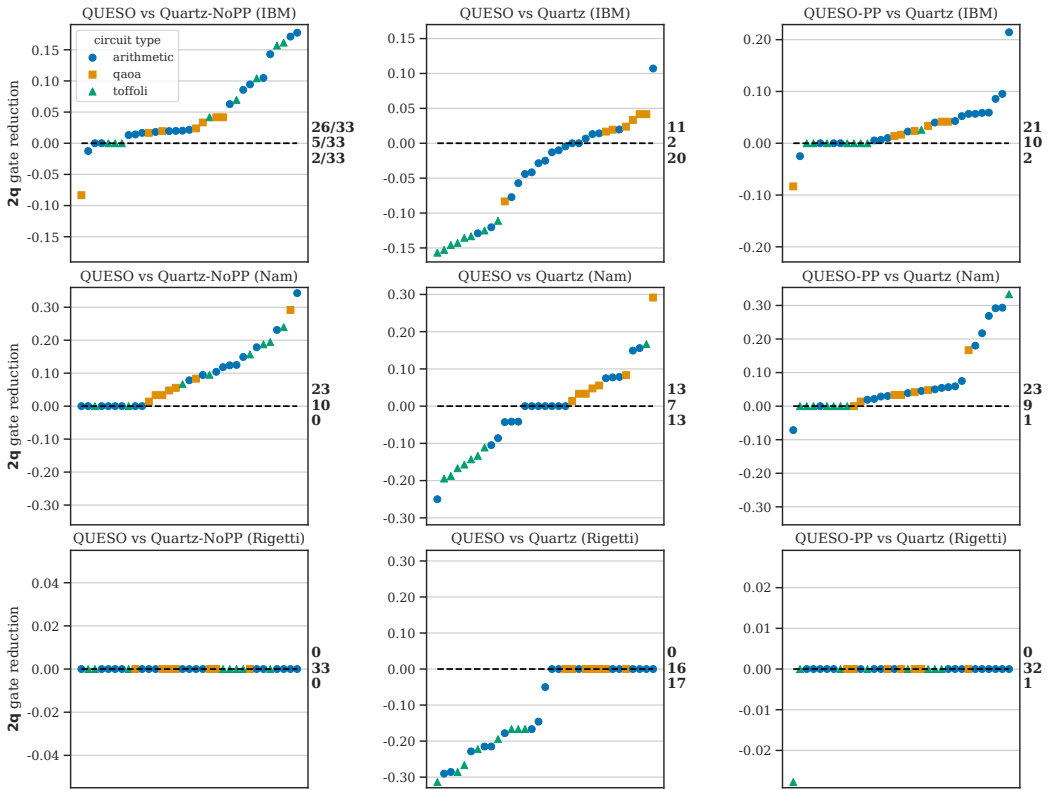


Fig. 30. 7 hour timeout comparison against Quartz.

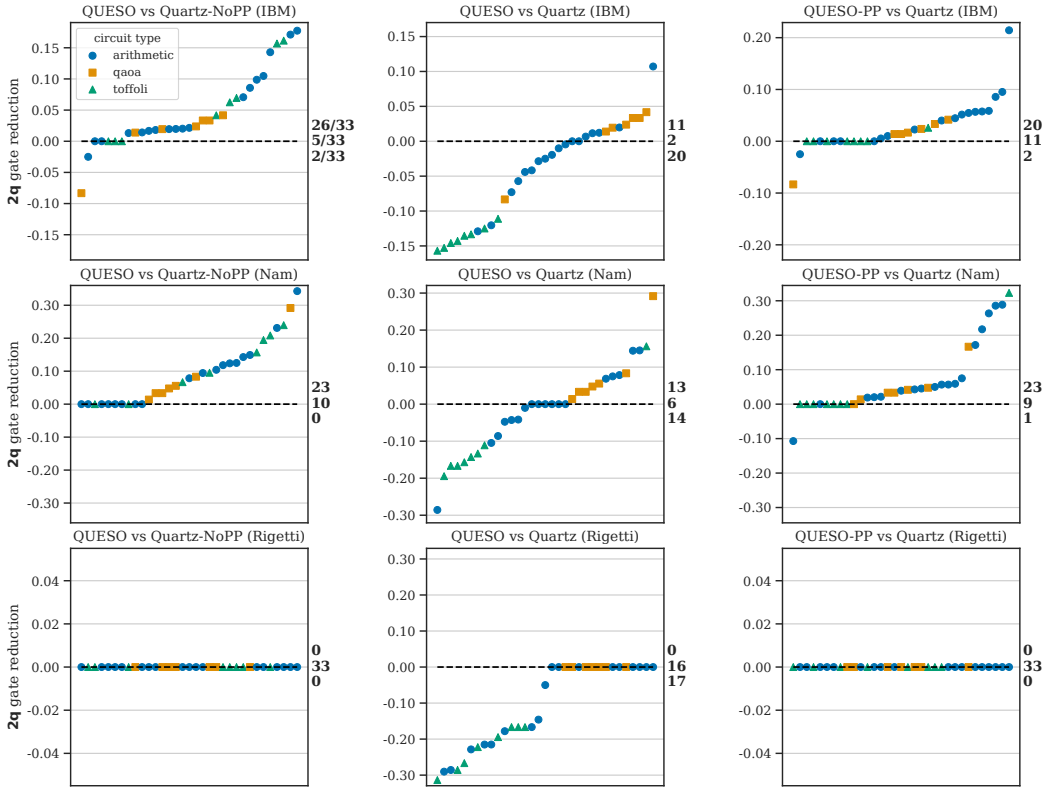


Fig. 31. 8 hour timeout comparison against Quartz.

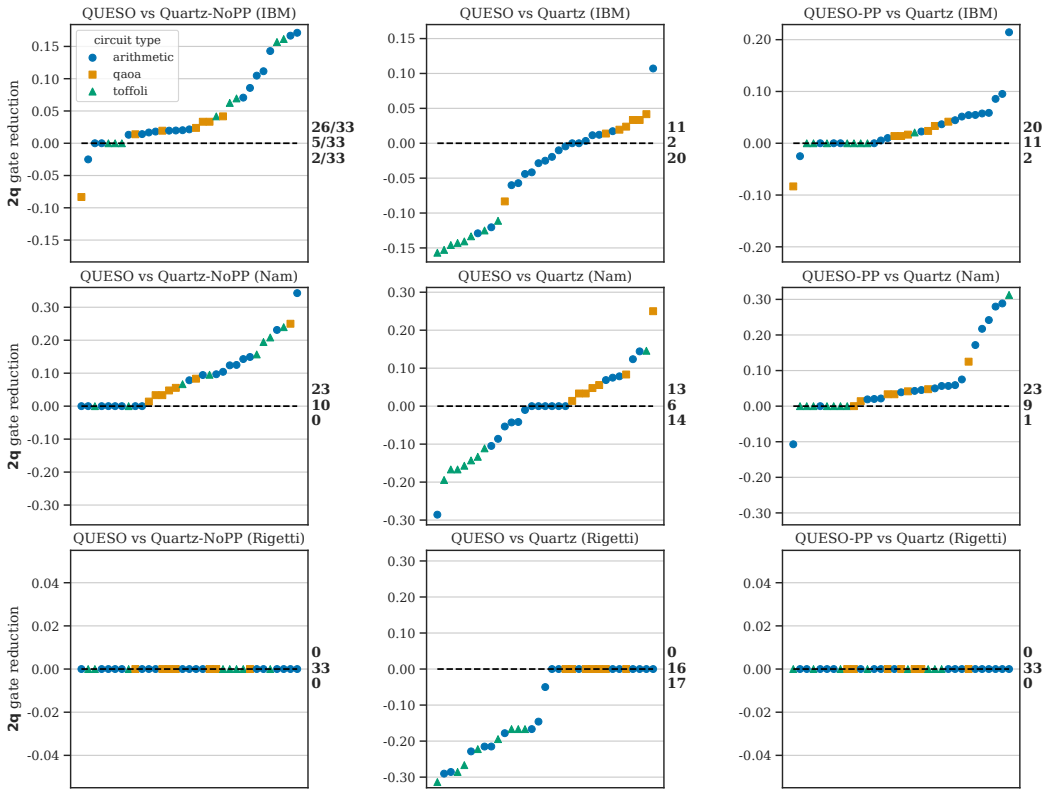


Fig. 32. 9 hour timeout comparison against Quartz.

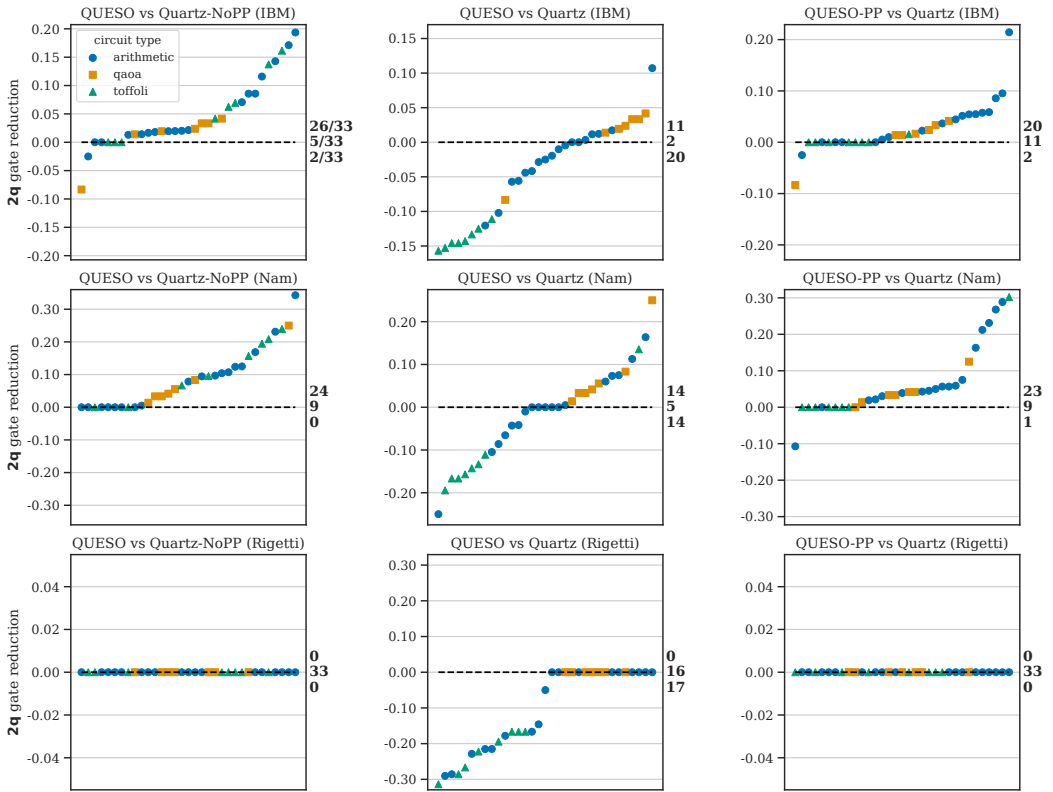


Fig. 33. 10 hour timeout comparison against Quartz.

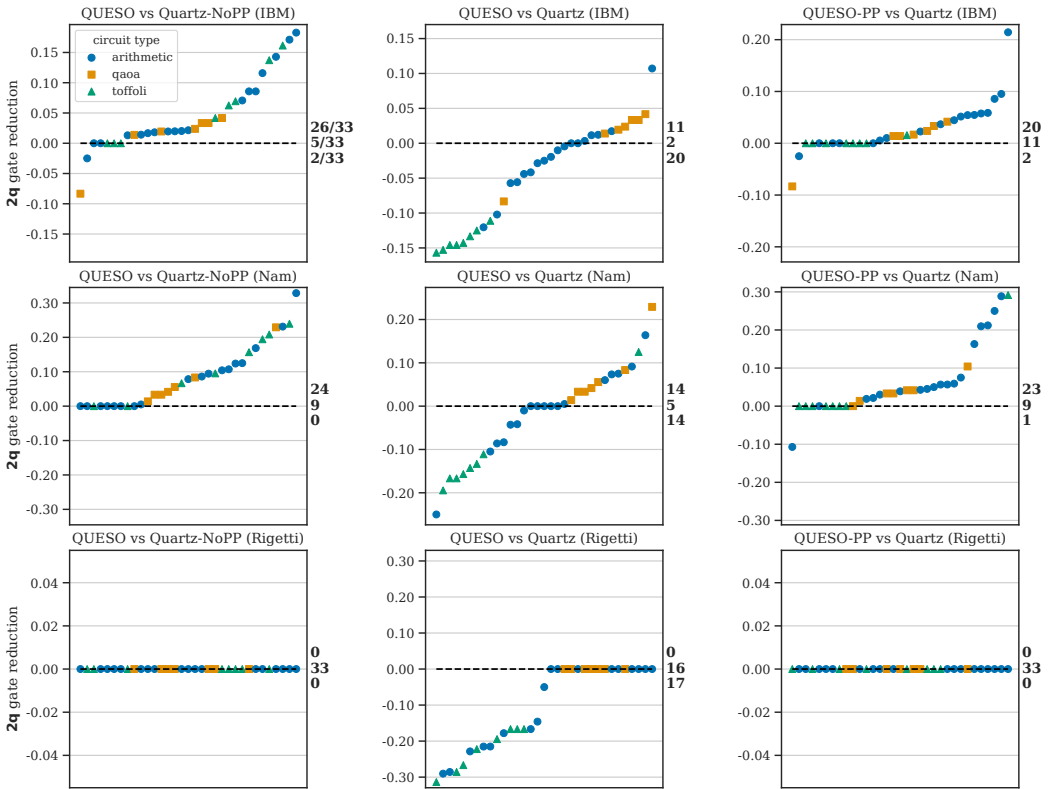


Fig. 34. 11 hour timeout comparison against Quartz.

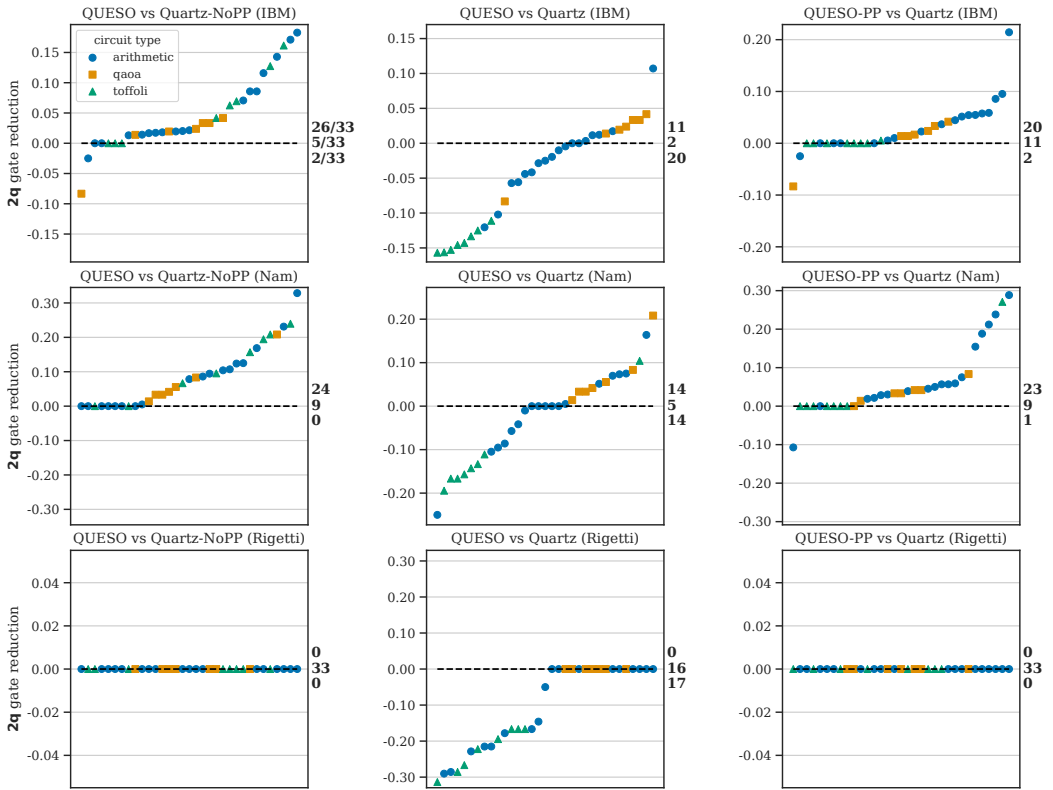


Fig. 35. 12 hour timeout comparison against Quartz.



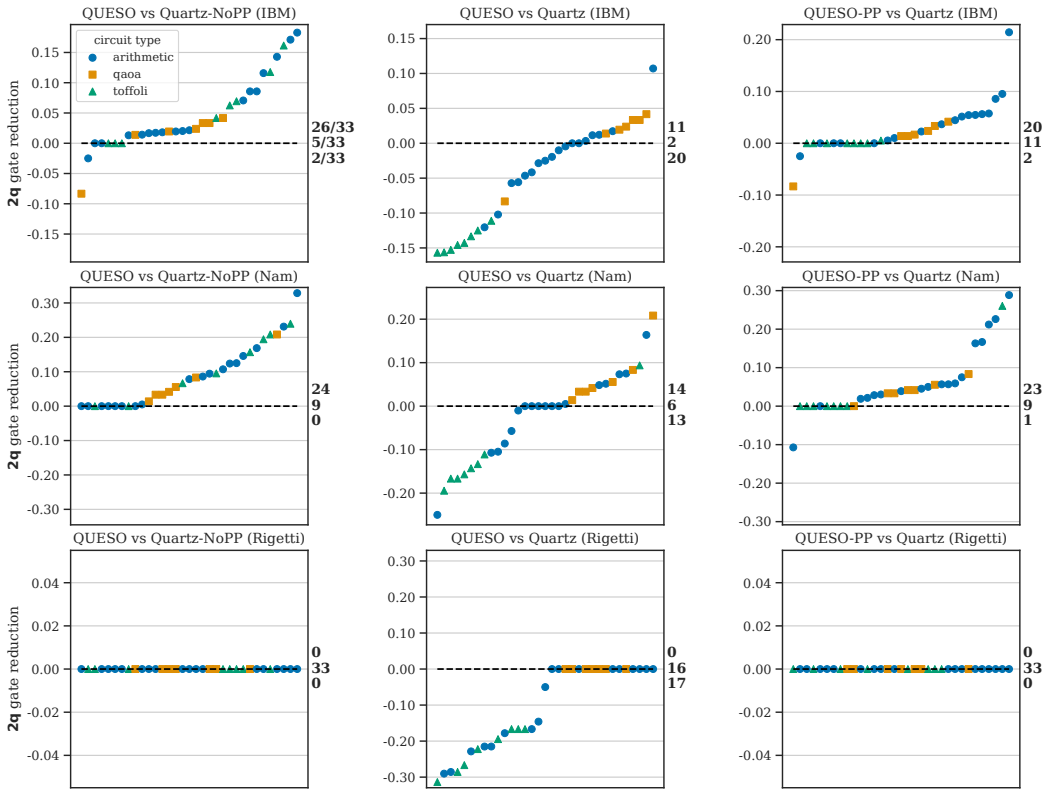


Fig. 36. 13 hour timeout comparison against Quartz.

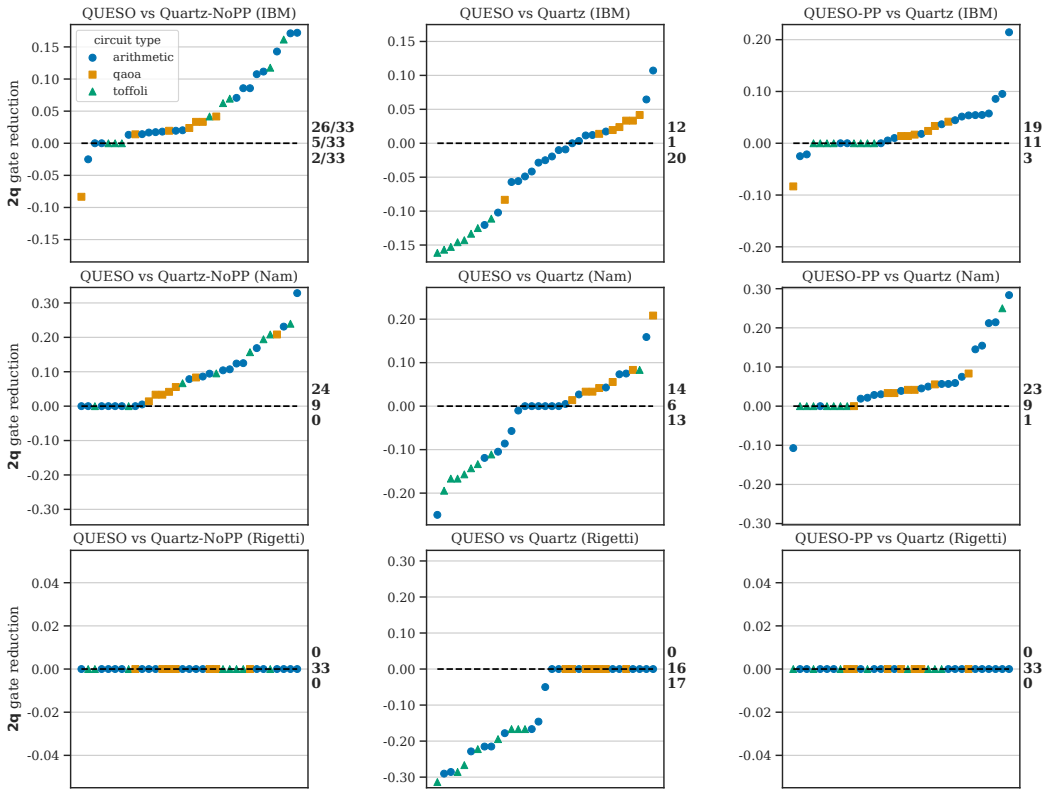


Fig. 37. 14 hour timeout comparison against Quartz.

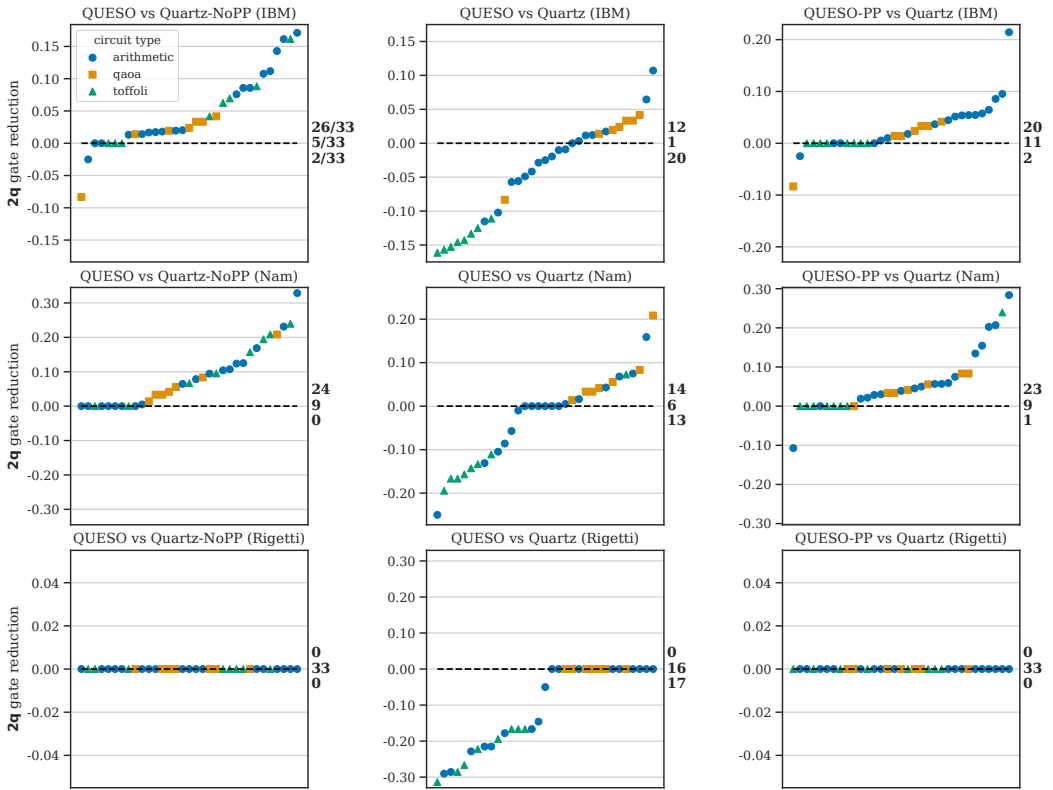


Fig. 38. 15 hour timeout comparison against Quartz.

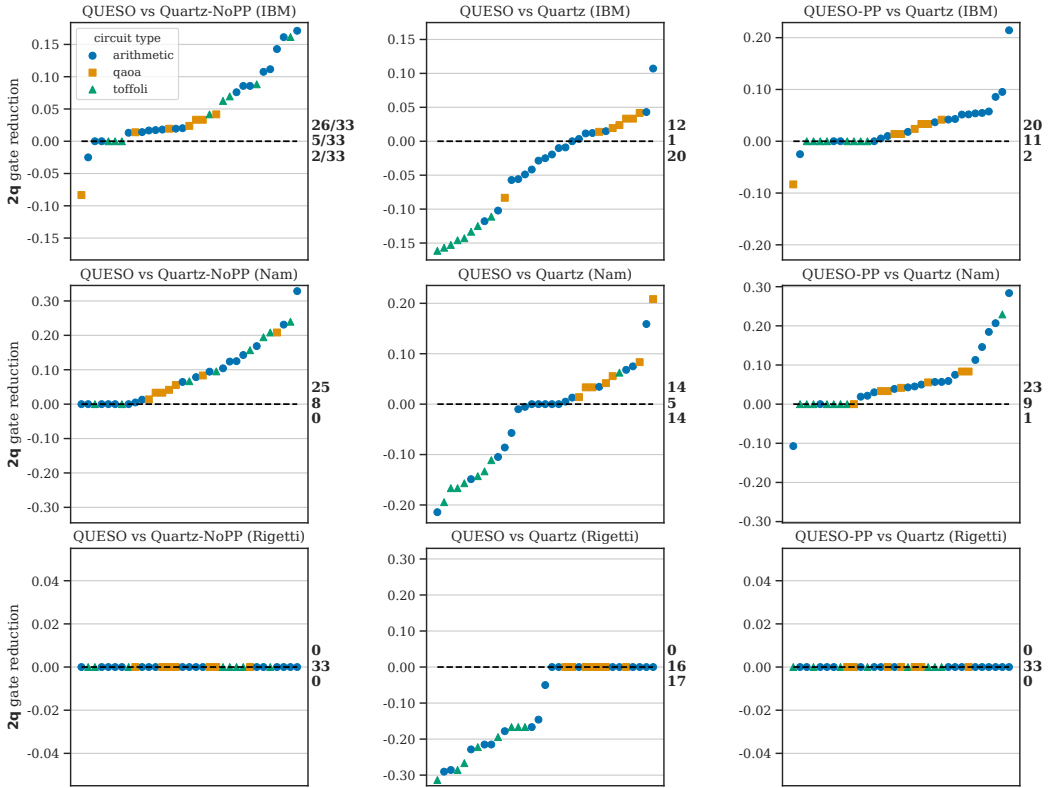


Fig. 39. 16 hour timeout comparison against Quartz.

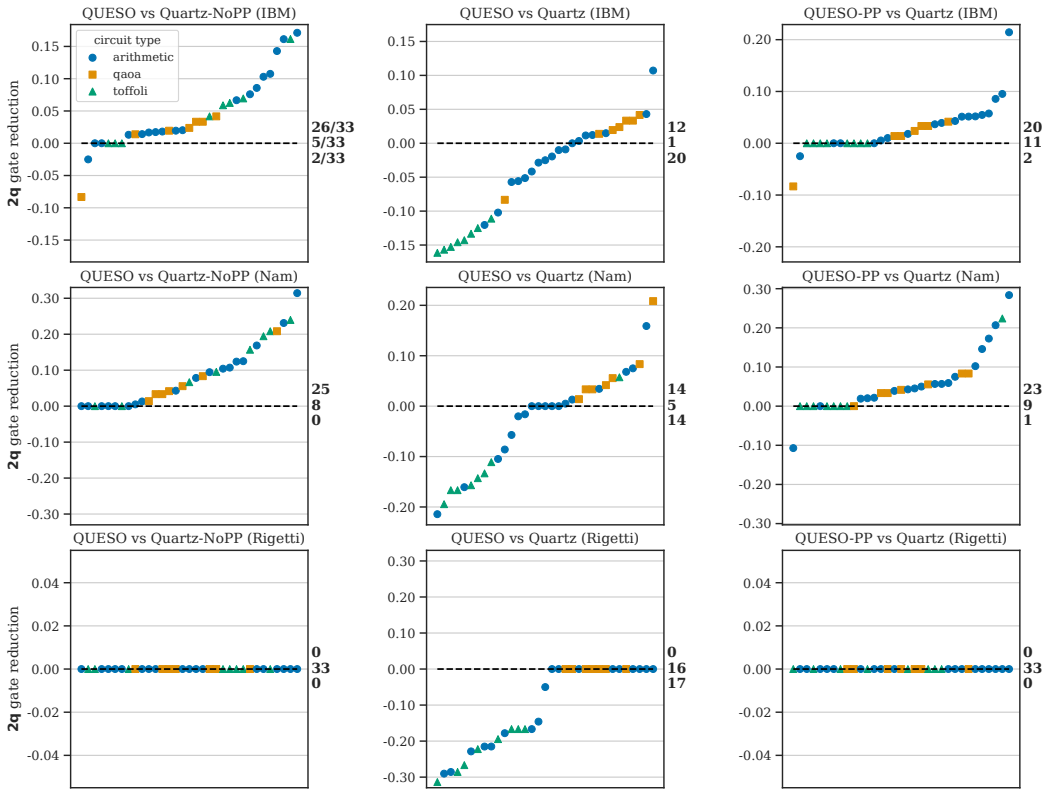


Fig. 40. 17 hour timeout comparison against Quartz.

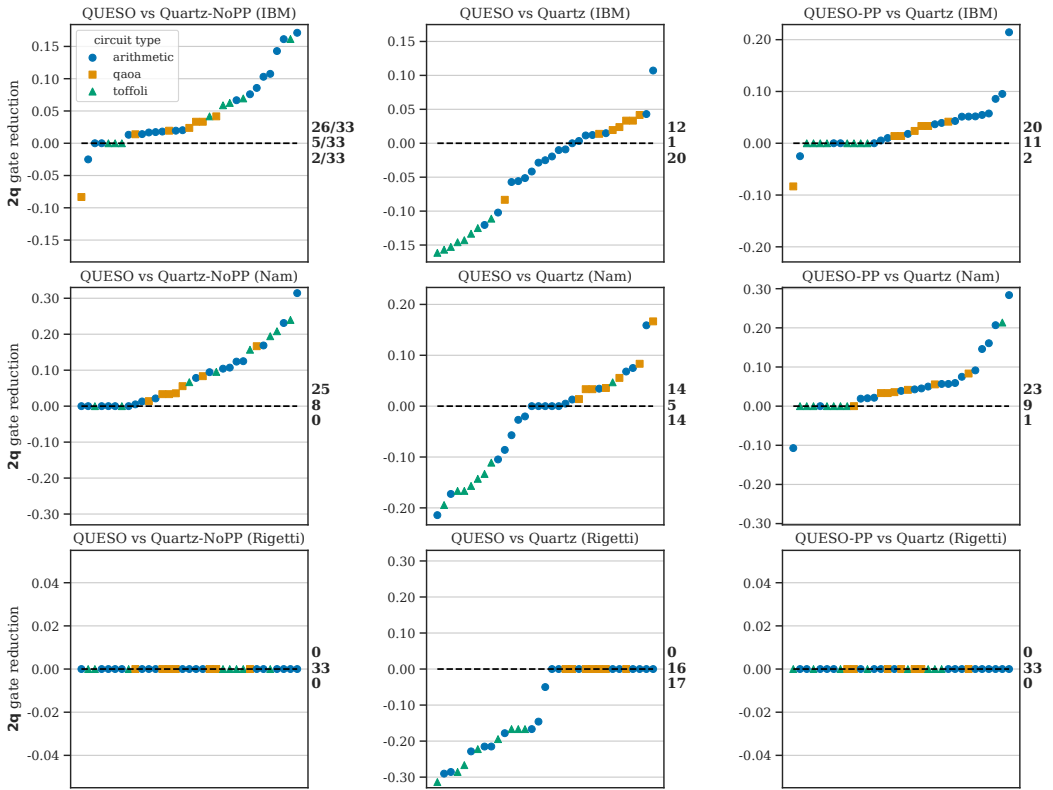


Fig. 41. 18 hour timeout comparison against Quartz.

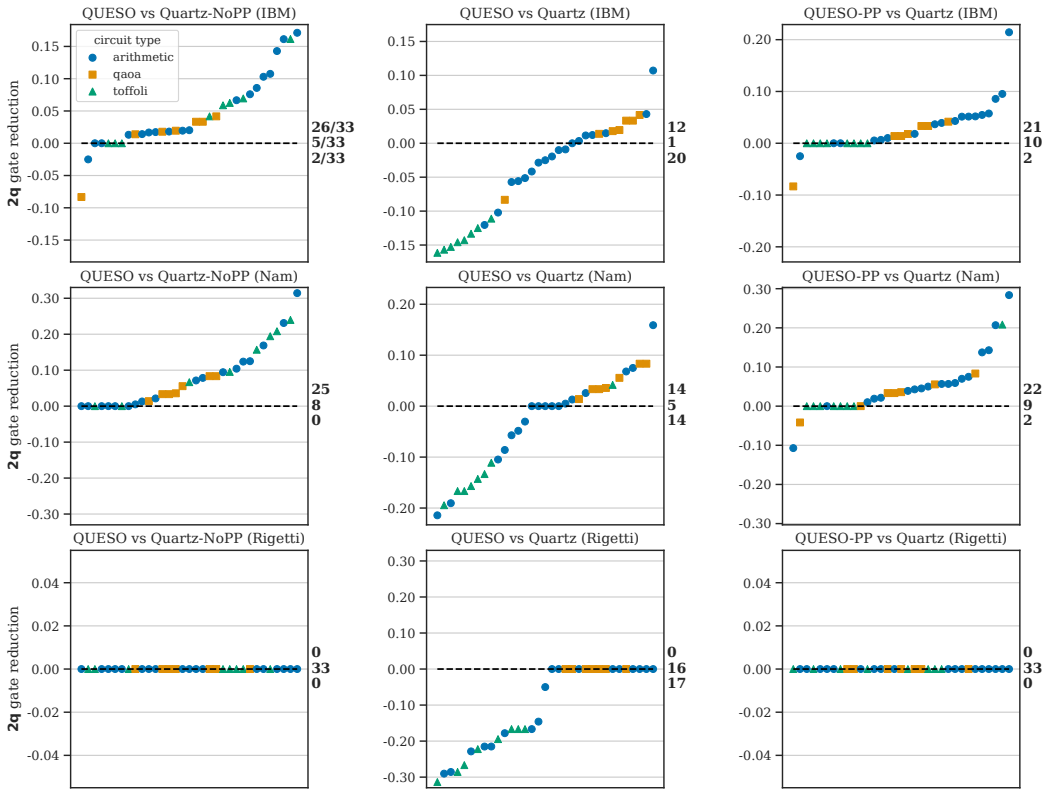


Fig. 42. 19 hour timeout comparison against Quartz.



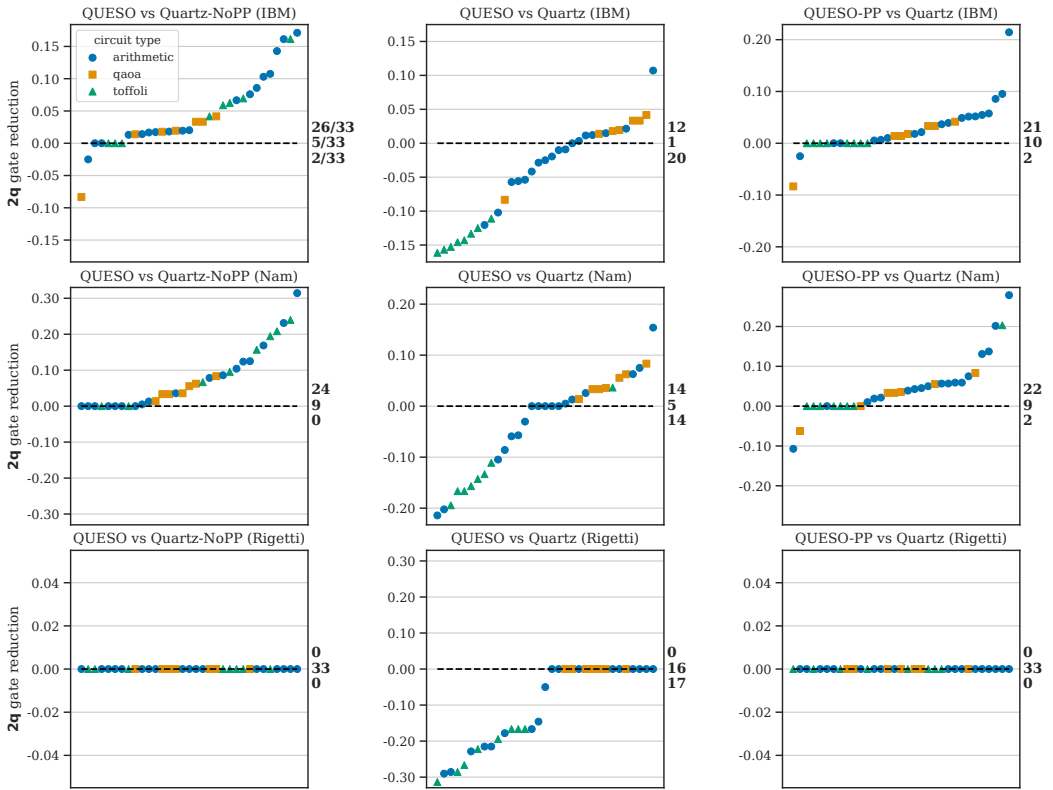


Fig. 43. 20 hour timeout comparison against Quartz.

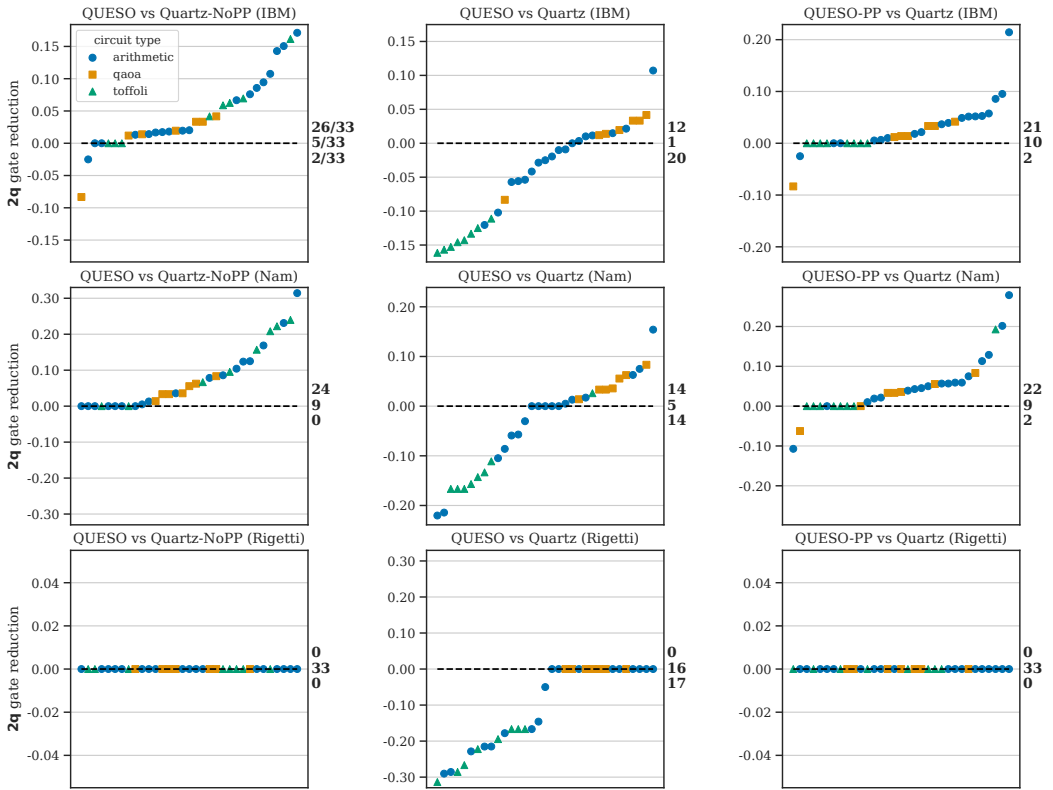


Fig. 44. 21 hour timeout comparison against Quartz.

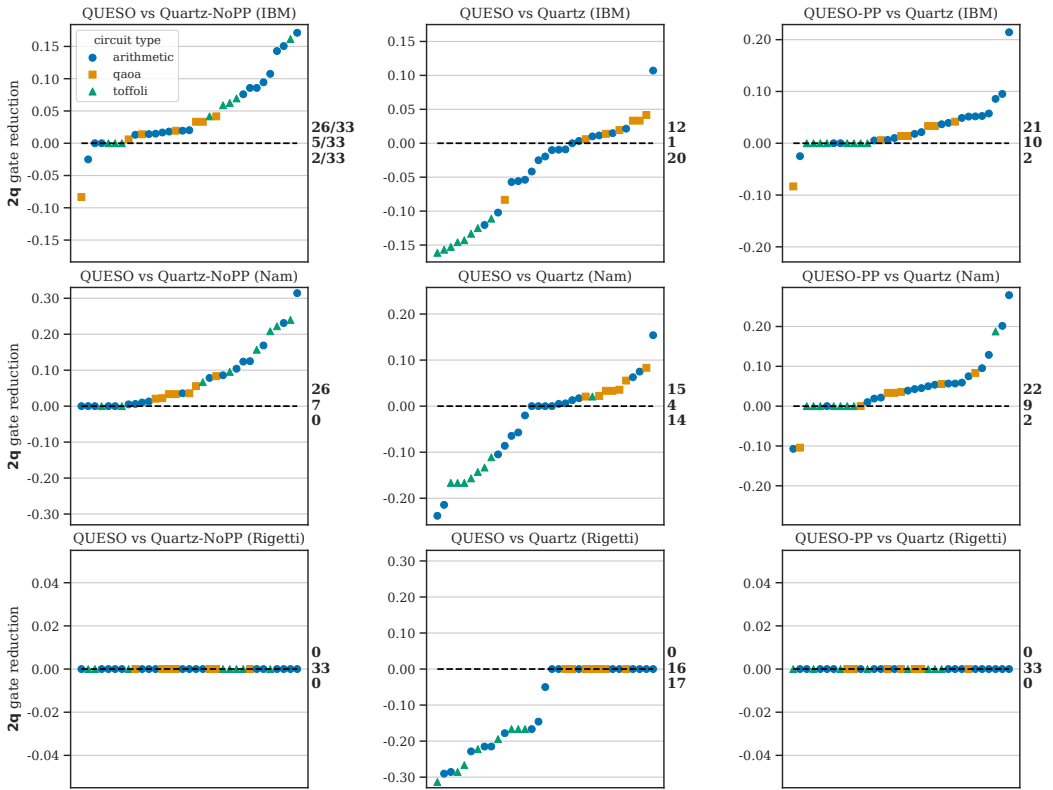


Fig. 45. 22 hour timeout comparison against Quartz.

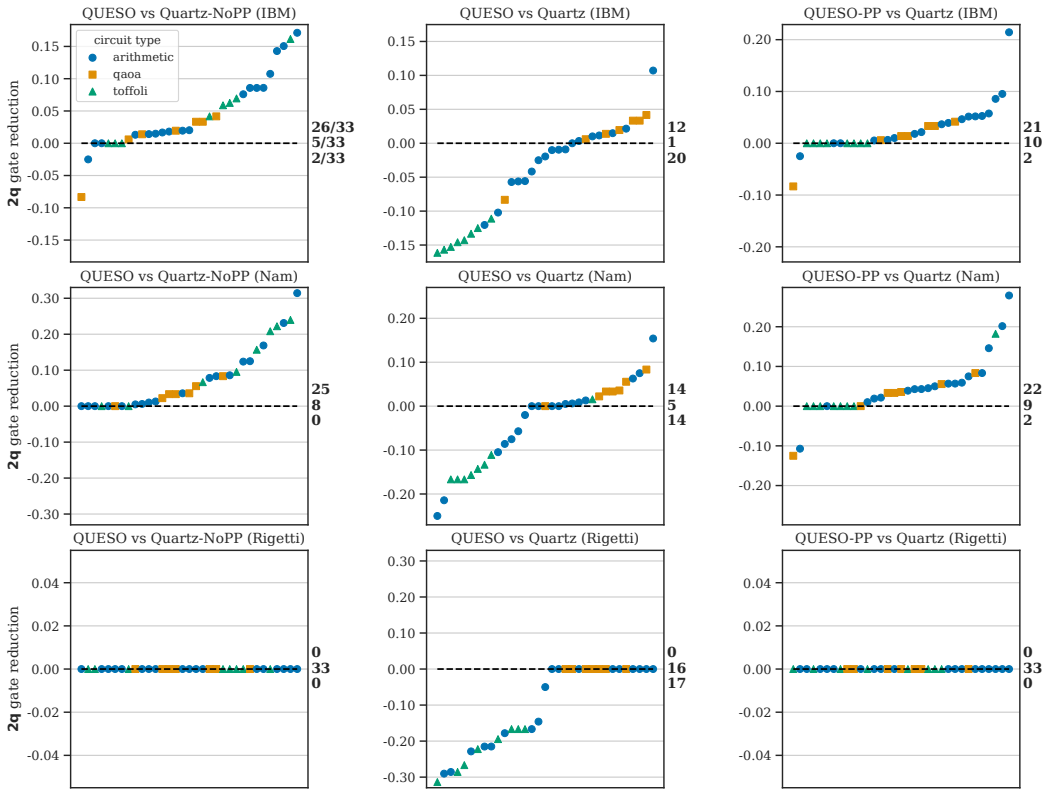


Fig. 46. 23 hour timeout comparison against Quartz.

## F EXPERIMENTAL RESULTS IN TABULAR FORM

### F.1 Total gate count 1 hour

Table 3. Total gate count results for IBM gate set with 1 hour timeout

Circuit	Original	voqc	Qiskit	TKET	Quartz	Quartz-NoPP	QUESO	QUESO-PP
adder_8	900	644	805	802	718	894	687	563
barenco_tof_3	58	43	51	51	36	47	44	36
barenco_tof_4	114	80	100	100	67	102	83	67
barenco_tof_5	170	117	149	149	98	154	122	98
barenco_tof_10	450	302	394	394	265	423	317	253
csla_mux_3	170	148	156	157	143	148	147	146
csum_mux_9	420	354	382	372	343	383	378	361
gf2^4_mult	225	185	206	206	179	218	191	179
gf2^5_mult	347	282	318	319	281	338	291	276
gf2^6_mult	495	399	454	454	394	483	426	385
gf2^7_mult	669	536	614	614	535	657	573	523
gf2^8_mult	883	691	804	806	695	877	759	672
gf2^9_mult	1095	870	1006	1009	874	1092	969	842
gf2^10_mult	1347	1068	1238	1240	1059	1345	1215	1017
mod5_4	63	53	58	58	51	56	52	38
mod_mult_55	119	99	106	103	91	94	103	96
mod_red_21	278	206	227	230	206	244	222	196
qcla_adder_10	521	403	469	464	398	498	430	371
qcla_com_7	443	292	398	384	270	408	341	267
qcla_mod_7	884	664	786	776	708	878	720	590
rc_adder_6	200	153	170	170	160	173	171	168
tof_3	45	36	40	40	31	36	36	31
tof_4	75	58	66	66	49	58	58	49
tof_5	105	80	92	92	67	89	80	67
tof_10	255	190	222	222	157	226	190	157
vbe_adder_3	150	94	136	138	84	135	94	71
qaoa_n4_p4	220	92	92	92	88	88	100	100
qaoa_n6_p4	330	138	138	138	135	135	154	154
qaoa_n8_p4	440	184	184	184	320	320	212	212
qaoa_n10_p4	550	230	230	230	479	479	266	266
qaoa_n14_p4	770	322	322	322	741	741	374	374
qaoa_n20_p4	1100	460	460	460	1089	1089	536	536
qaoa_n30_p4	1650	690	690	690	1647	1647	810	810

Table 4. Total gate count results for Rigetti gate set with 1 hour timeout

Circuit	Original	Quilc	Quartz	Quartz-NoPP	QUESO	QUESO-PP
adder_8	4412	3212	2767	4401	2142	1460
barenco_tof_3	268	193	148	242	134	86
barenco_tof_4	528	418	272	480	264	160
barenco_tof_5	788	553	386	716	394	228
barenco_tof_10	2088	1540	960	2052	1044	569
csla_mux_3	870	608	654	810	418	370
csum_mux_9	1848	1421	1100	1800	935	670
gf2^4_mult	1059	748	796	963	512	454
gf2^5_mult	1633	1197	1252	1571	809	696
gf2^6_mult	2329	1741	1867	2300	1154	992
gf2^7_mult	3147	2371	2560	3132	1564	1347
gf2^8_mult	4213	3057	3340	4204	2081	1741
gf2^9_mult	5149	3796	4205	5143	2579	2197
gf2^10_mult	6333	4724	5179	6329	3172	2685
mod5_4	305	225	197	279	143	116
mod_mult_55	545	408	361	503	267	212
mod_red_21	1208	845	738	1081	614	430
qcla_adder_10	2535	1769	1722	2510	1267	932
qcla_com_7	2048	1462	1131	2010	1020	638
qcla_mod_7	4186	3001	2762	4170	2022	1409
rc_adder_6	1010	750	606	920	485	353
tof_3	207	135	135	188	104	76
tof_4	345	218	199	315	172	114
tof_5	483	325	271	441	240	155
tof_10	1173	797	631	1071	580	360
vbe_adder_3	740	452	367	680	368	216
qaoa_n4_p4	712	332	472	576	268	259
qaoa_n6_p4	1068	501	712	864	385	390
qaoa_n8_p4	1424	664	1085	1319	579	527
qaoa_n10_p4	1780	805	1445	1724	714	655
qaoa_n14_p4	2492	1171	2146	2461	1010	914
qaoa_n20_p4	3560	1646	2997	3547	1428	1297
qaoa_n30_p4	5340	2375	4579	5333	2014	1966

Table 5. **Total gate count results for Ion gate set with 1 hour timeout**

<b>Circuit</b>	<b>Original</b>	<b>Qiskit</b>	<b>QUESO</b>	<b>QUESO-RZ-OBJ</b>
adder_8	2616	1381	1387	1507
barenco_tof_3	160	91	92	96
barenco_tof_4	316	176	175	187
barenco_tof_5	472	261	258	278
barenco_tof_10	1252	686	673	733
csla_mux_3	510	277	263	306
csum_mux_9	1120	664	656	692
gf2^4_mult	635	355	347	386
gf2^5_mult	981	543	536	599
gf2^6_mult	1401	777	763	858
gf2^7_mult	1895	1041	1031	1163
gf2^8_mult	2533	1381	1483	1542
gf2^9_mult	3105	1701	1765	1911
gf2^10_mult	3821	2095	2359	2354
mod5_4	181	101	100	109
mod_mult_55	325	178	165	192
mod_red_21	728	381	397	422
qcla_adder_10	1503	805	839	908
qcla_com_7	1226	654	693	725
qcla_mod_7	2494	1278	1309	1424
rc_adder_6	594	314	288	327
tof_3	123	71	71	73
tof_4	205	116	116	120
tof_5	287	161	161	167
tof_10	697	386	386	402
vbe_adder_3	440	229	245	265
qaoa_n4_p4	448	148	139	155
qaoa_n6_p4	672	219	211	235
qaoa_n8_p4	896	328	299	323
qaoa_n10_p4	1120	386	358	394
qaoa_n14_p4	1568	566	518	562
qaoa_n20_p4	2240	772	716	788
qaoa_n30_p4	3360	1171	1087	1191

Table 6. Total gate count results for Nam gate set with 1 hour timeout

Circuit	Original	voqc	Qiskit	Quartz	Quartz-NoPP	QUESO	QUESO-PP
adder_8	900	682	869	730	900	752	605
barenco_tof_3	58	50	56	38	54	48	38
barenco_tof_4	114	95	109	68	114	90	68
barenco_tof_5	170	140	162	102	170	150	98
barenco_tof_10	450	365	427	322	450	395	262
csla_mux_3	170	158	168	156	164	149	148
csum_mux_9	420	308	420	306	420	406	252
gf2^4_mult	225	192	213	180	219	202	177
gf2^5_mult	347	291	327	281	343	308	273
gf2^6_mult	495	410	465	399	493	450	381
gf2^7_mult	669	549	627	541	667	611	516
gf2^8_mult	883	705	819	703	883	832	682
gf2^9_mult	1095	885	1023	877	1093	1020	835
gf2^10_mult	1347	1084	1257	1060	1345	1257	1009
mod5_4	63	56	62	40	63	49	33
mod_mult_55	119	90	117	94	115	108	94
mod_red_21	278	214	261	228	272	230	196
qcla_adder_10	521	438	512	448	521	467	406
qcla_com_7	443	314	428	345	441	357	274
qcla_mod_7	884	723	853	725	884	786	651
rc_adder_6	200	157	195	154	200	182	152
tof_3	45	40	44	35	42	40	35
tof_4	75	65	73	55	75	65	55
tof_5	105	90	102	75	105	90	75
tof_10	255	215	247	195	255	215	175
vbe_adder_3	150	101	146	92	150	93	80
qaoa_n4_p4	220	124	124	205	205	106	128
qaoa_n6_p4	330	186	186	327	327	178	206
qaoa_n8_p4	440	248	248	437	437	244	276
qaoa_n10_p4	550	310	310	549	549	310	350
qaoa_n14_p4	770	434	434	769	769	426	482
qaoa_n20_p4	1100	620	620	1099	1099	616	696
qaoa_n30_p4	1650	930	930	1650	1650	930	1050



## F.2 Two-qubit gate count 1 hour

Table 7. Two-qubit gate count results for IBM gate set with 1 hour timeout

Circuit	Original	voqc	Qiskit	TKET	Quartz	Quartz-NoPP	QUESO	QUESO-PP
adder_8	409	331	385	383	391	409	347	298
barenco_tof_3	24	20	24	24	18	22	21	18
barenco_tof_4	48	38	48	48	34	48	41	34
barenco_tof_5	72	56	72	72	50	72	61	50
barenco_tof_10	192	146	192	192	142	192	161	130
csla_mux_3	80	74	71	71	73	75	73	73
csum_mux_9	168	168	168	168	168	168	168	168
gf2^4_mult	99	99	99	99	97	99	97	96
gf2^5_mult	154	154	154	154	153	154	151	148
gf2^6_mult	221	221	221	221	220	221	217	211
gf2^7_mult	300	300	300	300	299	300	295	287
gf2^8_mult	405	405	405	402	405	405	399	382
gf2^9_mult	494	494	494	494	494	494	487	466
gf2^10_mult	609	609	609	609	609	609	604	574
mod5_4	28	28	28	28	27	27	24	21
mod_mult_55	48	46	48	48	44	46	46	44
mod_red_21	105	99	105	104	92	105	94	81
qcla_adder_10	233	207	213	209	199	233	211	187
qcla_com_7	186	148	174	174	129	186	157	128
qcla_mod_7	382	344	366	366	364	382	358	301
rc_adder_6	93	81	81	81	87	91	87	87
tof_3	18	16	18	18	14	16	16	14
tof_4	30	26	30	30	22	26	26	22
tof_5	42	36	42	42	30	40	36	30
tof_10	102	86	102	102	70	102	86	70
vbe_adder_3	70	54	62	62	46	62	48	38
qaoa_n4_p4	48	48	48	48	37	37	40	40
qaoa_n6_p4	72	72	72	72	69	69	64	64
qaoa_n8_p4	96	96	96	96	96	96	92	92
qaoa_n10_p4	120	120	120	120	120	120	116	116
qaoa_n14_p4	168	168	168	168	168	168	164	164
qaoa_n20_p4	240	240	240	240	240	240	236	236
qaoa_n30_p4	360	360	360	360	360	360	360	360

Table 8. **Two-qubit** gate count results for Rigetti gate set with **1 hour timeout**

<b>Circuit</b>	<b>Original</b>	<b>Quilc</b>	<b>Quartz</b>	<b>Quartz-NoPP</b>	<b>QUESO</b>	<b>QUESO-PP</b>
adder_8	409	385	321	409	409	321
barenco_tof_3	24	24	20	24	24	20
barenco_tof_4	48	48	40	48	48	40
barenco_tof_5	72	72	60	72	72	60
barenco_tof_10	192	192	160	192	192	160
csla_mux_3	80	71	76	80	80	76
csum_mux_9	168	168	168	168	168	168
gf2^4_mult	99	99	99	99	99	99
gf2^5_mult	154	154	154	154	154	154
gf2^6_mult	221	221	221	221	221	221
gf2^7_mult	300	300	300	300	300	300
gf2^8_mult	405	405	405	405	405	405
gf2^9_mult	494	494	494	494	494	494
gf2^10_mult	609	609	609	609	609	609
mod5_4	28	28	28	28	28	28
mod_mult_55	48	48	40	48	48	40
mod_red_21	105	105	81	105	105	81
qcla_adder_10	233	213	199	233	233	199
qcla_com_7	186	174	132	186	186	132
qcla_mod_7	382	366	312	382	382	314
rc_adder_6	93	81	73	93	93	73
tof_3	18	18	14	18	18	14
tof_4	30	30	22	30	30	22
tof_5	42	42	30	42	42	30
tof_10	102	102	70	102	102	70
vbe_adder_3	70	62	52	70	70	50
qaoa_n4_p4	48	48	48	48	48	48
qaoa_n6_p4	72	72	72	72	72	72
qaoa_n8_p4	96	96	96	96	96	96
qaoa_n10_p4	120	120	120	120	120	120
qaoa_n14_p4	168	168	168	168	168	168
qaoa_n20_p4	240	240	240	240	240	240
qaoa_n30_p4	360	360	360	360	360	360

Table 9. **Two-qubit** gate count results for Ion gate set with **1 hour timeout**

<b>Circuit</b>	<b>Original</b>	<b>Qiskit</b>	<b>QUESO</b>	<b>QUESO-RZ-OBJ</b>
adder_8	409	385	409	409
barenco_tof_3	24	24	24	24
barenco_tof_4	48	48	48	48
barenco_tof_5	72	72	72	72
barenco_tof_10	192	192	192	192
csla_mux_3	80	71	80	80
csum_mux_9	168	168	168	168
gf2^4_mult	99	99	99	99
gf2^5_mult	154	154	154	154
gf2^6_mult	221	221	221	221
gf2^7_mult	300	300	300	300
gf2^8_mult	405	405	405	405
gf2^9_mult	494	494	494	494
gf2^10_mult	609	609	609	609
mod5_4	28	28	28	28
mod_mult_55	48	48	48	48
mod_red_21	105	105	105	105
qcla_adder_10	233	213	233	233
qcla_com_7	186	174	186	186
qcla_mod_7	382	366	382	382
rc_adder_6	93	81	89	93
tof_3	18	18	18	18
tof_4	30	30	30	30
tof_5	42	42	42	42
tof_10	102	102	102	102
vbe_adder_3	70	62	70	70
qaoa_n4_p4	48	48	48	48
qaoa_n6_p4	72	72	72	72
qaoa_n8_p4	96	96	96	96
qaoa_n10_p4	120	120	120	120
qaoa_n14_p4	168	168	168	168
qaoa_n20_p4	240	240	240	240
qaoa_n30_p4	360	360	360	360

Table 10. **Two-qubit** gate count results for Nam gate set with **1 hour timeout**

<b>Circuit</b>	<b>Original</b>	<b>voqc</b>	<b>Qiskit</b>	<b>Quartz</b>	<b>Quartz-NoPP</b>	<b>QUESO</b>	<b>QUESO-PP</b>
adder_8	409	337	409	407	409	348	298
barenco_tof_3	24	22	24	16	22	20	16
barenco_tof_4	48	44	48	30	48	39	30
barenco_tof_5	72	66	72	48	72	66	44
barenco_tof_10	192	176	192	188	192	176	128
csla_mux_3	80	74	80	76	80	70	70
csum_mux_9	168	168	168	166	168	168	112
gf2^4_mult	99	99	99	99	99	99	96
gf2^5_mult	154	154	154	154	154	154	148
gf2^6_mult	221	221	221	221	221	221	211
gf2^7_mult	300	300	300	300	300	300	285
gf2^8_mult	405	405	405	405	405	405	384
gf2^9_mult	494	494	494	494	494	494	466
gf2^10_mult	609	609	609	609	609	609	574
mod5_4	28	28	28	22	28	23	18
mod_mult_55	48	40	48	40	48	46	40
mod_red_21	105	93	105	105	105	92	79
qcla_adder_10	233	207	233	231	233	211	189
qcla_com_7	186	148	186	182	186	149	123
qcla_mod_7	382	338	382	380	382	352	306
rc_adder_6	93	73	93	73	93	81	71
tof_3	18	16	18	14	16	16	14
tof_4	30	26	30	22	30	26	22
tof_5	42	36	42	30	42	36	30
tof_10	102	86	102	90	102	86	70
vbe_adder_3	70	54	70	47	70	44	41
qaoa_n4_p4	48	48	48	44	44	30	36
qaoa_n6_p4	72	72	72	69	69	64	68
qaoa_n8_p4	96	96	96	96	96	92	92
qaoa_n10_p4	120	120	120	120	120	120	120
qaoa_n14_p4	168	168	168	167	167	160	160
qaoa_n20_p4	240	240	240	239	239	236	236
qaoa_n30_p4	360	360	360	360	360	360	360

### F.3 Total gate count 24 hour

Table 11. Total gate count results for IBM gate set with 24 hour timeout

Circuit	Original	voqc	Qiskit	TKET	Quartz	Quartz-NoPP	QUESO	QUESO-PP
adder_8	900	644	805	802	585	840	675	560
barenco_tof_3	58	43	51	51	36	47	44	36
barenco_tof_4	114	80	100	100	67	91	82	67
barenco_tof_5	170	117	149	149	98	138	120	98
barenco_tof_10	450	302	394	394	253	411	310	253
csla_mux_3	170	148	156	157	139	139	144	144
csum_mux_9	420	354	382	372	341	377	375	361
gf2^4_mult	225	185	206	206	178	217	187	178
gf2^5_mult	347	282	318	319	275	336	288	275
gf2^6_mult	495	399	454	454	388	483	417	385
gf2^7_mult	669	536	614	614	532	656	557	521
gf2^8_mult	883	691	804	806	693	866	743	672
gf2^9_mult	1095	870	1006	1009	868	1078	925	842
gf2^10_mult	1347	1068	1238	1240	1051	1328	1161	1016
mod5_4	63	53	58	58	51	55	52	38
mod_mult_55	119	99	106	103	91	94	103	96
mod_red_21	278	206	227	230	205	230	218	196
qcla_adder_10	521	403	469	464	379	479	407	364
qcla_com_7	443	292	398	384	268	388	316	265
qcla_mod_7	884	664	786	776	598	818	702	581
rc_adder_6	200	153	170	170	151	168	163	160
tof_3	45	36	40	40	31	36	36	31
tof_4	75	58	66	66	49	58	58	49
tof_5	105	80	92	92	67	80	80	67
tof_10	255	190	222	222	157	205	190	157
vbe_adder_3	150	94	136	138	82	113	94	71
qaoa_n4_p4	220	92	92	92	80	80	100	100
qaoa_n6_p4	330	138	138	138	131	131	154	154
qaoa_n8_p4	440	184	184	184	180	180	208	208
qaoa_n10_p4	550	230	230	230	230	230	266	266
qaoa_n14_p4	770	322	322	322	318	318	374	374
qaoa_n20_p4	1100	460	460	460	911	911	532	532
qaoa_n30_p4	1650	690	690	690	1605	1605	803	805

Table 12. Total gate count results for Rigetti gate set with 24 hour timeout

Circuit	Original	Quilc	Quartz	Quartz-NoPP	QUESO	QUESO-PP
adder_8	4412	3212	2553	4240	2132	1449
barenco_tof_3	268	193	148	242	134	86
barenco_tof_4	528	418	272	477	262	160
barenco_tof_5	788	553	386	716	390	226
barenco_tof_10	2088	1540	960	1896	1030	569
csla_mux_3	870	608	654	810	418	370
csum_mux_9	1848	1421	1100	1678	932	660
gf2^4_mult	1059	748	796	963	512	454
gf2^5_mult	1633	1197	1231	1479	794	696
gf2^6_mult	2329	1741	1751	2113	1130	990
gf2^7_mult	3147	2371	2371	2853	1529	1338
gf2^8_mult	4213	3057	3185	4104	2066	1739
gf2^9_mult	5149	3796	4130	5041	2558	2184
gf2^10_mult	6333	4724	5120	6258	3172	2685
mod5_4	305	225	197	279	143	116
mod_mult_55	545	408	361	501	263	212
mod_red_21	1208	845	738	1081	592	423
qcla_adder_10	2535	1769	1616	2331	1266	929
qcla_com_7	2048	1462	1095	1874	1020	636
qcla_mod_7	4186	3001	2527	4053	2020	1409
rc_adder_6	1010	750	606	920	481	353
tof_3	207	135	135	188	104	76
tof_4	345	218	199	313	172	114
tof_5	483	325	271	441	240	155
tof_10	1173	797	631	1071	580	360
vbe_adder_3	740	452	366	680	368	216
qaoa_n4_p4	712	332	472	576	268	257
qaoa_n6_p4	1068	501	712	864	380	385
qaoa_n8_p4	1424	664	952	1152	564	524
qaoa_n10_p4	1780	805	1192	1440	669	649
qaoa_n14_p4	2492	1171	1704	2016	935	914
qaoa_n20_p4	3560	1646	2757	3327	1338	1297
qaoa_n30_p4	5340	2375	4480	5236	1999	1966

Table 13. Total gate count results for Nam gate set with 24 hour timeout

Circuit	Original	voqc	Qiskit	Quartz	Quartz-NoPP	QUESO	QUESO-PP
adder_8	900	682	869	724	900	729	596
barenco_tof_3	58	50	56	38	50	48	38
barenco_tof_4	114	95	109	68	114	89	68
barenco_tof_5	170	140	162	98	170	130	98
barenco_tof_10	450	365	427	280	450	335	248
csla_mux_3	170	158	168	154	162	148	148
csum_mux_9	420	308	420	262	420	406	252
gf2^4_mult	225	192	213	177	219	198	176
gf2^5_mult	347	291	327	279	339	299	273
gf2^6_mult	495	410	465	391	485	441	381
gf2^7_mult	669	549	627	531	657	594	516
gf2^8_mult	883	705	819	703	883	803	680
gf2^9_mult	1095	885	1023	875	1091	943	835
gf2^10_mult	1347	1084	1257	1058	1345	1213	1008
mod5_4	63	56	62	26	48	45	33
mod_mult_55	119	90	117	93	108	98	92
mod_red_21	278	214	261	202	267	229	196
qcla_adder_10	521	438	512	428	519	466	394
qcla_com_7	443	314	428	290	441	335	272
qcla_mod_7	884	723	853	719	884	784	644
rc_adder_6	200	157	195	154	188	179	152
tof_3	45	40	44	35	40	40	35
tof_4	75	65	73	55	69	65	55
tof_5	105	90	102	75	101	90	75
tof_10	255	215	247	175	255	215	175
vbe_adder_3	150	101	146	85	146	93	76
qaoa_n4_p4	220	124	124	102	102	98	126
qaoa_n6_p4	330	186	186	186	186	178	202
qaoa_n8_p4	440	248	248	415	415	240	272
qaoa_n10_p4	550	310	310	533	533	306	346
qaoa_n14_p4	770	434	434	767	767	426	482
qaoa_n20_p4	1100	620	620	1099	1099	612	692
qaoa_n30_p4	1650	930	930	1650	1650	922	1050

#### F.4 Two-qubit gate count 24 hour

Table 14. Two-qubit gate count results for IBM gate set with 24 hour timeout

Circuit	Original	voqc	Qiskit	TKET	Quartz	Quartz-NoPP	QUESO	QUESO-PP
adder_8	409	331	385	383	314	409	339	297
barenco_tof_3	24	20	24	24	18	22	21	18
barenco_tof_4	48	38	48	48	34	44	41	34
barenco_tof_5	72	56	72	72	50	66	61	50
barenco_tof_10	192	146	192	192	130	192	161	130
csla_mux_3	80	74	71	71	70	70	72	72
csum_mux_9	168	168	168	168	168	168	168	168
gf2^4_mult	99	99	99	99	96	99	97	95
gf2^5_mult	154	154	154	154	148	154	151	147
gf2^6_mult	221	221	221	221	215	221	217	211
gf2^7_mult	300	300	300	300	296	300	295	285
gf2^8_mult	405	405	405	402	403	403	397	382
gf2^9_mult	494	494	494	494	492	494	487	466
gf2^10_mult	609	609	609	609	608	609	601	573
mod5_4	28	28	28	28	27	27	24	21
mod_mult_55	48	46	48	48	44	46	46	44
mod_red_21	105	99	105	104	91	101	92	81
qcla_adder_10	233	207	213	209	193	226	206	181
qcla_com_7	186	148	174	174	127	174	146	126
qcla_mod_7	382	344	366	366	307	382	353	292
rc_adder_6	93	81	81	81	81	89	79	79
tof_3	18	16	18	18	14	16	16	14
tof_4	30	26	30	30	22	26	26	22
tof_5	42	36	42	42	30	36	36	30
tof_10	102	86	102	102	70	92	86	70
vbe_adder_3	70	54	62	62	44	54	48	38
qaoa_n4_p4	48	48	48	48	36	36	40	40
qaoa_n6_p4	72	72	72	72	65	65	64	64
qaoa_n8_p4	96	96	96	96	92	92	88	88
qaoa_n10_p4	120	120	120	120	120	120	116	116
qaoa_n14_p4	168	168	168	168	164	164	164	164
qaoa_n20_p4	240	240	240	240	240	240	232	232
qaoa_n30_p4	360	360	360	360	360	360	353	355



Table 15. **Two-qubit** gate count results for Rigetti gate set with **24 hour timeout**

<b>Circuit</b>	<b>Original</b>	<b>Quilc</b>	<b>Quartz</b>	<b>Quartz-NoPP</b>	<b>QUESO</b>	<b>QUESO-PP</b>
adder_8	409	385	321	409	409	321
barenco_tof_3	24	24	20	24	24	20
barenco_tof_4	48	48	40	48	48	40
barenco_tof_5	72	72	58	72	72	58
barenco_tof_10	192	192	160	192	192	160
csla_mux_3	80	71	76	80	80	76
csum_mux_9	168	168	168	168	168	168
gf2^4_mult	99	99	99	99	99	99
gf2^5_mult	154	154	154	154	154	154
gf2^6_mult	221	221	221	221	221	221
gf2^7_mult	300	300	300	300	300	300
gf2^8_mult	405	405	405	405	405	405
gf2^9_mult	494	494	494	494	494	494
gf2^10_mult	609	609	609	609	609	609
mod5_4	28	28	28	28	28	28
mod_mult_55	48	48	40	48	48	40
mod_red_21	105	105	81	105	105	81
qcla_adder_10	233	213	199	233	233	199
qcla_com_7	186	174	132	186	186	132
qcla_mod_7	382	366	314	382	382	314
rc_adder_6	93	81	73	93	93	73
tof_3	18	18	14	18	18	14
tof_4	30	30	22	30	30	22
tof_5	42	42	30	42	42	30
tof_10	102	102	70	102	102	70
vbe_adder_3	70	62	50	70	70	50
qaoa_n4_p4	48	48	48	48	48	48
qaoa_n6_p4	72	72	72	72	72	72
qaoa_n8_p4	96	96	96	96	96	96
qaoa_n10_p4	120	120	120	120	120	120
qaoa_n14_p4	168	168	168	168	168	168
qaoa_n20_p4	240	240	240	240	240	240
qaoa_n30_p4	360	360	360	360	360	360

Table 16. **Two-qubit** gate count results for Nam gate set with **24 hour timeout**

<b>Circuit</b>	<b>Original</b>	<b>voqc</b>	<b>Qiskit</b>	<b>Quartz</b>	<b>Quartz-NoPP</b>	<b>QUESO</b>	<b>QUESO-PP</b>
adder_8	409	337	409	401	409	340	289
barenco_tof_3	24	22	24	16	20	20	16
barenco_tof_4	48	44	48	30	48	38	30
barenco_tof_5	72	66	72	44	72	56	44
barenco_tof_10	192	176	192	146	192	146	114
csla_mux_3	80	74	80	76	78	70	70
csum_mux_9	168	168	168	122	168	168	112
gf2^4_mult	99	99	99	96	99	98	95
gf2^5_mult	154	154	154	154	154	152	148
gf2^6_mult	221	221	221	221	221	221	211
gf2^7_mult	300	300	300	300	300	300	285
gf2^8_mult	405	405	405	405	405	403	382
gf2^9_mult	494	494	494	494	494	491	466
gf2^10_mult	609	609	609	609	609	609	573
mod5_4	28	28	28	15	22	21	18
mod_mult_55	48	40	48	39	43	39	39
mod_red_21	105	93	105	81	105	92	79
qcla_adder_10	233	207	233	211	231	211	179
qcla_com_7	186	148	186	129	186	143	121
qcla_mod_7	382	338	382	374	382	352	299
rc_adder_6	93	73	93	73	81	79	71
tof_3	18	16	18	14	16	16	14
tof_4	30	26	30	22	28	26	22
tof_5	42	36	42	30	40	36	30
tof_10	102	86	102	70	102	86	70
vbe_adder_3	70	54	70	40	66	44	37
qaoa_n4_p4	48	48	48	30	30	30	36
qaoa_n6_p4	72	72	72	68	68	64	64
qaoa_n8_p4	96	96	96	96	96	88	88
qaoa_n10_p4	120	120	120	120	120	116	116
qaoa_n14_p4	168	168	168	165	165	160	160
qaoa_n20_p4	240	240	240	239	239	232	232
qaoa_n30_p4	360	360	360	360	360	352	360

## F.5 T gate count

Table 17. T gate count results for Nam gate set with 1 hour timeout

Circuit	Original	voqc	Qiskit	PyZX	Quartz	Quartz-NoPP	QUESO	QUESO-PP
adder_8	399	215	361	170	231	399	265	219
barenco_tof_3	28	16	24	16	16	28	16	16
barenco_tof_4	56	28	48	28	28	56	28	28
barenco_tof_5	84	40	72	40	40	84	60	40
barenco_tof_10	224	100	192	100	100	224	160	100
csla_mux_3	70	64	68	46	64	70	64	64
csum_mux_9	196	84	196	78	84	196	168	84
gf2^4_mult	112	68	96	60	68	112	82	68
gf2^5_mult	175	115	155	94	115	175	135	115
gf2^6_mult	252	150	216	140	150	252	198	150
gf2^7_mult	343	217	301	217	217	343	273	214
gf2^8_mult	448	264	384	264	264	448	360	264
gf2^9_mult	567	351	495	351	351	567	459	351
gf2^10_mult	700	410	600	410	410	700	568	410
mod5_4	28	16	26	8	14	28	10	10
mod_mult_55	49	35	45	28	35	49	39	35
mod_red_21	119	73	107	72	77	119	75	73
qcla_adder_10	238	164	222	154	164	238	198	164
qcla_com_7	203	95	177	92	107	203	135	95
qcla_mod_7	413	249	361	227	245	413	321	245
rc_adder_6	77	47	67	47	47	77	65	47
tof_3	21	15	19	15	15	19	15	15
tof_4	35	23	31	23	23	35	23	23
tof_5	49	31	43	31	31	49	31	31
tof_10	119	71	103	71	71	119	71	71
vbe_adder_3	70	24	62	24	32	70	28	24

Received 2022-11-10; accepted 2023-03-31